2013

Effect of Doping on β-Tricalcium Phosphate Bioresorbable Bulk Material and Thin Film Coatings

Suhaila Abdalla
North Carolina Agricultural and Technical State University

Effect of Doping on β-Tricalcium Phosphate Bioresorbable Bulk Material and Thin Film Coatings

By

Suhaila Abdalla

North Carolina A&T State University

A dissertation submitted to the graduate faculty

in partial fulfillment of the requirements for the degree of

DOCTOR OF PHILOSOPHY

Department: Mechanical Engineering

Major: Mechanical Engineering

Major Professor: Dr. Dhananjay Kumar

Greensboro, North Carolina

2013

School of Graduate Studies
North Carolina Agricultural and Technical State University

This is to certify that the Doctoral Dissertation of

Suhaila Abdalla

has met the dissertation requirements of
North Carolina Agricultural and Technical State University

Greensboro, North Carolina
2013

Approved by:

Dr. Dhananjay Kumar Major Professor	Dr. Jagannathan Sankar Committee Member
Dr. Devdas Pai Committee Member	Dr. Cindy Waters Committee Member
Dr. Samuel Owusu-Ofori Department Chairperson	Dr. Sanjiv Sarin Dean, The Graduate School

Biographical Sketch

Suhaila Abdalla was born on April 2nd 1973, in Khartoum, Sudan. She completed her senior secondary school education at the Catholic Sisters' School in Khartoum, Sudan. She received her Bachelor of Science degree in Mechanical Engineering from the University of Khartoum, Sudan in 1999. Suhaila has worked as an RF engineer with Sprint PCS from 2001 to 2007.

Suhaila was admitted into the Ph.D. program at the Mechanical Engineering Department of North Carolina Agricultural & Technical State University in the spring of 2009. She performed her research on surface modification of biodegradable magnesium implants using pulsed laser deposition.

Dedication

I dedicate this doctoral dissertation to my family: my father Eltahir Mustafa Abdalla and my mother Gadria Salih, my siblings Mustafa, Julanar, Mulham, and Saria, who've always supported me and encouraged me.

Acknowledgements

I would like to express my gratitude and appreciation to my supervisor Dr. Dhananjay Kumar for his kind guidance, providing different solutions and inspiring motivation towards my doctoral thesis. He was also the person who suggested and introduced to me how to work with my topic and how to enhance my skills. He has provided his valuable time in discussing, going through my drafts, providing comments and advising me on how to improve my work from time to time.

I would also like to thank Dr. Jag Sankar for taking me on and allowing me to become a part of the ERC team, allowing me to be a part of researching such cutting edge technologies. I would also like to thank my committee members Dr. Devdas Pai and Dr. Cindy Waters. My special thanks goes to Dr. Ram Gupta for all his valuable input, suggestions and comments to guide me in the right direction towards completing my degree requirements. I would like to extend special thanks to Professor Samuel Owusu-Ofori for his support and encouragement throughout my graduate studies.

I would also like to thank certain ERC members for sharing their expert knowledge and knowhow that was necessary to help me conduct my research: Dr. Xu, Dr. Waterman, Dr. Jang, and Dr. Yarmolenko.

Last but not least, I would like to thank my lab mates, Kwadwo Mensah-Darkwa, Talisha Haywood, Sally Ibrahim, Svitlana Fialkova, Ruben Kotoka, Seyram Gbordzoe, and Chris Smith for all their support.

This work was financially supported by the National Science Foundation - Engineering Research Center for Revolutionizing Metallic Biomaterials (ERC-RMB). This support is greatly appreciated.

Table of Contents

List of Figures

List of Tables

Abstract

Magnesium has emerged as a revolutionary biodegradable metal for use as an orthopedic material, it has several advantages over the permanent metallic materials currently in use, including eliminating the effects of stress shielding, improving biocompatibility and degradation properties, thus removing the requirement of a second surgery for implant removal. Due to the rapid degradation of magnesium, it is necessary to control the corrosion rates of the materials to match the rates of bone healing. This dissertation reports on the effect of doping on the properties of β-tricalcium phosphate (β-TCP). It also reports on its application as a thin film coating on magnesium alloys for implant applications.

Adding various dopants to β-TCP significantly influences critical properties. In this study, discs were fabricated in two compositions: (i) undoped β-TCP, (ii) β-TCP doped with 1.0 wt % MgO, 0.5 wt % ZnO, and 1.0 wt % TiO_2. Films were fabricated from these compositions using the pulsed laser deposition (PLD) technique. These coatings were then characterized for corrosive, hardness, and cytocompatibility. The XRD patterns of the coating confirm the amorphous nature of the films. The presence of the metal oxides in β-TCP improved ceramic densification. The application of these doped coatings was also found to increase the hardness by 88 %, the modulus of elasticity by 66 %, and improve corrosion resistance of the magnesium alloy substrate; with a 2.4 % improvement in E_{corr} and 95 % decrease in i_{corr}. Cell viability was studied using an osteoblast precursor cell line MC3T3-E1 to assure that the biocompatibility of these ceramics was not altered due to the dopants. Long-term biodegradation studies were conducted by measuring weight change and surface microstructure as a function of time in simulated body fluid. The results suggest that these coatings could be used for bioresorbable implants with improved corrosion resistance and increased hardness.

CHAPTER 1

Introduction

This dissertation is organized into five chapters. Chapter 1 introduces the research subject, objectives and motivations for this work. It also gives a brief review of the current innovations. The second chapter is dedicated to presenting a comprehensive theoretical review of biomaterials, their current use and limitations. It also provides a literature review of metallic implant materials, bioceramics, and coating methods currently utilized, as well as the logic behind the ceramic, target and substrate selections for the present work. Chapter 3 presents the experimental methods and theory behind the characterization methods used in this research. It provides the parameters used in the PLD system followed by descriptions of the characterization techniques used in this work. Results and discussions are presented in Chapter 4. In chapter 5 a conclusion of the present work is given and suggestions for potential future work are described briefly.

1.1 Background

Soft tissue tears, bone fracture or joint dislocations all generally require a fixation device to be correctly treated (Rayburn, Riffle, Walburn, & Williams, 1998; Walz, Salzmann, Fabbro, Eichhorn, & Imhoff, 2008; Waris, Konttinen, Ashammakhi, Suuronen, & Santavirta, 2004). Bone is a highly specialized form of connective tissue that provides an internal support system in most vertebrates (Shea & Miller, 2005). It acts as the site for the attachment of muscles and tendons, essential for movement, protects the vital organs of the cranial and chest cavities, and it encloses the blood forming vessel elements of the bone marrow. In addition to these mechanical functions, bone plays an important metabolic role as a mobile store of calcium and phosphate, which can be drawn upon when needed.

Bone is a connective tissue composed of an organic collagenous matrix, a fine dispersion of reinforcing inorganic elements, and bone-forming and bone-degrading cells. These different components render bone tissue properties unique in terms of hardness, flexibility and regenerative capacity. Bone defects are frequently caused by trauma, disease and developmental deformity (Wiese & Pape, 2010). Repairing such bone sites involves various medical surgical techniques, some of which include the use of autografts, allografts, internal and external fixation devices, and replacement implants. A number of materials have been tested for use in the biomedical industry to treat these types of bone defects, which include metals, polymers, ceramics and composites (Altieri, Flores, Gonzalez, & Rodríguez; Lemons, 1993; T. Ogawa, 2006; Uchida et al., 1990; Wallace et al., 1988).

The mechanical and biological properties of bone implants need to be optimal to form a quick and firm connection with the bone tissue in load bearing applications. Metallic and certain polymeric materials with the right mechanical strength offer mechanical strength that is required to simulate bone tissue in load-bearing applications in terms of maximum load, bending and fatigue strength, such as titanium, stainless steel, Polyesters, PLA, and PGA, which are currently used for bone tissue engineering (Hutmacher, Hurzeler, & Schliephake, 1996; Yue, Pilliar, & Weatherly, 1984).

Magnesium and magnesium alloys are potential bioresorbable metals for orthopedic devices such as mini/micro-plate systems, screws, and rods. This is so because magnesium is one of the essential elements in the human body. The mechanical integrity of magnesium based devices to bones is high owing to magnesium's elastic modulus and compressive yield strength being closer to those of natural bone than other commonly used metallic implants (Staiger, Pietak, Huadmai, & Dias, 2006) as listed in Table 1.1 (Choi, Kong, Kim, & Lee, 1998;

DeGarmo, Black, & Kohser, 1997; L. J. Gibson & Ashby, 1999; Seeley, Bandyopadhyay, & Bose, 2007; Thamaraiselvi & Rajeswari, 2004). Degradation of bioresorbable metals should be inhibited until the fractured bone is sufficiently repaired to bear the load. However, the existing magnesium alloys do not show enough corrosion resistance for bone fixation devices. Improvement of the corrosion resistance is essential for the promotion of the practical use of magnesium alloys (A. Yamamoto, Watanabe, Sugahara, Tsubakino, & Fukumoto, 2001).

Table 1.1

Summary of physical and mechanical properties of various implant materials in comparison to natural bone

Properties	Natural Bone	Mg	Ti alloy	Co–Cr Alloy	Stainless Steel	TCP	HA
Density (g/cm^3)	1.8–2.1	1.74–2.0	4.4–4.5	8.3–9.2	7.9–8.1	3.14	3.1
Elastic modulus (Gpa)	3–20	41–45	110–117	230	189–205	120.69	73-117
Compressive yield strength (Mpa)	130–180	65–100	758–1117	450–1000	170–310	70-95	600
Fracture toughness (MPa $m^{1/2}$)	3–6	15–40	55–115	N/A	50–200	0.41-1.15	0.7

The interaction between the implanted material and the surrounding tissue at the implant interface is essential for success or failure of implants and thus the need arises for coatings that will improve the performance of the bone implant (H. Zreiqat et al., 2002). Surface modification is one of the methods to improve the corrosion resistance of magnesium and its alloys (Gupta, Mensah-Darkwa, & Kumar, 2013). Coatings with calcium phosphate compounds attracted attention because the calcium phosphate compounds precipitated from simulated body fluids (SBF) improved the corrosion resistance of magnesium (Clèries L, 2000).

In that respect, coatings can be applied to facilitate the process of bone healing and obtain a continuous transition from living tissue to the synthetic implant, thus, the most obvious candidates for application as implant coating are compounds that are inspired by the components of bone tissue, they can be inorganic (e.g., hydroxyapatite, tricalcium phosphate) or organic (e.g., collagen, extracellular matrix components, enzymes) (Geng, Tan, Zhang, et al., 2009; Mckee & Nanci, 1996; Morra et al., 2005; Oonishi et al., 1989; Robins et al., 2009). One of the limitations of using ceramic material components is that the implant suffers from early failures due to their low fracture toughness (Kalita, Bhardwaj, & Bhatt, 2007). Therefore, in an effort to improve the mechanical properties of these ceramics, metallic oxide dopants were added to the bulk ceramic to improve its fracture toughness, hardness and to improve corrosion resistance of the magnesium implant due to the physiological environment with the body.

As a new approach for a bioresorbable implant, this research work reports on the use of pulsed laser deposition (PLD) to uniformly coat magnesium and its alloys with the bioresorbable doped ceramic beta tricalcium phosphate for application as a bioresorbable bone fixation device.

1.2 Innovations

Metals and their alloys have a long history as orthopedic implants and bone graft

substitutes for their well-known strength (elastic modulus larger than 100 GPa), especially in load-bearing sites (M. Wang, 2003). Typically implants have been produced from stainless steel, cobalt–chromium (CoCr), or titanium alloys. A lot of methods of surface modification have been developed to enhance biological properties of these implants to promote bone fixation for use in orthopedic procedures (Bobyn JD, 1999).

Due to inherent properties, such as lightweight, high strength and biocompatibility, metallic alloys garnered considerable attention as implant materials. Their use is however also associated with several limitations, which include permanence, cracking, low volumetric porosity, relatively high modulus of elasticity compared to bone and the potential of releasing harmful metallic ions and introducing corrosion products into the body from these materials (J. Jacobs, Hallab, Skipor, & Urban, 2003; J. J. Jacobs et al., 1998; JJ., JL., & RM., 1998; Lhotka, Szekeres, Steffan, Zhuber, & Zweymuller, 2003; Puleo & Huh, 1995). Most metals are not biodegradable, thus, cannot be used to produce a complete tissue replacement for bone defects. Additionally, metal particles released from the implant have been found to affect the release of inflammatory factors, inhibit expression of osteogenic cell markers, and stimulate bone loss or recommencement. For instance, studies have shown that titanium and its alloy particles inhibit bone-cell proliferation and osteogenic differentiation (Goodman, Ma, Chiu, Ramachandran, & Lane Smith, 2006). Another draw back in the use of metal implants is their lack of bioactivity and a significant difference in stiffness between the metal and surrounding bone tissue rendering them not capable of integrating well with the implant site. These metal implants being stiffer than the natural bone tissue, leads to the stress shielding effect and poor osteointegration during the implants lifetime. Several modifications have been suggested to address some of the limitations of these traditional solid metals.

The use of magnesium is thought to be helpful in overcoming the limitations of conventional metals currently used in tissue engineering. Magnesium is lightweight and biodegradable making it potentially useful metal in bone substitution. The fracture toughness of magnesium is greater than that of ceramic biomaterials such as hydroxyapatite, while its elastic modulus and compressive yield strength are closer to those of the natural bone as compared to other commonly used metallic implants (DeGarmo et al., 1997). Moreover, magnesium can be found in bone tissue as a trace element, where it plays an essential role (DeGarmo et al., 1997; Hartwig, 2001; Okuma, 2001; Slinde, Grönberg, Engström, Rossander-Hulthén, & S., 2002; Vormann, 2003; Wolf & Cittadini, 2003). Magnesium is a co-factor for many enzymes, and helps to stabilize the structures of DNA and RNA (Hartwig, 2001). Reports suggested that magnesium might actually stimulate the growth of new bone tissue (Revell, Damien, Zhang, Evans, & Howlett, Dec; Yamasaki et al., 2003; Yamasaki Y, 2002 Oct; H. Zreiqat et al., 2002). Thus, magnesium and its alloys could be used for load bearing orthopedic implants, which would remain present in the body and maintain mechanical integrity over the healing period; eventually the implants are replaced by natural tissue (C. E. Wen et al., 2001; F. Witte et al., 2006).

One approach to providing a strong, long-lasting adhesive interface between a bone replacement implant and the surrounding tissue involves the use of bioactive materials that mimic the behavior of natural bone. The bioactive materials are put as a coating on the implant surfaces to improve the integration of metal implants to bone tissue, prolong their lifetime, and prevent adverse effects produced by metal implants. Examples of such materials include calcium phosphate salts, such as hydroxyapatite (HA), tricalcium phosphate (TCP), and Plaster of Paris (calcium sulfate dihydrate).

In the past decade, many studies were conducted to investigate coatings that will inhibit

degradation rate of magnesium in physiological environment. Geng et al. found that β-TCP coated porous magnesium scaffolds showed improved mechanical and biological properties (Geng, Tan, Zhang, et al., 2009). It was found to control the degradation rate of magnesium to create a suitable microenvironment and a bioactive surface for cell growth and proliferation, it promoted cell attachment and proliferation, and the growth of bone like apatite on the surface of the coated metals.

There are many techniques that have been used to create such coatings on metallic implant materials, for example, dip coating, electrophoretic deposition, hot isotatic pressing, pulsed laser deposition, sol-gel processing, and sputter coating have been used to deposit these coatings (Lacefield, 1998). Amongst all these methods, PLD has several characteristics that distinguish it from other growth methods and provide special advantages for the growth of chemically complex (multielement) and composite materials (Sharma, Kalyanaraman, Narayan, Oktyabrsky, & Narayan, 2001). The advantages of this technique are the capability for reactive deposition, energetic evaporants, fast deposition times, flexibility, improved film quality at lower temperatures, maintenance of stoichiometry, and simplicity for the growth of multilayered structures (Eason, 2006).

For PLD deposition ceramic powders must be fabricated into targets my means of pressing and sintering. Although TCP is a very attractive candidate for these coatings, sintering remains a major challenge. The sintering of TCP is much less reported than it is for HA. α-TCP and β-TCP are the two phases of interest in biological applications. β-TCP is the thermodynamically stable form at low temperature. It transforms into α-TCP in the temperature range 1275–1300 °C (Barralet, Gbureck, Grover, & Thull, 2004; Perera, Martínez-Vázquez, Miranda, Ortiz, & Pajares, 2010). β-TCP is generally preferred in sintered ceramic implants,

while α-TCP is more commonly used in bone graft cements because of its hydrolysis properties (Perera et al., 2010).

The main difficulty encountered in the sintering of β-TCP comes from the β → α phase transformation that occurs at ~1300 °C. It is accompanied by a sudden thermal expansion, which creates mechanical stresses inducing cracks within the sample (Itatani, Takahashi, Howell, & Aizawa, 2002; X. L. Wang, Fan, & Zhang, 2005). This leads to a low mechanical reliability of TCP ceramics sintered above the transformation temperature (Raynaud, Champion, Lafon, & Bernache-Assollant, 2002). Another point is that the reverse transformation α → β during cooling to room temperature does not occur in the same conditions as the β → α transformation, α-TCP being generally present in the cooled ceramics heated above the transformation temperature. Slow kinetics of the α → β transformation is often encountered in dimetallic phosphate compounds $Me_2(PO_4)_3$ (Averbuch-Pouchot & Durif, 1996).

According to the work of Monma and Goto, an annealing treatment of TCP for at least 5 h at 850 °C would be necessary to complete this transformation (Monma & Goto, 1983). To overcome these difficulties, some authors used MgO (Famery, Richard, & Boch, 1994; Rabadjieva et al., 2011), ZnO (Bandyopadhyay, Withey, Moore, & Bose, 2007; Carbajal, Caballero, & Sainz, 2012; Rabadjieva et al., 2011), MgO–ZnO (Xue, Dahlquist, Banerjee, Bandyopadhyay, & Bose, 2008), MgO–SrO (Banerjee, Tarafder, Davies, Bandyopadhyay, & Bose, 2010), SiO_2– ZnO (Fielding, Bandyopadhyay, & Bose, 2012) or $Ca_2P_2O_7$ (Ryu et al., 2002) as additives to increase the high-temperature limit of β-TCP. Similarly, the influence of TiO_2, Ag_2O, NaF, CaO or SiO_2 addition on the sintering of β-TCP has also been reported (Bandyopadhyay et al., 2007; Douard et al., 2011; Seeley et al., 2007; Seeley, Bandyopadhyay,

& Bose, 2008). All these oxides were also chosen because they were expected to improve the biological and/or mechanical properties of sintered ceramics.

1.3 Objective and Motivation

Magnesium alloys are susceptible to corrosion in the physiological environment of the body. There are two potential solutions to stop or reduce the corrosion of magnesium; the first one is to develop alloys of magnesium using metals that are biocompatible and the second solution is based on the application of surface modification. In this research, a combined approach has been used that allows the mechanical properties of the implants to be supported by the metallic structure, while the osteointegration is promoted by the applied coating. Attempts have been made to improve the mechanical properties of tricalcium phosphate through the addition of dopants. The significance of adding dopants to TCP is to modify the rate of resorption, improve the material's hardness and promote bioactivity, thus, controlling the rate of mechanical degradation and inhibiting corrosion of the magnesium alloys. The focus to improve densification was based on the combination and ratio of dopants added to TCP.

Sun et al. showed that addition of zinc (Zn) and calcium (Ca) enhances the corrosion potential of the magnesium alloy and the in vitro degradation rate of the Mg4Zn0.2Ca alloy was similar to that of high-purity magnesium in SBF (Sun, Zhang, Wang, Geng, & Jiao, 2012). After 30-day degradation in SBF solution, the values of the yield strength, the ultimate tensile strength and the elongation of the alloy were enough for the fixed bone. In vitro cytotoxicity experiments indicated good biocompatibility of the alloy. For this work a magnesium alloy of Mg2Zn0.3Ca cast in our lab was used as a substrate as well as commercially bought unalloyed magnesium.

The present research relates to bioceramic coating of metallic devices for use in bone fixation. Ca-P coating is believed to first allow strong tissue-material interaction and then

slowly dissolve away as tissue grows on the material. Pulsed laser deposition was chosen as the method to apply these coatings. The parameters to produce the smoothest and most stoichiometric films were optimized thorough experiments and characterized through structural, mechanical and biological tests to investigate the effect of dopant addition on these properties.

- X-ray diffraction was used to investigate any phase changes on the TCP films due to the addition of dopants and the crystallinity of the deposited films.
- The hardness and stiffness of the ceramics and films were studied using nanoindentation tests.
- Bio-mineralization due to exposure to SBF was studied by checking weight gain after soaking and SEM images were taken for each sample and time duration.
- Corrosion resistance of the films after TCP coating was checked using electrochemical corrosion studies.
- Biocompatibility of the fabricated coatings was studied using live-dead assay.

CHAPTER 2

Literature Review

Chapter 2 reviews the literature relevant to this research field. This chapter is divided into five components, (1) an introduction to the human skeletal system, the functions, composition, and mechanical properties of bone (2) biomaterials in orthopedics and their current use, (3) corrosion of implant materials, (4) choice of materials; metal substrates, bioceramics and metal oxide dopants used, and (5) an overview of the pulsed laser deposition technique used in the current research and methods used to characterize the newly developed implant material. Through this chapter, the reader can understand the importance of the role that metals and ceramics playing in tissue engineering.

2.1 Human Skeletal System – An Introduction

The human skeletal system provides support and protection for the body as well as sites for muscle attachments and the production of blood cells (Larry L. Hench, October 1993). The skeleton of an adult is made up on average of 206 bones, but with age this number decreases as some bones become fused together during the development of the circulatory and nervous system. Unlike adults the skeleton of an embryo is comprised of about 350 completely cartilaginous bones, over 140 more than adults. In an adult skeleton, the cartilage almost completely disappears: it remains in a few places which include certain parts of the ear, the nose, the mouth, the anterior parts of the ribs, and on the surface of the joints (Figure 2.1).

The human skeleton reaches full maturity at about 25 years of age and is comprised of two categories: the axial skeleton, which includes the cranium, the spinal column, and the thorax. The basic function of this section of the skeleton is to protect the internal organs: and the appendicular skeleton, which includes the upper and lower limbs, and the pelvis; its basic

function is to enable movement and support. Of the 206 bones in the human skeletal system, approximately 29 of them are defined as cranial bones; 26 make up the spinal column, roughly 25 can be found in the upper torso, also 64 make up both upper limbs including the hands, and 62 make up both lower limbs (Giovanni Iazzetti, 2002).

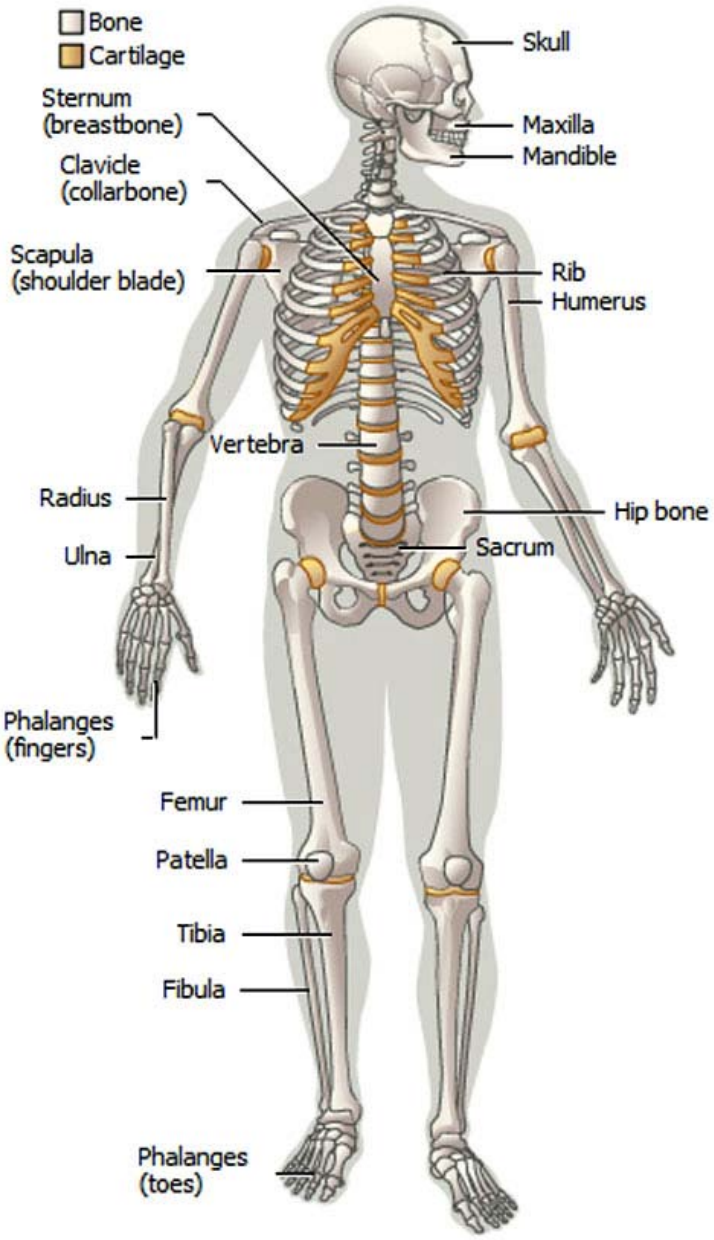

Figure 2.1 The Human Skeletal System (Webnode).

2.2 Functions and Composition of Bone

The four primary functions of bone are as follows: first, bones provide structural support for all organs and tissues in the body and act as a surface for muscle attachment to facilitate movement of the body. Second, the skeleton system provides protection for all internal organs. Third, bones act as a storage facility by maintaining and storing over 99 % of the body's total calcium supply. Finally, marrow within bones is the site of production of white and red blood cells and plays an important role in the development of the body's immune system (Iwasaki, Torres, Ohashi, Robinson, & Barber, 1997).

Bones make up about one sixth of the total body mass and have a density of approximately 1.9 g/cm^3. The principal constituent of bone is calcium phosphates in the form of the ceramic phase hydroxyapatite (HA) ($Ca_{10}(PO_4)_6(OH)_2$) (Mow, 2005). Another major constituent is the mineral phase of bone, which includes calcium (Ca), phosphorous (P), sodium (Na), potassium (K), magnesium (Mg), fluorine (F), chlorine (Cl), carbonate (CO_3^{-2}) and some other trace elements are strontium (Sr), lead (Pb), barium (Ba), iron (Fe), zinc (Zn), copper (Cu) (Agna, Knowles, & Alverson, 1958).

2.3 Mechanical Properties of Bone

Bone tissue is a calcium phosphate ceramic based material, with specific mechanical properties such as toughness, compressive strength, low density, lightness, corrosion, and fatigue resistant. However, bone material primarily is brittle and viscoelastic in nature whose mechanical properties are determined by porosity, degree of mineralization, and other structural factors. The mechanical properties of the human skeletal system have been studied and summarized by many authors (Ellis Iii, 1993; Matthews, Khambay, Ayoub, Koppel, & Wood, 2003; Shadanbaz & Dias, 2012; Wood, Zollman, Reuben, & Brandt, 1975).

Bone has a varied arrangement of material structures at many length scales that work in concert to perform diverse mechanical, biological and chemical functions such as structural support, protection and storage of blood cells, and mineral ion stability. In order to understand the mechanical properties of bone material, it is important to understand the mechanical properties of its component phases, and the structural relationship between them at the various levels of hierarchical structural organization (Bauer, Schmuki, von der Mark, & Park, 2013; Böstman & Pihlajamäki, 2000; Y. B. Wang et al., 2011). These levels and structures are:

1. The macrostructure (from 10 to 500 mm): This consists of cancellous and cortical bone.
2. The microstructure: containing the Haversian systems, osteons, and single trabecular.
3. The sub-microstructure (1–10 mm): enclosing the lamellae.
4. The nanostructure (from a few hundred nanometers to 1 mm): This holds the fibrillar collagen and embedded mineral.
5. And finally the subnanostructure (below a few hundred nanometers): which is comprised of a molecular structure of constituent elements, such as mineral, collagen, and non-collagenous organic proteins (Gao, 2006).

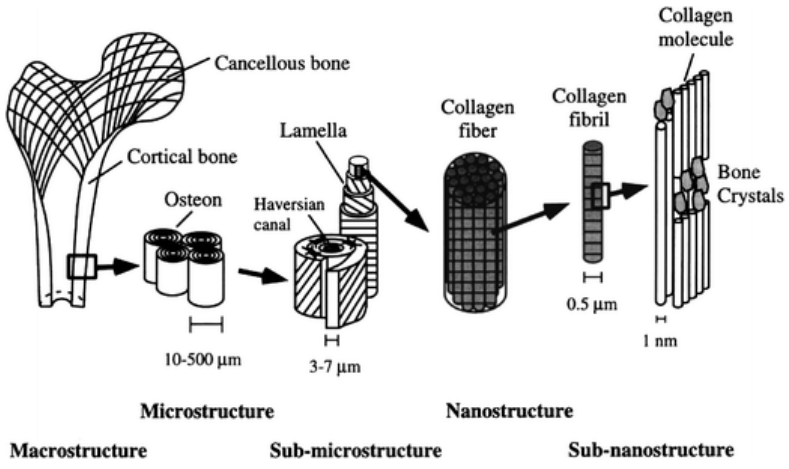

Figure 2.2 The hierarchical levels of bone structure (Rogel, Qiu, & Ameer, 2008).

This hierarchically organized structure has an irregular, yet optimized, arrangement and orientation of the components, making the material of bone heterogeneous and anisotropic. Based on the properties of bone shown in Table 2.1 (Larry L. Hench, October 1993) *(D. Shi, 2004), various materials have been used in bone engineering; in the following section some of these materials and methods of their application will be discussed.

Table 2.1

Mechanical properties of bone

Property	Cortical Bone	Cancellous Bone	Articular Cartilage
Compressive Strength (MPa)	*137.8 100-230	*41.4 2-12	-
Flexural, Tensile Strength (MPa)	50-150 *68.6	10-20 *3.5	10-40
Strain to Failure	1-3	5-7	15-50 %
Young's Modulus (Tensile) (GPa)	14-20	0.5-0.05 *3	0.001-0.01
Fracture Toughness (K_{1c})(MPa $m^{1/2}$)	2-12	-	-

2.4 Biomaterials in Orthopedics

A biomaterial is a material that interacts with human tissue and body fluids to treat, improve, or replace functional elements of the human body. Biomaterial devices used in orthopedics are commonly called implants; these are manufactured for numerous orthopedic applications, they are meant to be implanted in the human body as components of devices that are designed to perform certain biological functions by substituting, repairing or supporting

different tissues such as teeth, bone, cartilage or ligaments and tendons, and even by guiding bone repair when necessary (Figure 2.3). Often metals and other materials have been used for this purpose. Metals in biomedical device are exploited due to their inertness and structural functions. They are generally preferred over polymers or ceramics especially in applications where the implants are subjected to static, dynamic or cyclic loads requiring a combination of strength and ductility.

Figure 2.3 (a) Hip implant, (b) tooth implant, (c) & (d) knuckle implants.

The late l9th century steered in the concept of sterile surgery, and with research, development, and the optimization of implant materials, came the possibility of implanting foreign materials into the body with low risk of rejection due to infection or other adverse reactions. However, at this time there existed no suitable material to withstand the challenges posed by the biologic environment, particularly in regard to strength and corrosion resistance.

Biocompatibility is the primary characteristic that a medical device should have in any orthopedic application; that is, it must not adversely affect the local and general host. The human body, however, consists of a highly corrosive environment; consequently, the first generation of biomaterials was required to be as inert as possible to reduce corrosion and the release of ions and particles during the implant lifetime (Larry L. Hench & Polak, 2002).

Mechanical properties play a leading role in the selection of candidate materials for implant manufacture. Generally the mechanical properties of a material are described in terms of

the deformation or strain produced by an applied stress. A fracture-fixation device typically remains in service for a period of months or years and must endure repeated loading under corrosive conditions. The mechanical properties of fatigue, creep, and stress relaxation reflect time-dependent materials' behavior and are important mechanical parameters in the selection process. Figure 2.4 illustrates the uses of biomaterials in the human body.

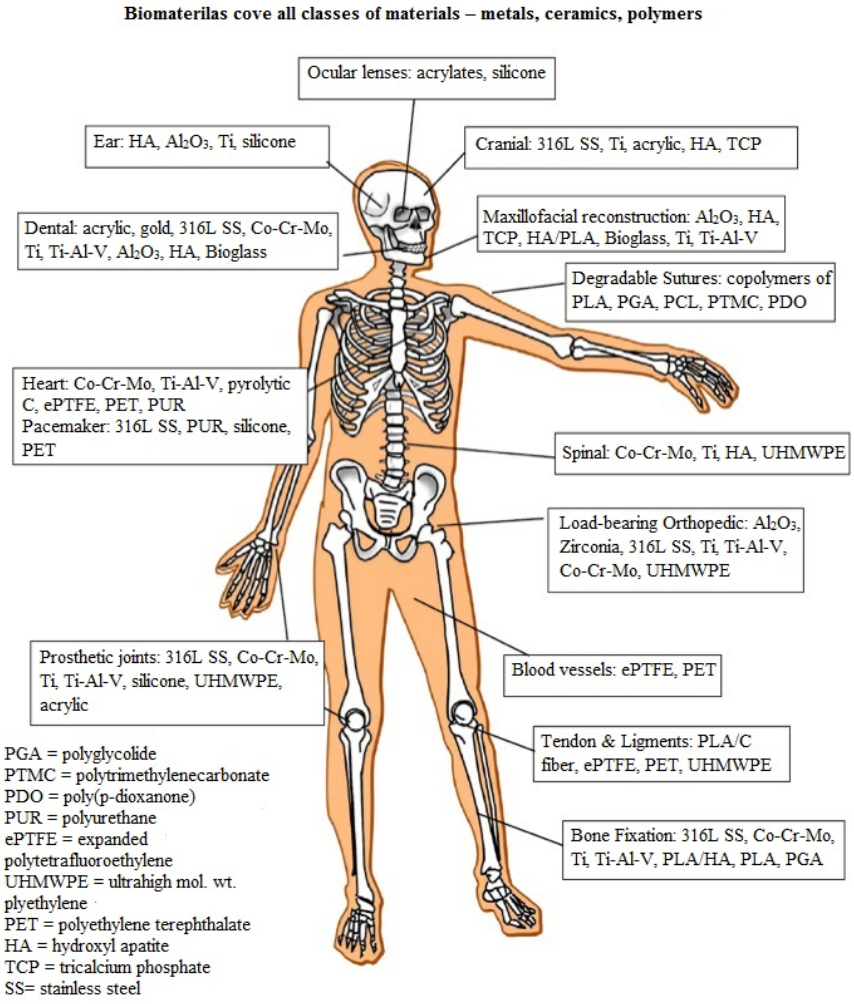

Figure 2.4 Applications of biomaterials [After (OpenCourseWare)].

2.5 Bone Implants and Fixation Devices

Metal alloys such as Ti alloys, stainless steel and CoCr alloys are currently the most popular materials for manufacture of implants and fracture-fixation devices. Two major

disadvantages of these materials are their extreme stiffness, which causes stress shielding of the underlying bone, and the necessity of removing metallic implants after fracture healing is complete, in certain cases. To overcome the shortcomings of these metal alloys, bioresorbable materials for use in fracture fixation have been extensively studied and researched. Unfortunately, the currently available bioresorbable materials lack strength and stiffness and are associated with inflammatory reactions in a significant number of cases (Navarro, Michiardi, Castaiio, & Planell, 2008).

Fractures have been treated with many different methods throughout history, depending on the fracture; one might be treated in a cast or splint, whereas another would require open reduction and internal fixation. Immobilization by casting, bracing, or splinting a joint above and below the fracture was used for most long bone fractures (Farlex, 2013). The ultimate aim of applying a fracture fixation device is to restore the structural integrity of the damaged bone; this is dependent upon a number of materials properties, device design, and physiologic requirements. It is important to take into consideration the site and type of fracture, the possible operative approaches, and the rapidity of bone healing. Specifically, the materials selection process must incorporate the chemical and mechanical demands of the biologic environment to achieve the desired outcome.

Wires, screws, pins, plates, rods, and nails are some structures currently in use extensively to restore the function of traumatized or degenerated bone tissues. Mechanical failure of these internal fixation devices may occur during orthopedic surgery, which may be caused by poor material quality, inadequate design, or wrong material choice. The biomaterials for bone fixation devices may include stainless steel, Ti alloys, Co-Cr alloys, iron, magnesium, polymers, and ceramics. Each of these materials has a set of typical mechanical properties, including

Young's modulus, hardness, tensile strength, compressive strength, shear strength and ductility. The design of these bone fixation devices must be adapted considering these properties and possible forces applied during implantation. Commonly there are two types of fixation devices internal and external devices.

2.5.1 External fixation devices. External fixation entails the use of pins and/or wires secured to external scaffolding to provide support to a limb (Figure 2.5). In this way, this device is a stabilizing frame that holds the bones in the proper position while they heal. Some of the advantages of external fixation are that it is quickly and easily applied. When compared with internal plates and screws, external fixators cause less disruption of the soft tissues and blood supply (Claes, Heitemeyer, Krischak, Braun, & Hierholzer, 1999). The risk of infection at the site of the fracture is minimal, but there is a risk of infection where the pins are inserted from the skin into the bone. They are mainly used where the skin and other soft tissues around the fracture are badly damaged.

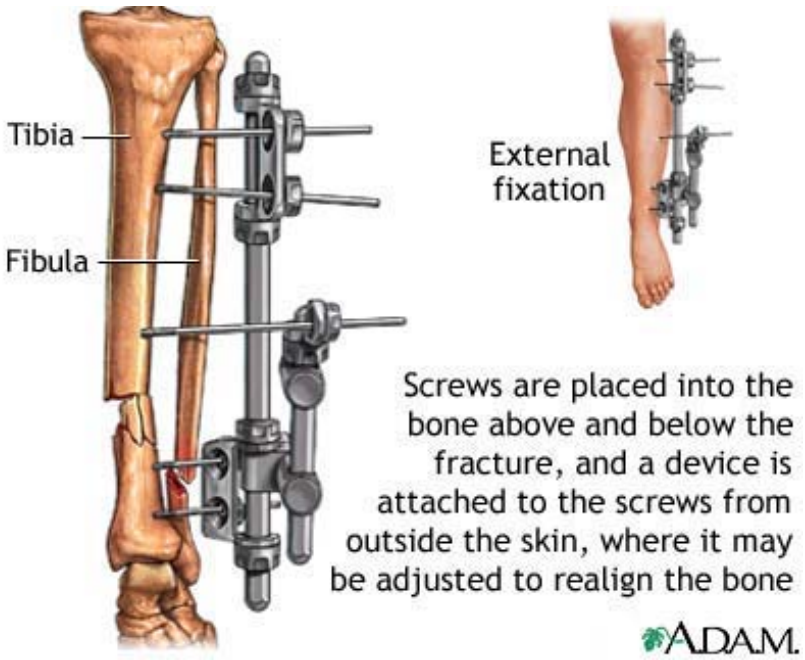

Figure 2.5 External bone fixation device (A.D.A.M., 2006).

2.5.2 Internal fixation devices. Metal implants are used successfully for fracture stabilization because they reproduce the supportive and protective functions of bone without impairing bone healing, remodeling, or growth. In an internal fixation device, the implant is able to withstand tension, unlike the fractured bone, which is best suited to resist compression; the most efficient biomechanical internal fixation takes advantage of this difference by loading the bone in compression and the metal in tension (Bone & Expressed, 1976). It involves the surgical implementation of implants for the purpose of repairing a bone. During this operation, the bone fragments are first repositioned (reduced) in their normal alignment, and then held together with special screws or by attaching metal plates to the outer surface of the bone (Figure 2.6). In the presence of fragments, they may also be held together by inserting rods down through the marrow space in the center of the bone to guide the healing process of a bone, as well as the setting of the bone itself, this procedure is known as open reduction internal fixation.

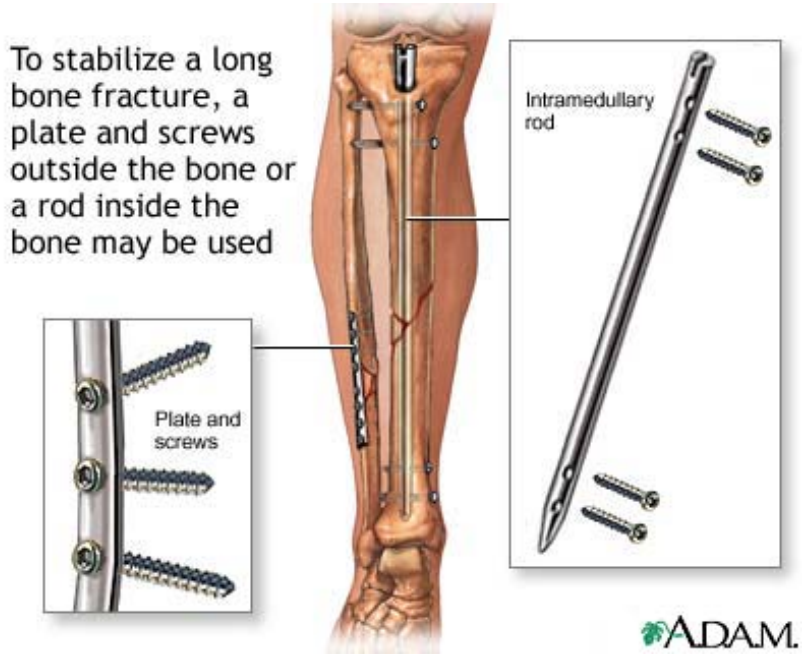

Figure 2.6 Internal bone fixation device (A.D.A.M., 2006).

There is currently no perfect material for use in internal fixation; therefore, a variety of

issues must be examined when specific metals are considered as surgical implant. The material must be systemically nontoxic, non-immunogenic, and non-carcinogenic; it should have good mechanical strength, such as tensile, compressive, and torsional strength, stiffness, fatigue resistance, and easy to shape and form. It should be visible in X-ray, resistant to degradation and erosion or bio-corrosion, easily integrated and have minimal adverse effects on imaging such as magnetic resonance imaging (MRI). Numerous materials have been studied for use to fabricate these bone stabilizing devices, including metals, polymers and ceramics. The following section will give an overview of some of the materials currently in use for the fabrication of such devices.

2.6 Metals for Implants

Metals have been used as implants material for more than 100 years, when Lane first introduced metal plate for bone fracture fixation (Lane, 1895) . In the early development, metal implants faced corrosion and insufficient strength problems (Lambotte, 1909; Sherman, 1912). Shortly after the introduction of the stainless steel in 1920s, which has had far-superior corrosion resistance to anything in that time, it immediately attracted the interest of the clinicians. Thereafter, metal implants experienced vast development and clinical use depending on specific implant applications.

The majority of elements in the periodic table are metals, remarkably few warrant even preliminary consideration for uses as implant materials since the majority of metals and alloys are not suitable for biologic implantation due to the relatively corrosive environment combined with the poor tolerance of the body to even minute concentrations of most metallic corrosion products, this eliminates from discussion most metallic materials. However, with advances in biotechnology, many metals and alloy systems have been developed with a high degree of

corrosion resistance.

Metallic biomaterials do not possess bio-functionalities like blood compatibility, bone conductivity and bioactivity (Niinomi, 2002). Hence, surface modifications are often times required. Improving their bone conductivity has been done by coating with bioactive ceramics like hydroxyapatite (Habibovic, Barrere, van Blitterswijk, de Groot, & Layrolle, 2002), or blood compatibility by coating with biopolymers (Lahann et al., 1999). Nowadays, large number of metallic biomaterials composed of nontoxic and allergy-free elements are being developed. Even more, new types of biodegradable metals have been proposed as temporary implants (H. Hermawan & Mantovani, 2009). Generally, all metal implants are exploited due to their inertness and structural functions; they are generally non-magnetic and high in density, making them compatible with magnetic resonance imaging techniques and visible under X-ray imaging.

Metals are highly superior to polymers and ceramics, due to the fact that artificial implants are subjected to loads, either static or repetitive, and this condition requires an excellent combination of strength and ductility (Hendra Hermawan, 2012). Specific requirements of metals depend on the specific implant applications. Stents and stent grafts are implanted to open blood vessels; therefore, it requires plasticity for expansion and rigidity to maintain dilatation. For orthopedic implants, metals are required to have excellent toughness, elasticity, rigidity, strength and resistance to fracture, shown in Figure 2.7 (F. Witte, Crostack, Nellesen, & Beckmann, 2011). For total joint replacement, metals need to be wear resistant to avoid debris formation resulting from friction. Dental restoration requires strong and rigid metals and even the shape memory effect for better results. Magnesium has mechanical properties closest to those of bone when compared to the properties of other metallic materials currently in use for orthopedic implants.

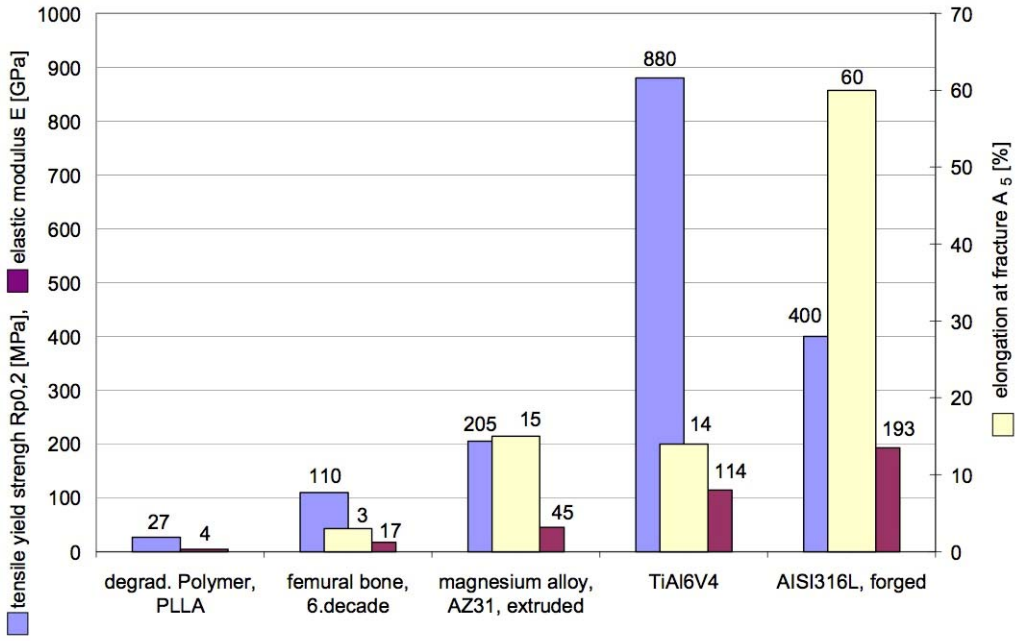

Figure 2.7 Mechanical properties of bone and implant materials.

Of the possible metallic candidates, tantalum and the noble metals do not have suitable mechanical properties for the construction of most orthopedic tools and implants, while zirconium is in general too expensive. Some of the most popular metals currently in use as implants include:

- **Stainless Steel**

The most used types of stainless steels for implant fabrication are Types 316 and 316L. Forged stainless steel has greater yield strength than cast stainless steels, but has lower fatigue strength than other implant alloys. However, stainless steel is more ductile and more easily machined, and recent advancements have significantly enhanced its properties (Hayes & Richards, 2010). Stainless steel that has a low content of impurities and a passivated surface was found to be suitable for implantation in the human body. Despite these qualities, stainless steel is inferior to other super alloys, as it has less desirable erosion, biocompatibility, and fatigue life properties; for this reason it is no longer used routinely (Weckbach, Losacco, Hahnhaussen,

Gebhard, & Stahel, 2012).

- **Cobalt Chrome Alloys**

Cobalt-based alloys are highly resistant to corrosion and especially to attack by chloride byproducts, making them quite resistant to fatigue and corrosion induced cracking. However, as is true of other alloys, cobalt based alloys may fail because of fatigue fracture. As in all highly alloyed metals in the body environment, galvanic corrosion can occur, but to a lesser extent than in the iron-based alloys (M. Ogawa, Tohma, Ohgushi, Takakura, & Tanaka, 2012).

There are basically two types of cobalt chromium alloys. CoCrMo alloy, which is usually castable and the other is CoNiCrMo alloy, which is usually wrought by (hot) forging. The wrought CoNiCrMo alloy is usually used for making the stems of prosthesis for heavily loaded joints such as the knee and hip. The castable CoCrMo alloy has been used for many decades in dentistry and recently has found a market in the making of artificial joints (Damron, 2008).

- **Titanium and Titanium-Based Alloys**

The first recorded use of titanium for implant fabrication dates back to the late 1930's. Titanium's lightness and good mechanical and chemical properties makes them outstanding features for implant applications (Disegi & Wyss, 1989). One of the most commonly used titanium alloy in the manufacture of implants is (Ti6Al4V), its main alloying elements are aluminum and vanadium. Titanium alloys outperform any other implant material; they outperform stainless steel when compared by specific strength. One of the shortcomings of titanium is its poor shear strength causing stress shielding, thus, making it less desirable for use on bone screws, plates and similar applications.

Titanium-based alloys that have a high coefficient of friction that can cause problems, they tend to seize when in contact with other surfaces. Wear particles are formed if two parts of

an implant rub against one another, therefore, implants of titanium upon titanium generally are not used as joint surfaces (Watzinger et al., 2000). The corrosion resistance of titanium is attributed to the formation of a surface oxide film on exposure to air. Under in viv' conditions, the oxide is the only stable reaction product.

Table 2.2

Implants division and type of metals used

Division	Example of implants	Type of metal
Cardiovascular	Stent, Artificial valve	316L SS; CoCrMo; Ti Ti6Al4V
Orthopedic	Bone fixation (plate, screw, pin), Artificial joints	316L SS; Ti; Ti6Al4V; CoCrMo; Ti6Al4V; Ti6Al7Nb
Dentistry	Orthodontic wire Filling	316L SS; CoCrMo; TiNi; TiMo AgSn(Cu) amalgam, Au
Craniofacial	Plate and screw	316L SS; CoCrMo; Ti; Ti6Al4V
Otorhinolaryngology	Artificial eardrum	316L SS

2.7 Magnesium as a Metal Implant

The major advantages of magnesium alloys as temporary biomaterials are their good mechanical properties, biocompatibilities, but being one of the most electrochemically active metals they are prone to corrosion. Various magnesium alloys have been investigated as biodegradable materials and some of them have been shown good biocompatibility. For example, AZ31, AZ91, WE43, LAE442, Mg-Ca and Mg-Zn have been investigated for bone implant application (X. Gu, Zheng, Cheng, Zhong, & Xi, 2009; Y. Z. Wan et al., 2008; Xu, Zhang, Yin, Zeng, & Yang, 2008; Zeng, Dietzel, Witte, Hort, & Blawert, 2008).

Magnesium is essential to human metabolism and is the fourth most abundant cation in

the human body. The human body has an estimated 25 g of magnesium stored in bone tissue (Hartwig, 2001; Okuma, 2001; N. E. L. Saris, E. Mervaala, H. Karppanen, J. A. Khawaja, & A. Lewenstam, 2000; Vormann, 2003; Wolf & Cittadini, 2003). Magnesium is a cofactor for many enzymes and stabilized the structures of DNA and RNA (N.-E. L. Saris, E. Mervaala, H. Karppanen, J. A. Khawaja, & A. Lewenstam, 2000; Staiger et al., 2006). Magnesium and magnesium alloys have density ranging from 1.74 to 2.0 g/cm^3, which is much less than that of the biomedical Ti alloy (4.4–4.5 g/cm^3) and close to that of the bone (1.8– 2.1 g/cm^3) (Staiger et al., 2006). The fracture toughness of magnesium is greater than ceramic biomaterials, while the elastic modulus (41–45 GPa) is close to that of the bone that avoids the stress shielding effect (J. Jacobs et al., 2003). Magnesium has standard electrode potential – 2.37 V, and bare magnesium metal exhibits even poorer corrosion resistance in Cl^- containing physiologic environment. Therefore, magnesium alloys could be developed as a new biodegradable metal, taking advantage of their fast corrosion rate in the physiologic environment.

Magnesium-based materials were first introduced as orthopedic biomaterials in the first half of the century. Lambotte first reported on the use of magnesium as an orthopedic implant (Lambotte, 1909), a plate of magnesium with gold-plated steel nails were used to secure a fracture involving the bones of the lower leg (Lambotte, 1932). The implant was unsuccessful as the magnesium metal corroded only 8 days after surgery and produced a large amount of gas beneath the skin. In an attempt to slow the corrosion process and increase the mechanical integrity of the implants, in vivo works have investigated various magnesium alloys (McBride, 1938; Troitskii & Tsitrin, 1944; F. Witte et al., 2005).

Troitskii and Tsitrin, reported on 34 cases where magnesium alloyed with small levels of cadmium, was constructed into plates and screws and used to secure various fractures. 9 of these

trials were unsuccessful; these failures were attributed to infection, or difficulties arising from not allow for treatment of subcutaneous gas bubble formation, although no adverse inflammatory reactions to the implant were observed. The material is reported to have stimulated the development of a hardening at the fracture site and there was hydrogen gas evolution during the corrosion process, however, using a subcutaneous needle to drawing off the gas easily treated this problem. The mechanical integrity of most was maintained for 6–8 weeks, with complete resorption occurring in 10–12 months. On the other hand, it was also reported that some implants only survived 3–5 weeks, which was attributed to increased acidity in the site of some fractures (Troitskii & Tsitrin, 1944). Similar results were reported by Znamenski, where magnesium alloy containing 10 wt % aluminum was used to treat gunshot wounds in two young men (Znamenskii, 1945). In both cases, fractures fused in 6 weeks, with the magnesium plate no longer detectable after 6 weeks, and the pins no longer detected after 4 weeks.

McBride reports on the use of screws, pegs, plates and bands prepared from Mg–Al–Mn alloys to secure 20 fractures and bone grafts. No systemic reactions to the use of magnesium alloys or inflammatory reactions adjacent to the implant are observed. A positive effect on the bone tissue and deposits of the osseous callous were observed despite there being no effect on the cancellous bone tissues (McBride, 1938). McBride also reported that while the absorption rate was higher for traumatized bone tissue, a typical magnesium–aluminum–manganese 1 gram screw would completely absorb in 120 days (McBride, 1938).

These early examples imply that magnesium-based materials are non-toxic and may actually stimulate bone tissue healing. However, the rate of corrosion of magnesium, or these simple alloys, occurs at a rate that is too rapid to allow sufficient time for healing as it is desirable to have the implanted fixture present for at least 12 weeks (F. Witte et al., 2005). In the

following sections, the science behind the corrosion of these metal implants will be discusses, as well as some methods currently being studied to inhibit such corrosive behavior.

2.8 Corrosion of Implant Materials

The manner in which that material will affect the body must be considered any time a foreign material is placed inside the human body. Because all metals corrode, preventing corrosion is difficult; thus, choosing better quality materials is one apparent solution to this problem. Efforts should also be made to use materials whose corrosion does not create adverse effects inside the body. These efforts can reduce the complications associated with corrosion such as the increase in pain for the patient and reduction in the functional capacity of the implant.

The selection of a metallic biomaterial to be employed as a load-bearing orthopedic device should be based on a reliable analysis of relevant materials properties. Several reports indicate that fatigue-related mechanisms are responsible for the most part of mechanical failures of implantable medical metallic components (Fleck & Eifler, 2010; Giori, 2010; Niinomi, 2007; Vadiraj & Kamaraj, 2007). Chao and López reported that nearly 90 % of the surface fracture of cementless hip prosthesis manufactured with Ti–6Al–4V alloy was due to fatigue mechanisms (Chao & López, 2007). In addition to oscillating mechanical loads, implants are exposed to the physiological fluid that consists of a saline solution including Na^+, Mg^{2+}, Cl^-, SO_4^{2-} and HCO_3^{2-} (Bloyer et al., 2007).

Metallic implants owe their corrosion resistance to the formation of a passive film, which is a stable, compact and continuous oxide surface film that prevents the underlying bare metal surface from coming into contact with these corrosive ions (Antunes & de Oliveira, 2009). However, in case the passive film is locally dissolved by chloride ions, pits are generated that rapidly propagates, leading to pitting corrosion. Sudarshan et al. related nucleation of fatigue

cracks to the presence of pits on the surface of metallic materials (Sudarshan, Srivatsan, & Harvey, 1990). This is due to the fact that the environment can accelerate the initiation of a surface flaw and propagate it to a critical size, leading to fracture. This process is known as corrosion fatigue, denoting the failure of a material under the simultaneous action of cyclic loads and chemical attack (Suresh, 2004). The reduction in fatigue life of metallic implants under corrosion fatigue has been well documented (Azevedo, 2003; Giordani, Guimarães, Pinto, & Ferreira, 2004; Magnissalis, Zinelis, Karachalios, & Hartofilakidis, 2003).

2.8.1 Corrosion of magnesium-based alloys. Magnesium alloys are currently considered for applications as load-bearing implant devices such as plates, screws and pins for repairing bone fracture (Frank Witte et al., 2008). This arises from the low corrosion resistance properties of magnesium alloys in aqueous environments (Staiger et al., 2006). While for most engineering applications the susceptibility to corrosion is a critical limitation of these materials, for biomedical purposes it is a desirable property. If the material is employed as a fixture device, degradation may be beneficial to the patient, enabling it to be absorbed by the body, eliminating the need for a new surgical procedure to remove the device (Jamesh, Kumar, & Narayanan, 2011).

Biodegradable magnesium-based implants are very attractive since the in vivo corrosion of these materials generates mainly non-toxic, soluble byproducts (Abidin, Martin, & Atrens, 2011; Harandi, Idris, & Jafari, 2011; J. Yang, Cui, Lee, & Wang, 2010). However, the evolution of hydrogen gas during in vivo degradation of magnesium alloys is a major drawback. If the degradation is too fast, hydrogen may accumulate as subcutaneous gas bubbles, causing the implant device to lose its mechanical integrity before the effective healing of the fractured bone (Xu, Yu, Zhang, Pan, & Yang, 2007; E. Zhang, Yin, Xu, Yang, & Yang, 2009). Hence,

controlling the corrosion rate of magnesium-based biomedical alloys is of utmost importance.

Several studies have concentrated on this subject, investigating the effect of different alloying elements and coatings on the corrosion properties of biodegradable magnesium alloys (Y. W. Song, Shan, & Han, 2008; Z. Wen, Wu, Dai, & Yang, 2009; S. Zhang et al., 2010; Y. Zhang, Yang, Cui, Lee, & Lee, 2010). Reports have focused mainly on aluminum and rare earth (RE) containing magnesium alloys due to the positive effect that these elements have on arresting the corrosion of magnesium in physiological environments (Avedesian, Baker, & Committee, 1999). However, Witte et al. (Frank Witte et al., 2008) have recently recommended that magnesium alloyed with Al and RE systems should avoided due to their cytotoxic effects and the possible harmful effects of these elements on osteoblasts (El-Rahman, 2003; Ku, Piolettli, Browne, & Gregson, 2002; W. Yang, Zhang, Liu, & Xue, 2006). As a result, new biodegradable magnesium alloys have recently been developed for biomedical purposes and their in vitro corrosion resistance in physiological fluids evaluated (X. N. Gu et al., 2011; Y. Z. Wan et al., 2008; E. Zhang, Yang, Xu, & Chen, 2010).

Magnesium alloys corrode in aqueous materials by several different oxidation-reduction reactions, which are influenced by the alloying elements. Generally, the corrosion of magnesium in water will yield magnesium hydroxide and hydrogen gas evolution (F. Witte et al., 2009). The following net reaction (1) from half-cell reactions are given below:

$$Mg\,(s) + 2H_2O\,(aq) \rightarrow Mg(OH)_2\,(s) + H_2\,(g) \quad (1)$$

Contributing Half-cell reactions:

$$Mg\,(s) \rightarrow Mg^{2+}\,(aq) + 2\,e^- \; Mg\,(s) \quad \text{(Oxidation Reaction)} \quad (2)$$

$$2\,H_2O\,(aq) + 2\,e^- \rightarrow H_2\,(g) + 2\,OH^-(aq) \quad \text{(Reduction Reaction)} \quad (3)$$

$$Mg^{2+}\,(aq) + 2\,OH^- \rightarrow Mg\,(OH)_2\,(s) \quad \text{(Byproduct Formation)} \quad (4)$$

As seen from these equations, magnesium's reaction with aqueous solutions results in the production of hydrogen gas. In orthopedic applications where development of blood vessels and transport is minimal, this might lead to the formation of potentially harmful subcutaneous hydrogen pockets. Experimentation has shown that the addition of zinc has the ability to significantly decrease the amount of hydrogen gas evolved when measured by electrical corrosion testing (F. Witte et al., 2010).

The types of corrosion that are evidenced on the surface of the material are dependent upon the electrolytic medium in which the corrosion of the material is taking place (G. Song, 2007; F. Witte et al., 2005). The medium in which the material is placed greatly influences the parameters and degree to which the corrosion occurs, since corrosion is a surface effect. It has been noted that the corrosion of magnesium in water forms a hydroxide layer on the surface of the material. If the corrosive medium contains any chlorides with concentrations above 30 mmol/L, the hydroxide will be converted to magnesium chloride ($MgCl_2$) rather than magnesium hydroxide (Saw, 2003). In the case of biological fluids where chloride concentrations are approximately 150 mmol/L, surface pitting corrosion is observed (G. Song, 2007).

Many methods are being developed to inhibit the corrosive properties of magnesium, such as alloying, heat treatment and surface modification. In this research the use of ceramic coating to ihibit these corrosive properties is proposed. In the following sections we will discuss the the properties of bioceramics and the reason behind their selection.

2.9 Bioceramics

Ceramics used for the repair and reconstruction of diseased or damaged parts of the musculo-skeletal system, termed bioceramics, may be bioinert (e.g., alumina and zirconia), resorbable (e.g., tricalcium phosphate), bioactive (e.g., hydroxyapatite, bioactive glasses, and

glass-ceramics), or porous for tissue ingrowth (e.g., Ca-P-coated metals). Applications include coatings of orthopedic and dental implants, maxillofacial surgery, ear, nose, and throat (ENT) diseases and scaffolds for bone growth and as powders in total hip and knee surgery (F. Zhang, Chang, Lu, Lin, & Ning, 2007).

Bioceramic is the name given to this class of ceramics used for repair and reconstruction of these diseased and damaged parts of the musculoskeletal system. These ceramics including calcium phosphate and materials such as calcium aluminates, titanates, zirconates, alumina and silica have been used for surgical implantations. Many of these ceramics are mostly inert or insoluble in human body fluids, they are at their most stable form and cannot be oxidized any further, some are bioactive or surface reactive and bioresorbable or biodegradable, (Wise et al., 2000) examples of these bioinert materials include zirconia, silicon nitrides, and alumina. Some glass ceramics and dense hydroxyapatite are bioactive whereas tetra calcium phosphate and tricalcium phosphate are bioresorbable ceramics (Park, 2000). Calcium phosphate bioceramics may be bioactive or bioresorbable depending on the phase being used. The presence of water and the temperature, both during processing and in service, determine the stable phases of calcium phosphate.

2.9.1 Bioactive ceramics. Examples of bioactive ceramics are low silica glasses, and various calcium phosphates. In general, a material that elicits a specific biological response at the interface of the material is termed a bioactive material. This response results in a formation of a bond between the tissue and that material; thus, they can be used to transfer loads to and from living cells. Normally cells grow directly adjacent to the material and in some cases may actually dissolve the material over time. These calcium phosphates are very similar to bone material (P. Ducheyne & Qiu, 1999). The high porosity of bioactive ceramics is often what

increases their surface activity. Uniform porosity in the order of 0.3 - 0.4 mm is desirable to facilitate the in-growth of bone into pores in alumina (bioinert material) or hydroxyapatite (bioactive material).

One of the main disadvantages of bioactive ceramics is their low strength. For this reason they are most often used in composites. Usually they are used to coat a bioinert metal, and many different combinations and morphologies have been used successfully (Cao & Hench, 1996). Fiber and particulate reinforcement are commonly used with bioactive materials as well.

2.9.2 Bioresorbable ceramics. Often times foreign materials are needed to be placed temporarily inside the body for a certain length of time in order to promote natural healing of the surrounding tissues, for example in the cases of hip replacements, vascular stints, or bone grafts. In those situations the foreign material needs to be removed after it has outlived its usefulness. However, it is imperative to shorten the total recovery time of the patients and decrease the risk of exposure to various other complications. This can be achieved through the use of bioresorbable materials that degrade in the body over time; thus, a second surgery to remove implanted devices can be avoided. Furthermore, bioresorbable materials can be implanted to support new tissue growth until such a time as the tissue is no longer needed and completely replaced by the newly grown tissue (D. D. Lee, Rey, & Aiolova, 2000).

Bioresorbable ceramics typically are calcium-based materials such as calcium sulfate (Plaster of Paris), hydroxyapatite, tricalcium phosphate, and other calcium salts. These materials are designed to degrade in the body over time allowing complete replacement of the implant by new growth of the host tissue. This eliminates the problem of limited service life often

encountered with implants since the biological tissue that replaced the implant will have the ability to grow and repair itself.

Challenges with resorbable ceramics include: the maintenance of the strength of the implant, the interface during the period of degradation, tissue growth to meet short term performance needs, and the matching of the material resorption rate to the rate of new tissue growth. Also, larger implants will leave a large quantity of material that must be absorbed by the body; therefore, the selected material must break down into components that are easily metabolized by the body, thus, the predominant use of calcium phosphates (M. Brown & Farrar, 2008).

2.10 Calcium Phosphates Ceramics

Calcium phosphate-based bioceramics have been in use in medicine and dentistry for more than 20 years (Barrère, Mahmood, de Groot, & van Blitterswijk, 2008; de Groot; Hulbert, Bokros, Hench, Wilson, & Heimke, 1987; Jarcho, 1985; Maurus & Kaeding, 2004). Applications include replacements for teeth, hips, knees, tendons, and ligaments and repair for periodontal disease, oral reconstruction, augmentation and stabilization of the jawbone, spinal fusion, and bone repair after major surgery. Different phases of calcium phosphate ceramics are used depending upon whether a resorbable or bioactive material desire.

Calcium phosphates, such as beta tricalcium phosphate, [β-$Ca_3(PO_4)_2$] and hydroxyapatite, [$Ca_{10}(PO_4)_6(OH)_2$] are promising compounds for bone and tooth implant materials (L. L. Hench, 1998; Jarcho, Salsbury, Thomas, & Doremus, 1979). While calcium hydroxyapatite $Ca_{10}(PO_4)_6(OH)_2$ or (HA), is the primary inorganic component of natural bone (Yamashita et al., 2005), trace elements are also present (Driessens & Verbeeck, 1990). HA is but one of a number of calcium-phosphorous (Ca-P) compounds which are biocompatible.

Others include octocalcium phosphate (W. E. Brown, Mathew, & Tung, 1981) and both phases of tricalcium phosphate $Ca_3(PO_4)_2$ (α-TCP/β-TCP) (J. C. Elliot, 1994). Compounds, particularly HA, may show differing degrees of stoichiometry with the Ca/P ratio ranging from 1.55 to 2.2 (Meyer & Fowler, 1997). Such materials can be artificially created by conventional high-temperature ceramic processing (Roberto, 1995) or by low-temperature aqueous chemistry (P. Brown & Hocker, 1991; P. W. Brown & Fulmer, 2005).

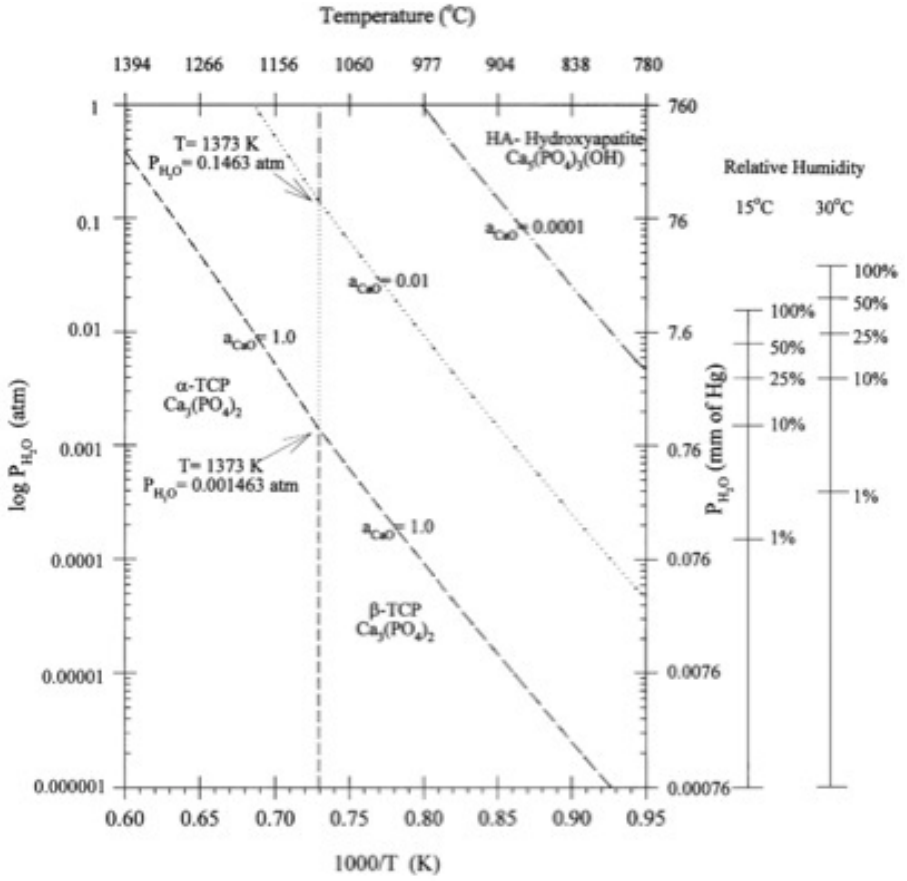

Figure 2.8 Diagram illustrating the stabilities of HA and TCP (Langstaff et al., 1999).

Figure 2.8 shows the calculated phase diagram expected for the Ca-P system as a function of inverse temperature (K^{-1}) and partial pressure of H_2O in the thermal processing atmosphere. The diagram applies to a closed chemical system and utilizes a large database of literature values for the Gibbs free energies of formation. The most stable phase(s) are computed

for a large matrix of coordinates, which lead to the placement of the phase boundaries. HA decomposes into β-TCP at temperatures below 1100 °C under low partial pressure of H_2O. α-TCP is formed at temperatures above about 1100 °C. The predictions are consistent with high-temperature crystallographic data for HA ceramics (Dickens, Schroeder, & Brown, 1974; Welch & Gutt, 1961).

2.10.1 Hydroxyapatite. The term apatite describes a family of compounds having similar structures but not necessarily having identical compositions. Hence, apatite is a description and not a composition. Stoichiometric hydroxyapatite belongs to the general and wide apatitic group, represented by the formula $M_{10}(RO_4)X_2$, where R is most commonly phosphorous, M could be one of several metals although it is usually calcium, and X is commonly hydroxide or a halogen such as fluorine or chlorine.

Hydroxyapatite is one of the most biocompatible materials known that has been in use as a coating for metal implants. Hydroxyapatite, specifically, calcium hydroxyapatite is the most commonly used calcium phosphate in the medical industry, as it possesses excellent biocompatibility and osteo-conductivity (Suchanek & Yoshimura, 1998). The Ca/P molar ratio for HA is 1.67:1 and its theoretical density is 3.156 g/cm^3. HA has hexagonal rhombic prisms crystal structure. It enhances bone healing adjacent to implants and establishes high interfacial bone-implant strength (Wise et al., 2000).

The principal objective of using dense or porous HA implants, is to obtain a structure with sufficient strength and function to osseointegrate with bone during healing. Porous HA has comparatively low mechanical properties, thus, it is mainly used as cancellous bone substitute or as specific fillers for periodontal defects and maxillofacial reconstruction (Hing, Best, & Bonfield, 1999).

2.10.2 Tricalcium phosphate. Tricalcium phosphate with chemical formula $Ca_3(PO_4)_2$, has four polymorphs, α, β, γ, and super-α. The γ polymorph is a high-pressure phase, and the super-α phase is observed at temperatures above 1500 °C (I. Gibson, Akao, Best, & Boneield, 1996). Hence, the most frequently observed polymorphs of TCP bioceramics are the alpha and beta phases. According to Elliot, β-TCP has the rhombohedral space group R3c with unit cell a=1.0439 nm, c=3.7375 nm (hexagonal setting) with 21 formula units per hexagonal unit cell (J. Elliot, 1994). In order to make it more easy to described mathematically, a non-primitive hexagonal unit cell is always used to express a rhombohedral lattice by adopting the axes a, b, and c indicated by the arrows in Figure 2.9, which has the cell transferred to one centered at the points 1/3, 2/3, 2/3 and 2/3, 1/3, 1/3 and thus, the cell is three times as large, but has the shape of the conventional hexagonal cell with the c-direction as the unique axis (Liao, 2006). Lattices, which have rhombohedral centering, are normally given the symbol R.

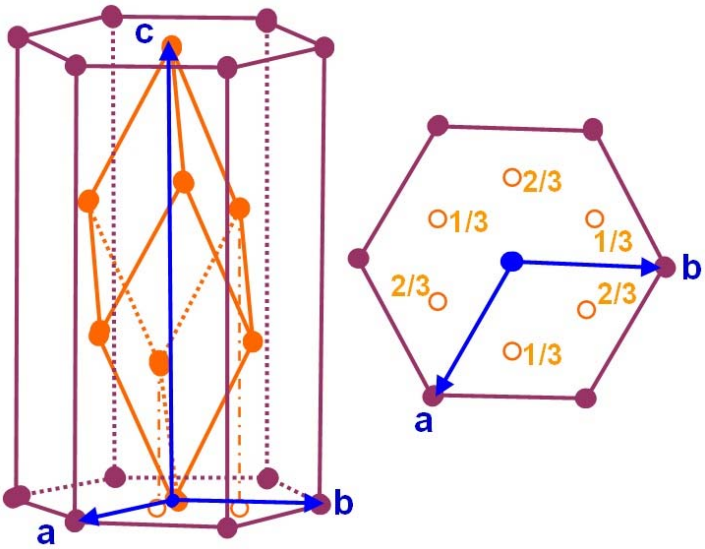

Figure 2.9 Schematic illustrating the relationship between the hexagonal and primitive rhombohedral unit cells.

Figure 2.10 illustrates the structure viewed along the [0001] plane (Jay, Mallinson, Fong,

Metcalfe, & Grimes, 2011). Here, calcium sites are blue, phosphorous ions are purple and oxygen ions are red with grey tetrahedra. The five cation sites are presented below the structure to emphasize their polyhedra, with the central ion representing the cation and surrounding red atoms, oxygen. The five cation sites are described individually (Ca (1)–(5)), with the central ion representing the cation and surrounding red atoms, oxygen.

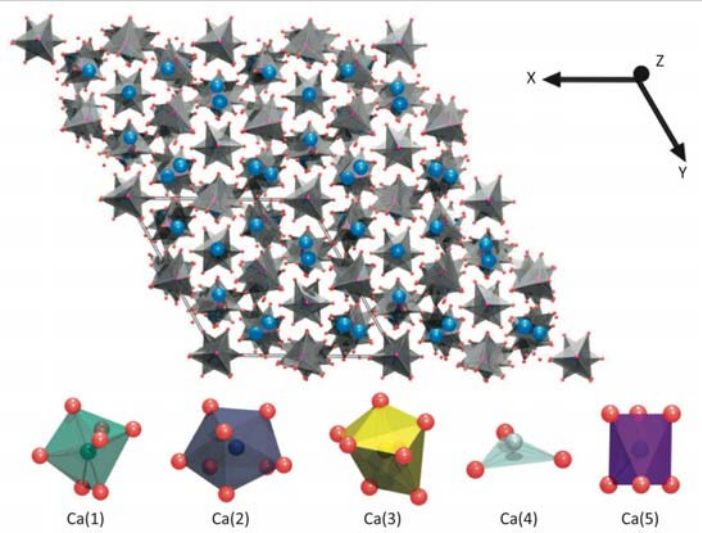

Figure 2.10 The β-$Ca_3(PO_4)_2$ structure viewed along [0001].

β-TCP is stable up to 1125 °C, but above this temperature and up to 1430 °C, α-TCP becomes the stable phase (J. Elliot, 1994). The dissolution rate of TCP was investigated by various researchers (Black & Hastings, 1998). Comparing the relative dissolution ratios of dense HA and TCP, the dissolution rate of TCP was found to be 12.3 times higher than that of HA in buffered lactic acid solution (0.4 M, pH 5.2) and was 22.3 times higher than that of HA in buffered ethylene diamine tetracetic acid (EDTA) solution (0.05 M, pH 8.2) (Jarco, Kay, Gumaer, & Doremus, 1977). Ducheyne et al. (P Ducheyne et al., 1980) compared the dissolution rate of six calcium phosphates in calcium and phosphate free solution at pH 7.3, the dissolution rate increased in the following order:

HA < β-TCP < α-TCP < TTCP

Mechanical properties of TCP are rarely available, but it was reported that TCP has slightly higher fracture toughness than HA (Santos, Jha, & Monteiro, 1996). Fully dense and translucent β-TCP totally free from α modification can attain a maximum strength value of 120 MPa (Tampieri, Fiorani, & Barone, 1995).

The hydroxyapatite is relatively leess resorbable than tricalcium phosphate when used as a coating material on the implant surface (Ando, 1958; L.L. Hench & Wilson, 1993). This behavior allows tricalcium phosphates to be used as resorbable implants and coatings on inert materials to improve the interface between a prosthesis and surrounding tissues (Ando, 1958). In general, biodegradation of calcium phosphate ceramics is caused by physiological dissolution, which depends on the local pH of the environment, solubility product of the material and, physical disintegration into small particles as a result of preferential chemical attack on the grain boundaries. Biological factors such as phagocytosis (the ingestion of living cells) that causes a decrease in local pH value are also a factor in the dissolution of the ceramics.

Numerous studies have been conducted to improve on the properties of bioceramics with the use of metal dopants, in the current research MgO, ZnO, and TiO_2 have been selected as dopants to improve on the sintering process, the mechanical, and corrosion properties. In the upcoming sections, justification of the selection of these materials is discussed.

2.11 Metal Ion Dopants

One of most important goals is the densification of β-TCP ceramics using high temperature without the phase transition of β to α (Famery et al., 1994). The principal difficulties in the use β-TCP ceramics are achievement of high-strength and single-phase composition. The flexural strength of dense β-TCP ceramic is reported at 138 MPa which value is lower than that

for dense human bones (Akao, Aoki, Kato, & Sato, 1982). Bonfield argues that implant materials with similar mechanical properties should be the goal when bone is to be replaced (W Bonfield, 1999).

Research of β-$Ca_3(PO_4)_2$ properties shows that there are some advantages in the use of metal-oxides as MgO in the densification of bioceramic compacts (Itatani et al., 2002). The presence of magnesium in calcified living tissues (about 0.5 % in bone or tooth enamel and more than 1 % in tooth dentine) suggests that this element could improve the biocompatibility of TCP materials (Christel et al., 1988). In this work beta tricalcium phosphate [β-$Ca_3(PO_4)_2$] was doped with MgO, ZnO, and TiO_2 to improve biocompatibility and improve hardness, corrosion resistance, as well as densification during sintering.

2.11.1 Magnesium oxide. Magnesium oxide, also called magnesia, is a colorless, amorphous powder, which occurs in nature as periclase. It is also a source of magnesium. Magnesium oxide has numerous benefits and applications especially in the health care industry. It is necessary for the majority of bodily functions including the heart. Magnesium oxide is vital to maintain the integrity of the skeletal system and enhances bone density. It can slow down or reverse osteoporosis, i.e., abnormal bone loss due to lack of calcium. Magnesium oxide also maintains important bodily balance with other minerals and is associated with protein and carbohydrate metabolism (Lindberg, Zobitz, Poindexter, & Pak, 1990). Magnesium oxide is a basis of good health in many respects, according to the May 2009 edition of Disaster Medicine and Public Health Preparedness. For example, it aids in energy production and assists the electric conduction of the heart, thus minimizing the risk of heart attack. It is also observed to play an important role in hypertension, diabetes and stroke (Dean, 2012).

Magnesium is the fourth most abundant mineral in the body and is essential to good health. Magnesium is needed for bone, protein, and fatty acid formation, making new cells, activating B vitamins, relaxing muscles, clotting blood, and forming adenosine triphosphate (ATP; the energy the body runs on). The secretion and action of insulin also require magnesium. Approximately 60 % of total body magnesium is found in bone, the other half is found predominantly inside cells of body tissues and organs. Only 1 % of magnesium is found in blood, but the body works very hard to keep blood levels of magnesium constant (Rude, 1998). Also, there is growing evidence that magnesium may be an important factor in the qualitative changes of the bone matrix that determine bone fragility. Magnesium depletion adversely affects all stages of skeletal metabolism, causing ceasing of bone growth, decreased osteoblast and osteoclast activities and induce bone fragility (Percival, 1999).

Figure 2.11 illustrates the crystal structure of magnesium oxide, the grey indicates the position of the magnesium atoms and the red indicates oxygen atoms in the lattice of the crystal respectively (Winter, 1993-2012).

Table 2.3

General properties of magnesium oxide

Crystal Structure	Cubic FCC (a=4.216 Å)
Density (g/cm^3)	3.58
Boiling Point (°C)	3600
Melting Point (°C)	2852
Color	White
Solubility	0.0086 g/100mL water
Formula weight (g/mol)	40.30

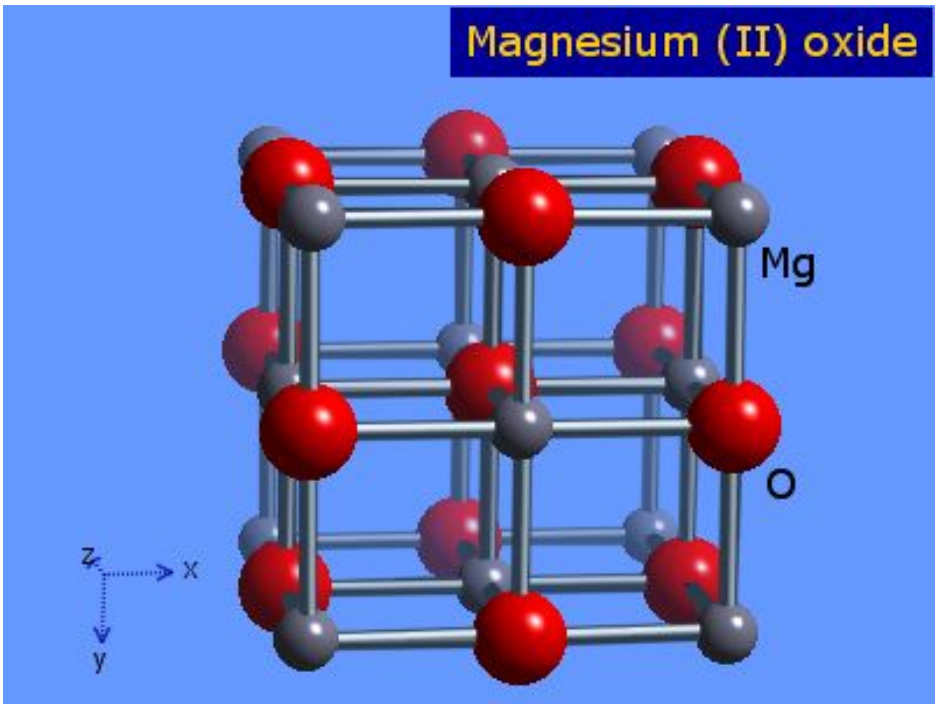

Figure 2.11 Solid crystal structure diagram of magnesium oxide.

It has been found that the optimum amount of MgO doping into TCP was 1 wt %; this percentage has shown good biocompatibility without cytotoxicity (Hyun Seung Yu, 2003). It was found that Mg^{2+} substitution into β-TCP tends to is a known to stabilize the rhombohedral crystal structure of TCP (Ando, 1958). It was also found to decrease the rate of degradation (L.L. Hench & Wilson, 1993). According to Calderin, magnesium is substituted into tri-calcium phosphate in the formula $Mg_xCa_{3-x}(PO_4)_2$ (x = 1, 2, and 3) as shown in Figure 2.12 (Calderin, Xilin, Stott, & Sayer, 2002). As expected, because of the smaller ionic radius, the magnesium atoms reside closer to the axis of the cluster than the Ca atoms. When a Mg atom is substituted into the TCP structure the Mg-O bond becomes stronger whereas, the Ca-O bonds are weakened by the increase in bond length compared to the Mg-O interaction, therefore, this may be the reason for magnesium stabilizing the structure of TCP (Calderin et al., 2002). Figure 2.12 indicates the equilibrium interatomic distances and bond angles.

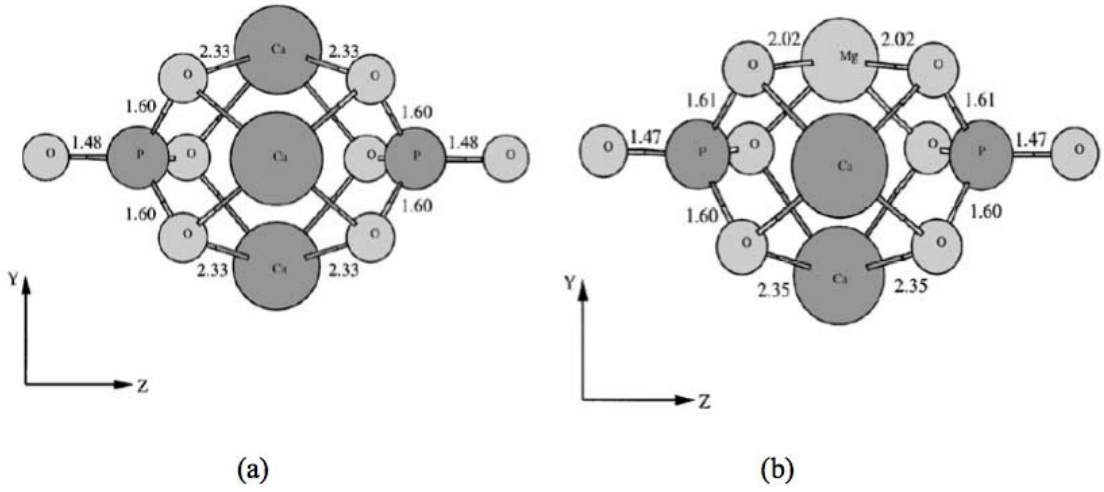

Figure 2.12 Equilibrium interatomic distances (Å) and bond angles (degree) of (a) fully relaxed $Ca_3(PO_4)_2$ (TCP) fragment (b) fully relaxed $MgCa_{3-1}(PO_4)_2$ fragment.

2.11.2 Zinc oxide. The health benefits of zinc include proper functioning of immune system, digestion, control of diabetes, improves stress level, energy metabolism, acne and wounds healing. Also, pregnancy, hair care, eczema, weight loss, night blindness, cold, eye care, appetite loss and many other factors are included as health benefits of zinc (Maret & Sandstead, 2006).

There are organs of the human body, which secrete zinc such as salivary gland, prostate gland and pancreas, and the immune cells also secrete zinc. It plays a crucial role in growth and cell division where it is required for protein synthesis and also for DNA and RNA synthesis in body cells. Zinc accelerates the process of healing of wounds. It combines with the hormone insulin but it is not required for the activity of insulin (Maret & Sandstead, 2006).

As a component of many enzymes, zinc is involved in the metabolism of proteins, carbohydrates, lipids and energy. The body contains about 2-3 g of zinc. There are no specific storage sites known for zinc; it is found in traces in all body tissues. The highest concentration

of it occurs in the liver, pancreas, kidneys and brain. It is also present in red blood cells and blood serum. The deficiency of zinc among human being is rare. There are reports that fibroses of the liver, extreme anemia, and heart diseases occur due to low zinc level in the blood (Chen et al., 1985). In certain cases zinc deficiency is associated with growth failure (dwarfism) and it is believed to causes sex glands to produce little or no hormones. The first signs of zinc deficiency are poor immune response and skin problems (Walker & Black, 2004).

Incorporation of Zn into bioglasses, Ca–P and Ca–Si system bioceramics to enhance their mechanical properties and cell–materials interactions has drawn considerable attention (Lusvardi et al., 2009; Miao et al., 2008; Ramaswamy, Wu, Zhou, & Zreiqat, 2008; Tang, Chappell, Dove, Reeder, & Lee, 2009; Wu et al., 2008; Hala Zreiqat et al., 2010). Zinc is an essential trace element with stimulatory effects on bone formation. It was found that zinc doped into beta-tricalcium phosphate to develop zinc-releasing biomaterials could promote bone formation (Rabadjieva et al., 2011; Wu et al., 2008; Xue et al., 2008). Also, when the zinc content was higher than 1.20 wt % in TCP, release of zinc from the zinc oxide caused cytotoxicity (Bandyopadhyay et al., 2007). Therefore, the zinc content of the composite ceramic must be <1.20 wt % (Kawamura et al., 2000). The density of zinc is 5.61 (g/cm^3) and its melting point is approximately 1975 °C.

TCP based materials doped with some trace elements such as zinc promotes excellent bioactivity, which does not exist in the parent materials (Kawamura et al., 1993). As an essential trace metal, Zn inhibits the differentiation of osteoclasts and/or promotes the activity of osteoblasts, affecting the formation of hard tissues, but a high Zn concentration can have serious toxic side effects on cells (Bettger & Odell, 1993). Kawamura et al. also found that Zn-containing calcium phosphate ceramics stimulated bone formation around the ceramics

implanted in rabbit femora, and attributed the effect to the Zn ions released from the ceramics. Therefore, it is important to use Zn-TCP for bone regeneration applications (Kawamura et al., 2000).

Table 2.3

General properties of zinc oxide

Crystal Structure	Hexagonal wurtzite (a=3.2495 Å)
Density (g/cm^3)	5.61
Boiling Point (°C)	1800
Melting Point (°C)	1300
Color	White
Solubility	0.16 g/100mL water
Formula weight (g/mol)	81.41

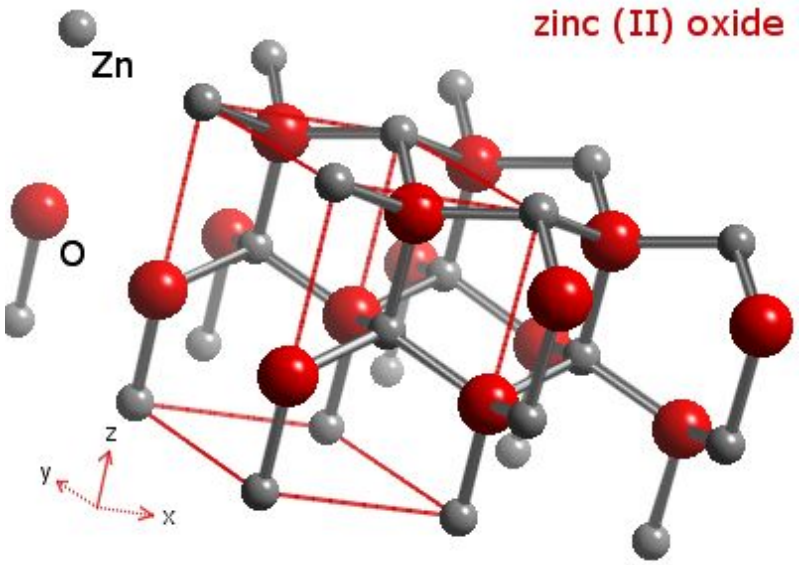

Figure 2.13 Solid crystal structure diagram of zinc oxide (Winter, 1993-2012).

Zinc is added into TCP by substitution method and can be seen in Figure 2.14 (Calderin et al., 2002). Zinc replaces the Ca atom causing some distortion in the crystal structure and is believe to be the reason for improved bioactivity in TCP (Yin et al., 2002).

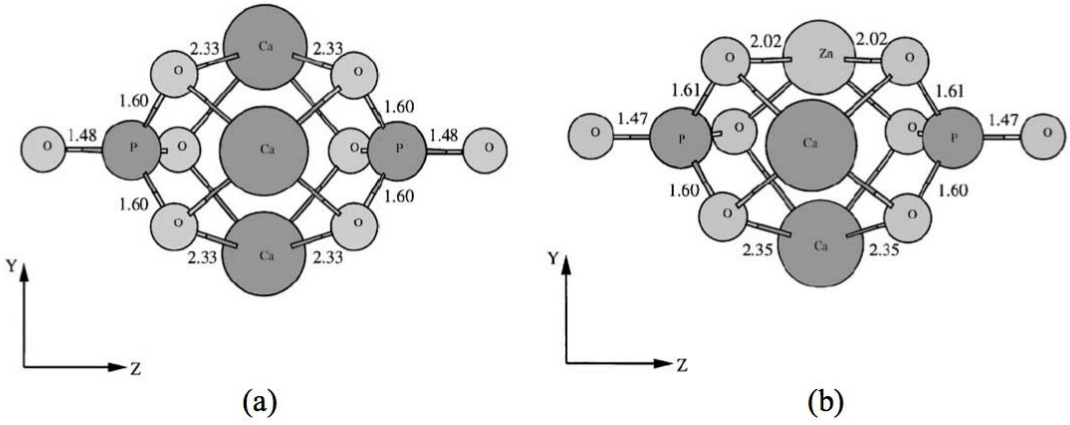

Figure 2.14 Equilibrium interatomic distances (Å) and bond angles (degree) of (a) fully relaxed $Ca_3(PO_4)_2$ (TCP) fragment (b) fully relaxed $ZnCa_{3-1}(PO_4)_2$ fragment.

2.11.3 Titanium dioxide. Titanium (Ti) is widely used as material for permanent implants in orthopedic and dental applications. It is well known that Ti shows a mechanically stable interface towards bone (osseointegration) (Seeley et al., 2007; Wolff, Ramalho, & Acchar, 2006). The good biological properties are due to the beneficial properties of the native oxide (TiO_2) that forms on Ti when exposed to oxygen. The native titanium oxide on Ti is usually amorphous and very thin, 2–7 nm (Jennifer & Michael, 2003; Lausmaa, Kasemo, & Mattsson, 1990; Zhou et al., 2007). In addition to being stable in the physiological environment, titanium oxides increase calcium ion interactions, which are important for protein and subsequent osteoblast adhesion (Ellingsen, 1991; Kasuga, Kondo, & Nogami, 2002).

This oxidized surface of Ti also increases some of the differentiation markers of the osteoblast promoting traits toward bioactivity and bonding to the natural bone (Kasuga et al.,

2002; Ramires, Romito, Cosentino, & Milella, 2001). Titanium dioxide also grows bone-like apatite when submersed in a simulated body fluid and thus it has the potential to be bioactive and bond with bone tissue (Moritz, Jokinen, Peltola, Areva, & Yli-Urpo, 2003; Ng, Annergren, Soutar, Khor, & Jarfors, 2005; Piveteau et al., 1999). Addition of titanium dioxide to TCP has also shown to improve the sintering characteristics of the ceramic composite (Caroff, Oh, Famery, & Boch, 1998).

It is well known that titanium with a thin titanium oxide surface is a biocompatible orthopedic material that provides an excellent physical bonding with the surface of bone. The bone bonding generally occurs without the common connective tissue layer that forms from the body's immune response (foreign body reaction) between the implant metal and the underlying bone surface (Linder, Carlsson, Marsal, Bjursten, & Branemark, 1988; Pilliar, Lee, & Maniatopoulos, 1986; Satomi, Akagawa, Nikai, & Tsuru, 1988). TiO_2 has good biocompatibility with bone and is known to induce: (i) osteoblast function, (ii) apatite nucleation and (iii) protein adsorption.

Influence of an addition of titanium dioxide on thermal properties of sintered HA has attracted significant attention because titania ceramics are potentially useful as porous cell carrier material whose properties, such as good permeability and high biocompatibility, serve to enhance cell vitality (Vu & Heimann, 1997; Weng, Liu, Zhang, & Ji, 1994). The effectiveness of different titanium dioxide materials on cell growth and distribution has been studied (Blum et al., 1996). The effect of TiO_2 incorporation on the shear strength and adhesive strength of HA coatings has been studied by Li et al. It is found that the shear strength slightly increases with the increase of TiO_2 content in the coatings (H. Li, Khor, & Cheang, 2002). However, to-date, the reports focus mainly on bulk HA composite materials. Investigation on alternative Ca-P coatings

is rare. The effect of TiO_2 on the structure and mechanical properties of PLD deposited TCP coatings are still under investigation.

Table 2.4

General properties of titanium dioxide

Crystal Structure	Tetragonal (a=4.5937 Å)
Density (g/cm^3)	4.23
Boiling Point (°C)	2972
Melting Point (°C)	2843
Color	White
Solubility	Insoluble in water
Formula weight (g/mol)	79.87

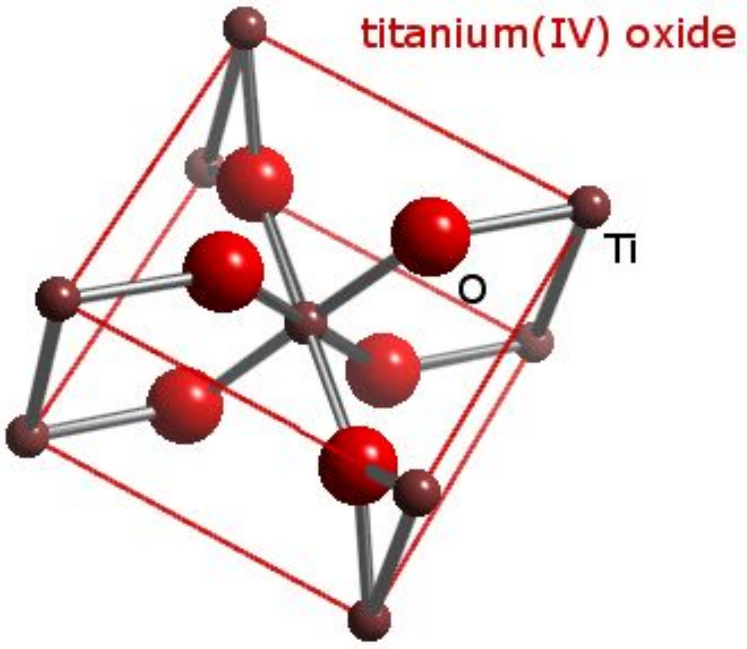

Figure 2.15 Solid crystal structure diagram of rutile (Winter, 1993-2012).

Table 2.5

Atomic radii of atoms in TCP and the dopants used

Element	Atomic radius (pm)
Calcium (Ca)	197
Phosphorous (P)	98
Oxygen (O)	73
Magnesium (Mg)	160
Zinc (Zn)	134
Titanium (Ti)	176

2.12 Surface Modification of Magnesium

Previously, orthopedic implants were designed simply as mechanical devices; the biological aspects of the implant were not the primary focus when designing these devices. The primary goal was to supply internal/external fixation to the injured bone tissue during healing. More recently, biologic coatings have been incorporated into orthopedic implants in order to modify and control the interaction of these devices with the surrounding biological environment.

It is believed that magnesium and its alloys may find applications in biomedical fields as implants, bone fixation devices, and tissue engineering scaffolds. The presence of magnesium ions has been shown to accelerate the growth of new bone tissue (F. Witte et al., 2005). Unfortunately, the poor corrosion resistance properties of magnesium-based materials in vivo impede their clinical use. The degradation time of the magnesium implants cannot match the rate of healing or regeneration of damaged bone. These shortcomings of metal alloys have led to the study of surface modification in an effort to prevent its initial degradation to maintain its desired mechanical strength.

Magnesium has been tested as internal fixation of bone fractures for decades. However, fast degradation and the production of hydrogen during in vivo degradation after implantation

hinders its clinical use (Lambotte, 1932). Recently, several methods have been suggested to slow down the biodegradation rate of magnesium alloys, such as element alloying, ion implantation, and mechanical treatment (Bobby Kannan, Singh Raman, Witte, Blawert, & Dietzel, 2011; McBride, 1938; Znamenskii, 1945). The fracture toughness of magnesium alloys is higher than that of bioceramics and polymers, but lower than that of stainless steels and titanium alloys, whilst the elastic modulus is closer to that of natural bone than other implant materials, making at very attractive material for implant applications (Evans, 1976; Feng & Han, 2010; Maurus & Kaeding, 2004; Navarro et al., 2008; Frank Witte et al., 2008).

For implant applications, a small number of preliminary surface treatment methods for magnesium alloys have been reported, including carbonate treatment (Al-Abdullat et al.), alkali–heat treatment (L. Li, Gao, & Wang, 2004; Atsushi Yamamoto & Tsubakino, 2003), ion plating of Ti (E. Zhang, Xu, & Yang, 2005), fluoride-conversion coating (Chiu, Wong, Cheng, & Man, 2007), and microarc oxidation (P. Shi, Ng, Wong, & Cheng, 2009), each with its merits and limitations. Another important method to reduce the degradation rate of Mg is surface modification. Many researchers have pointed out that surface modification with an appropriate coating is an effective approach, which could improve the corrosion resistance and surface biocompatibility of Mg-based implants (G. L. Song & Atrens, 1999; C. Wen et al., 2009; F. Witte et al., 2010; Wong et al., 2010; Xu et al., 2009).

Calcium–phosphate (Ca–P) coatings have been widely used in biomedical applications due to their favorable biocompatibility and osteo-conductive properties (Geng, Tan, Jin, Yang, & Yang, 2009; Lin et al., 1995; C. Wen et al., 2009). Many studies have been conducted on metal implants with Ca–P coatings to combine the biocompatibility of ceramics with the excellent strength of metals (Y. Li, Lee, Cui, & Choi, 2008; Y. W. Song et al., 2008). The mechanical

strength of these ceramics is known to be too poor to be used for load-bearing applications; thus, HA/TCP are often used as a bioactive coating on metallic substrates such as Ti alloys (Bigi et al., 2008; Huang, Best, Bonfield, & Buckland, 2010; H. X. Wang, Guan, Wang, Ren, & Wang, 2010). Recently, there are such reports about HA coating on biodegradable Mg-based materials (Gray-Munro & Strong, 2009; Onoki, Yamamoto, Onodera, & Nakahira, 2011; H. X. Wang et al., 2010). β-tricalcium phosphate, which has good chemical stability, relatively high mechanical strength, and favorable bioresorption rate is a promising material to be coated on magnesium to improve the possibility of applying magnesium in biomedical fields (Famery et al., 1994). To expand the repertoire in this respect, the present study attempts to prepare a bioresorbable coating with good mechanical properties, biocompatibility and biodegradation on magnesium alloys. The method selected for the application of these coatings was pulsed laser deposition technique. This section gives an overview on the science behind this method and justification of the reason behind its selection.

2.13 Pulsed Laser Deposition Technique

2.13.1 Introduction. Laser was first demonstrated in 1960. Since then it has been developed into a powerful tool in many application. It is especially useful in material processing (S. M. Metev & Veĭko, 1994). Laser possesses many unique properties such as narrow frequency bandwidth, coherence and high power density. Often the light beam is intense enough to vaporize the hardest and most heat resistant materials. Due to its high precision, reliability and spatial resolution, it is widely used in the industry for machining of thin films, modification of materials, material surface heat treatment, welding and micro patterning and multi-component materials can be ablated and deposited onto substrates to form stoichiometric thin films (Chrisey & Hubler, 1994).

To fine-tune the desired film properties, only a few parameters need to be controlled during the PLD process, such as laser energy density and pulse repetition rate. The targets used in PLD are small compared with the large size required for other sputtering techniques. It is quite easy to produce multi-layered films of different materials by sequential ablation of assorted targets. By controlling the number of pulses, a fine control of film thickness down to atomic monolayer can be achieved. The most important feature of PLD is that the stoichiometry of the target can be retained in the deposited films. This is the result of the extremely high heating rate of the target surface (10^{11} K/s) due to pulsed laser irradiation (Christen & Eres, 2008). It leads to the corresponding evaporation of the target irrespective of the evaporating point of the basic elements or compounds of the target.

2.13.2 A general description of pulsed laser deposition technique. The principle of pulsed laser deposition, in contrast to the simplicity of the system set-up, is a very complex physical phenomenon. It involves all the physical processes of laser-material interaction during the impact of the high-power pulsed radiation on a solid target. It also includes the formation of the plasma plume with high energetic species, the subsequent transfer of the ablated material through the plasma plume onto the heated substrate surface and the final film growth process. Thus PLD generally can be divided into the following four stages.

1. Laser radiation interaction with the target
2. Dynamic of the ablation materials
3. Decomposition of the ablation materials onto the substrate
4. Nucleation and growth of a thin film on the substrate surface

In the first stage, the laser beam is focused onto the surface of the target. At sufficiently high energy density and short pulse duration, the laser intensity exceeds the ablation threshold of

the target; the laser beam evaporates and ionizes material, creating a plasma plume above the material surface. Materials are dissociated from the target and ablated out with stoichiometry as in the target. The instantaneous ablation rate is highly dependent on the fluence of the laser irradiating on the target. The ablation mechanisms involve many complex physical phenomena such as collisional, thermal and electronic excitation, exfoliation and hydrodynamics. Initially the atoms, molecules and ions undergo collisions in the high-density region near the target forming the so-called Knudsen layer, leading to a highly directional expansion perpendicular to the target. The expansion dynamics of the laser-produced plasma plume have been described using semi-quantitative models (R.K. Singh, Holland, & Narayan, 1990; R. K. Singh & Narayan, 1990).

During the second stage the emitted materials tend to move towards the substrate according to the laws of gas-dynamic and show the forward peaking phenomenon (Namiki, Kawai, & Ichige, 1986). R.K. Singh reported that the spatial thickness varied as a function of $\cos^n \theta$, where n>>1 (Rajiv K. Singh & Carignan, 1991). The laser spot size and the plasma temperature have significant effects on the deposited film uniformity. The target-to-substrate distance is another parameter that governs the angular spread of the ablated materials. Hanabusa also found that a mask placed close to the substrate could reduce the spreading (Hanabusa, 1993).

The third stage is important to determine the quality of thin film. The ejected high-energy species impinge onto the substrate surface and may induce various type of damage to the substrate. The mechanism of the interaction is illustrated in Figure 2.16. These energetic species sputter some of the surface atoms and a collision region is established between the incident flow and the sputtered atoms. Film grows immediately after this thermalized region (collision region)

is formed. The region serves as a source for condensation of particles. When the condensation rate is higher than the rate of particles supplied by the sputtering, thermal equilibrium condition can be reached quickly and film grows on the substrate surface at the expense of the direct flow of the ablation particles.

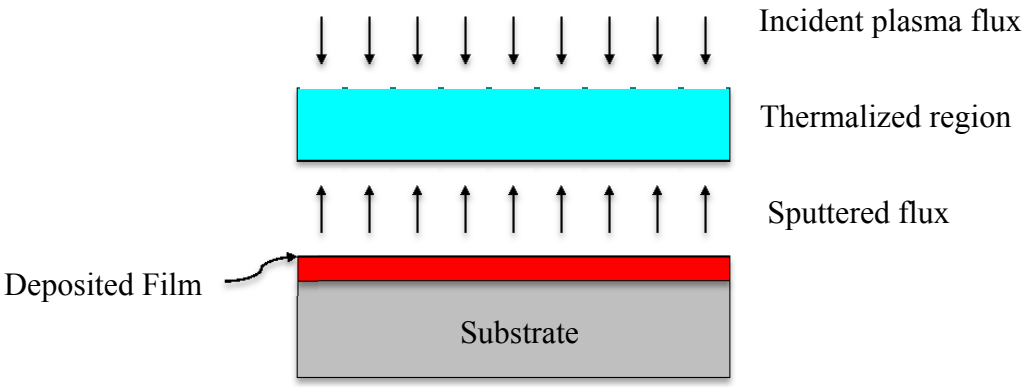

Figure 2.16 Schematic diagram of plasma-substrate interaction.

Nucleation-and-growth of crystalline films depends on many factors such as the density, energy, degree of ionization, and the type of the condensing material, as well as the temperature and the physical-chemical properties of the substrate. The two main thermodynamic parameters for the growth mechanism are the substrate temperature T and the supersaturation Δ m. They can be related by the following equation:

$$\Delta m = \mathrm{kT}\ln(\mathrm{R}/\mathrm{R_e}) \qquad (5)$$

where k is the Boltzmann constant, R is the actual deposition rate, and Re is the equilibrium value at temperature T.

The nucleation process depends on the interfacial energies between the three phases present – substrate, the condensing material and the vapor. The critical size of the nucleus depends on the deposition rate and the substrate temperature. For the large nuclei, a characteristic of small supersaturation, they create isolate patches (islands) of the film on the substrates, which

subsequently grow and coalesce together. As the supersaturation increases, the critical nucleus shrinks until its height reaches an atomic diameter and its shape is that of a two-dimensional layer.

The crystalline film growth depends on the surface mobility of the vapor atoms (adatom). Normally, the adatom will diffuse through several atomic distances before sticking to a stable position within the newly formed film. The surface temperature of the substrate determines the adatom's surface diffusibility. High temperature favors rapid and defect free crystal growth, whereas low temperature or large supersaturation crystal growth may be overwhelmed by energetic particle impingement, resulting in disordered or even amorphous structures.

Metev and Veilo suggested that the N_{99}, the mean thickness at which the growing, thin and discontinuous film reaching continuity is given by the formula:

$$\mathrm{N_{99}} = \mathrm{A(1/R)^{1/3}exp(-1/T)} \qquad (6)$$

where R is the deposition rate (supersaturation related) and T is the temperature of the substrate and A is a constant related to the materials (Goodwin, Leppert, Risbud, Kennedy, & Lee, 1997; S. Metev & Meteva, 1989).

In the PLD process, due to the short laser pulsed duration (~10 ns) and the small temporal spread (<10 μs) of the ablated materials, the deposition rate can be enormous (~10 $\mu m/s$). Consequently a layer-by-layer nucleation is favored and ultra-thin and smooth film can be produced (R. Kelly & Miotello, 1996). In addition the rapid deposition of the energetic ablation species helps to raise the substrate surface temperature. In this respect PLD tends to demand a lower substrate temperature for crystalline film growth.

A PLD system basically consists of three main components: Laser, deposition system, and the optics between the former two. Figure 2.17 shows the diagram of the PLD system that is

used in this work. Usually any type of laser can be used in a PLD system if the power of out-put laser beam is high enough. The lasers that had already been used in the PLD technique included ruby laser, CO_2 gas laser, Nd-YAG laser, Nd-glass laser, and excimer lasers, etc. However, due to its unique characteristics, excimer laser has become the number one choice in the PLD system.

Excimer laser is a gas laser operated in the UV range. It is also a pulsed laser with the repetition rate up to several hundred hertz and a common pulse width of 25 nanoseconds. Depending on the gas used, the operating wavelength of excimer laser can be changed from 157 nm for F2 to 351 nm for XeF. Table 2.6 lists the wavelengths for the commercial excimer laser systems. Compared to other commercial lasers, excimer laser also has output energy as high as 1J/pulse (Basting & Stamm, 2001). The higher output energy and the short operating wavelength make excimer laser the ideal one for PLD systems since most of the materials used for the deposition have strong absorption in range of 200 nm to 400 nm.

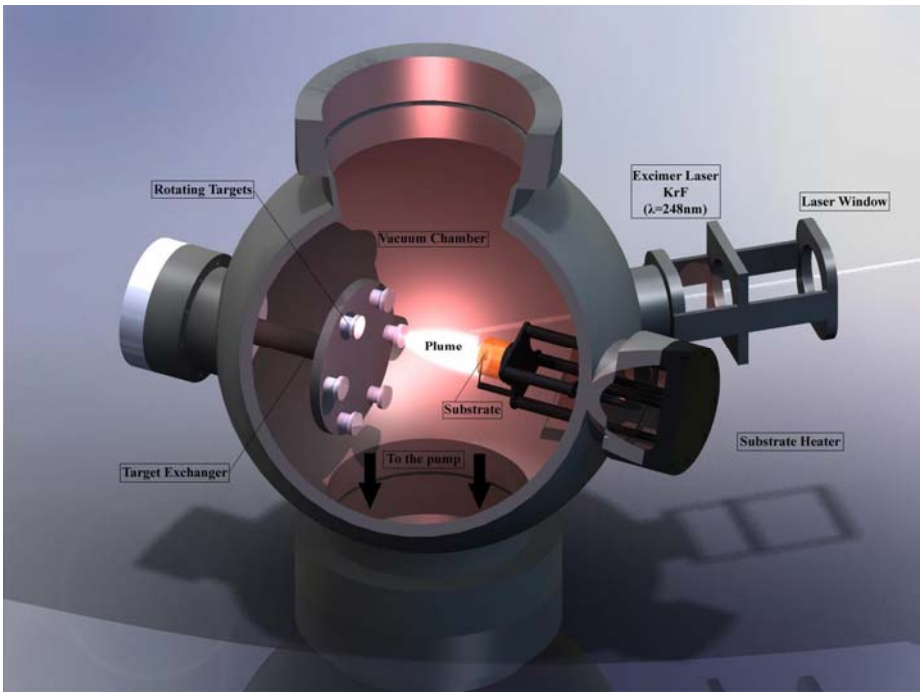

Figure 2.17 Diagram of PLD system used for this work.

Table 2.6

Operating wavelengths of excimer laser for different gases

Excimer	Wavelength (nm)
F2	157
ArF	193
KrCl	222
KrF	248
XeCl	308
XeF	351

In a PLD system, thin films are grown in a high vacuum chamber. The vacuum may vary from 10^{-6} Torr for the general purpose to 10^{-11} Torr for the laser molecular beam epitaxy (MBE) systems. One of the advantages of PLD is that it requires very simple and relatively economical pump and gas-flow systems. The basic elements inside the vacuum chamber include substrate holder, targets holder, vacuum gauges, etc. The multiple-target mounting assembly is usually adopted for the PLD system. In the system used for this work, six targets can be loaded into the vacuum chamber at the same time. The multiple-target assembly gives another advantage of PLD technique, by which in situ multilayer structures can be easily developed.

For all the PLD system, the optical elements are needed to achieve the optimized focused beam for ablating the target material. These optical elements, such as mirror, aperture, beam splitter, and lens are placed between the output port of the laser and the laser window of the vacuum chamber.

2.13.3 Plume-background gas interaction. The interaction of pulsed laser ablation plumes with a background gas has received increased attention recently due to its importance in

laser deposition, nanoparticle formation and growth, cluster production etc. In addition to these applications, these studies are very important for modeling of various processes in space physics, plasma chemistry and hydrodynamics (Chrisey & Hubler, 1994; Geohegan, Puretzky, Duscher, & Pennycook, 1998; Kroto, Heath, O'Brien, Curl, & Smalley, 1985).

The plasma expands freely in vacuum or low background pressures. As the background pressure increases, the plume behavior is characterized by strong mutual penetration of the laser plasma and ambient low-density gas. The expansion dynamics of the plume in this pressure regime is determined by the properties of the plasma as well as the background gas, and collisional affects starts to play a role. At still higher background pressures, the expansion dynamics of the plasma are fully governed by the nature and pressure of the ambient gas used (Geiohegan, 1994). In general, an increase in background pressure results in the following effects: (i) an increase in fluorescence from all species due to enhanced collisions on the expansion front and subsequent inter-plume collisions, (ii) shock front formation, (iii) slowing of the plume compared to propagation in vacuum resulting in spatial confinement of the plasma.

Compared to the expansion into a vacuum, the interaction of the plume with an ambient gas is a far more complex gas dynamic process due to the rise of new physical processes involved such as deceleration, attenuation, thermalization of the ablated species, diffusion, recombination, formation of shock waves and clustering (Bulgakov & Bulgakova, 1995, 1998; Geiohegan, 1994; Geohegan et al., 1998; Geohegan, Puretzky, & Rader, 1999; Harilal, 2001; Harilal, Bindhu, Nampoori, & Vallabhan, 1998).

In TCP, phosphorus is bound as PO_4, so higher Ca/P ratio can be caused by preferential resputtering of phosphorus before PO_4 is formed in the growing film. In a previous work Lee et al. observed an increased amount of phosphorus in PLD films with increasing H_2O pressure,

although the flux of phosphorus from the target should be reduced by scattering of the plume by the background gas (W. J. Lee, Lee, Kim, Kim, & Han, 2005). Therefore, the preferential resputtering of phosphorus from the growing film by the plume is important for determining the amount of deposited phosphorus. A preferential resputtering of phosphorus from a calcium phosphate film was also reported by van Dijk et al. for the sputter deposition of the film from a HA target (van Dijk et al., 1995; van Dijk, Verhoeven, Marée, Habraken, & Jansen, 1997). They also reported that a better stoichiometry of the deposited films with respect to HA was obtained by the introduction of O_2 into the sputter gas. Ahn et al. showed that the growth rates of thin films were found to be larger in an argon atmosphere than in vacuum over the entire range of target-substrate distances. In addition, the growth rate increased greatly when the substrate was placed within the plume for the deposition under an argon gas atmosphere. The enhanced deposition rates were of the order of 10^{-2} nm per pulse (Ahn et al., 2007). In the case of thin films deposited in an ambient argon gas, the compositions of the films were found to be very close to the target's composition when substrate was placed inside the plume. On the other hand, it is found to be very difficult to optimize the deposition parameters controlling the composition for PLD under vacuum.

In the PLD process of this work, argon ambient gas reacts with the growing film to enhance the formation of PO_4 in the film. Consequently, preferential resputtering of phosphorus is suppressed, resulting in better stoichiometry and Ca/P ratios that are lower than those obtained with vacuum depositions.

CHAPTER 3

Experimental Procedure

Chapter 3 was focused on the materials and methodology of the project. Magnesium and beta-tricalcium phosphate were used as the raw materials to fabricate the implant device. In this study, a magnesium alloy [Mg2Zn0.3Ca] was used as the substrate in conjunction with magnesium for comparison. These substrates were then coated with doped TCP targets in order to further increase the substrate's compressive strength, inhibit its corrosive nature, and promote bioactivity. The metal oxides chosen for doping were MgO, ZnO, and TiO_2. The ceramic TCP target to be used was doped with these metal oxides, fabricated, and characterized. These targets were obtained when green compacts were sintered at 1250 °C for 2 hours. Results from the hardness tests, corrosion tests, and in vitro biological tests will be presented in Chapter 4. The sample characterization techniques used were XRD analysis, imaging of the ceramic compacts and films produced by scanning electron microscopy, mechanical testing by nanoindentation and corrosion studies, and in vitro biological test (including image of the apatite growth on the ceramics and films and cell viability testing). This study examined effect of the dopant addition on the mechanical and biological properties of tricalcium phosphate.

3.1 Substrate Preparation

It is well known that magnesium has poor corrosion resistance properties and can be effectively improved by the appropriate selection of alloying elements (Baker & Committee, 1999). A lot of metals are toxic when implanted, thus, the range of alloying elements used in the degradable magnesium alloys is rather limited, zinc (Zn), manganese (Mn), calcium (Ca) and perhaps a very small amount of low toxicity rare earth (RE) can be tolerated in the human body and can also retard the biodegradation. Therefore, Mg-Ca binary alloys attract attention of

researchers because calcium is an important element of human bones. Controlling the calcium content and processing treatment can adjust the mechanical properties and biocompatibility of Mg-Ca binary alloy. However, inadequate mechanical properties as well as lower corrosion resistances of Mg-Ca binary alloys are the biggest drawback of these alloys (Z. Li, Gu, Lou, & Zheng, 2008; Y. Wan et al., 2008). Fortunately, in latest recent years, Mg-Zn system is paid more attention because zinc is one of abundant nutritional elements in human body (Tapiero & Tew, 2003; S. Zhang et al., 2010). Additionally, it is a great potential alloying element to improve the mechanical properties and corrosion resistance of magnesium alloys (Ben-Hamu, Eliezer, Dietzel, & Shin, 2008; Jardim, Solorzano, & Vander Sande, 2004). The addition of other alloying element can further improve the mechanical properties of Mg-Zn alloys (Ortega, Monge, & Pareja, 2008; Tapiero & Tew, 2003).

Studies conducted by Wang at al. (H. X. Wang et al., 2010) indicate that the Mg-Zn-Ca alloys have an excellent corrosion resistance in Kokubo's simulated body fluid (SBF). L. Mao et al. studied the effects of zinc on microstructure and mechanical properties of biomedical Mg-Zn-Ca alloys (Mao, Wang, Wan, He, & Huang, 2009). The results show that the microstructure is refined and the mechanical properties can be improved evidently with zinc content increasing. The mechanical properties of bending and compression can meet the requirements for hard tissue metal implants.

This research is geared towards revolutionizing of biodegradable magnesium alloys; and since small amounts of zinc, calcium and magnesium are all essential for human body, cast Mg2Zn0.3Ca alloy, which was prepared in our laboratory and high purity magnesium 99.97 % (Goodfellow, Germany) were used in this study. These rods were cut into 12.4 mm circular disc with of 5 mm thickness. The substrates were then mechanically polished progressively with

silicon carbide paper from #600 up to grade #1200 ascending grit; isopropyl alcohol was used for lubrication. The substrates were then washed in ultrasonic baths using acetone, and isopropyl alcohol for 15 minutes each. The substrates were then mounted on the substrate heater with double side copper tape for room temperature deposition.

3.2 Target preparation

Oxide based dopants used included magnesium oxide (96 %), titanium dioxide (99 %), and zinc oxide (99.9 %) all purchased from Fisher Scientific. Synthetic β-tricalcium phosphate (BABI-TCP-N100) nano powder was obtained from Berkley Advanced Biomaterials Inc. with an average particle size of 100 nm. These dopants were independently added to tricalcium phosphate in multiple weight percentages, which included 0.25, 0.5, and 1.0 wt. %.

Powders were weighed and mixed in 250 mL translucent polypropylene bottles, and 150g of zirconia milling media balls were added. Batches were made based on 30 g of β-TCP. After dopant addition, ball milling was done for 6 hours at 70 rpm to minimize the formation of agglomerates and increase the homogeneity of the powders. Figure 3.1 shows a flow chart of the process of target fabrication.

After milling, milling media was removed from the powders using a sifter. All powders were appropriately labeled. Powders were measured for each composition and pressed using a uniaxial press at 250 MPa of pressure using polyvinyl acetate (PVC) as a binder. The disk mold press produced 12 mm in diameter by 5 mm thick green compacts. After pressing, all green compacts were placed in a muffle furnace for densification at 1250 $^{\circ}$C for 2 hours. Bulk densities for green and sintered targets were measured for all compositions.

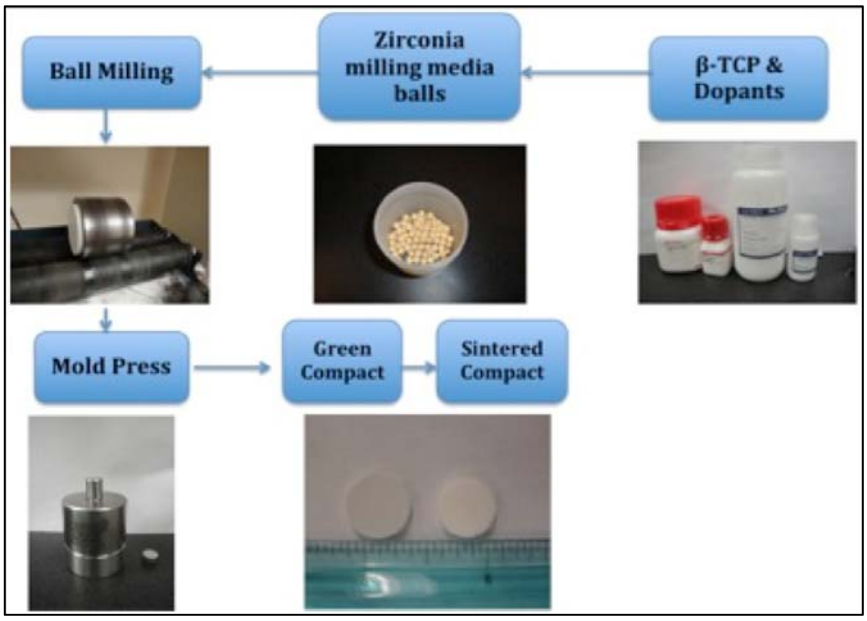

Figure 3.1 Processing of TCP with metal ion dopants flow chart.

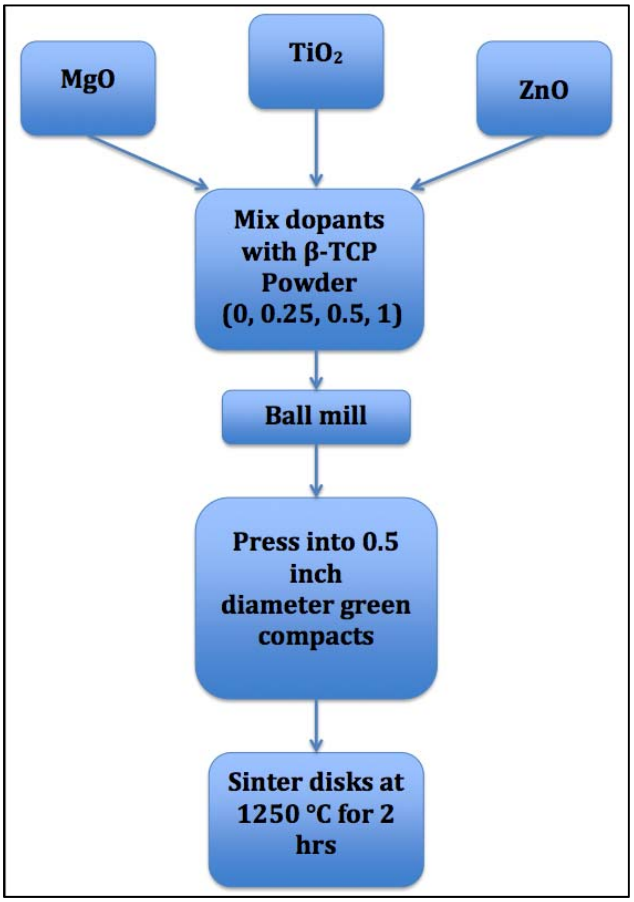

Figure 3.2 Target preparation process.

After preparing the green compacts, they were placed in a furnace for sintering and densification. The following section will elaborate on the sintering process used to densify the green power compacts.

Binder

When ceramics are sintered cracks are prone to occur in the sample, because of shrinkage, which, consequently, causes a severe reduction in strength. So in fabrication of all the compacts, use of binder is a requisite for sintering ceramic. Polymers are usually used, examples are polystyrene (PS), polyvinyl acetate (PVC) (Kruth, Wang, Laoui, & Froyen, 2003; Quadir, 1994), as the binder, since it would be expected to improve the strength of the body, which, in turn, would prevent it from cracking (Koh et al., 2006). The presence of small pores formed by the removal of the polymer on the ceramic during sintering, the polymer could also be used for increasing ceramic‘s porosity (Ruksudjarit, Pengpat, Rujijanagul, & Tunkasiri, 2008). However, if polymer is over-added into the ceramic, the mechanical properties would decrease instead. In Yook’s experiment, where a polystyrene (PS) polymer was used as the binder, he pointed out that the compressive strength of the porous HA scaffolds was significantly affected by the PS content, when increasing PS content from 0 to 20 vol. %, the compressive strength of the sample was significantly increased. However, a higher PS content of 30 vol. % was observed to lead to a lower compressive strength (Ruksudjarit et al., 2008). Safronova’s report indicated that the presence of 0.25 % – 0.50 % PVC (Polyvinyl chloride) strongly influences the mechanical properties of the powder (Safronova, Shekhirev, & Putlyaev, 2007). In the present research PVA was used as the binder when processing the powder compacts.

3.2.1 Sintering process. Sintering of ceramic materials is the method involving consolidation of ceramic powder particles by heating the green compact to a high temperature

below the melting point, when the material of the separate particles diffuse to the neighboring powder particles. The driving force of sintering process is reduction of surface energy of the particles caused by decreasing their vapor-solid interfaces.

During the diffusion process the pores in the green compact diminish or even close up, resulting in densification of the part and improvement of its mechanical properties. The level of the initial porosity of the green compact, sintering temperature and time, determines decrease of the porosity, caused by the sintering process. Sintering of pure oxide ceramics require a relatively long time and high temperature because the diffusion proceeds in solid state.

Sintering is a processing technique used to produce density-controlled materials and components from metal or/and ceramic powders by applying thermal energy. In general, the aim of sintering is to produce sintered parts with control of grain size, sintered density, and size and distribution of other phases including pores.

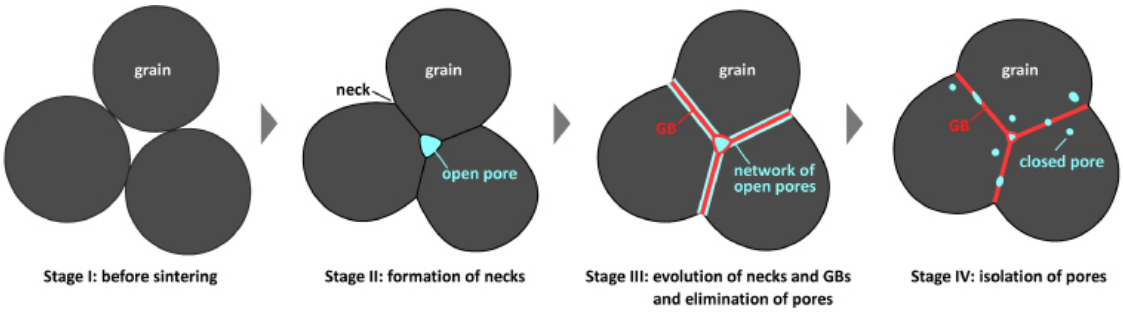

Figure 3.3 Schematic of coalescence process during sintering (Tanaka, Yamamoto, Shimoyama, Ogino, & Kishio, 2012).

During the sintering process the heating rate can affect the final density and phase purity of the material. Higher ramp rates can give a higher final density, but a rate greater than 10 °C/min has been shown to result in decomposition (W. Bonfield, Grynpas, Tully, Bowman, & Abram, 1981). In this step, a heating rate of 3 °C/min was used for sintering the green compacts. The sintering was carried out in a furnace, using a heating rate of 3 °C/min up to sintering

temperature, which was held for 2 hours, followed by cooling to room temperature. The reason for setting 3 °C/min as the heating rate was that if the heating rate was too high, cracks may be created on the ceramic target. There were seven stages in the schedule (Figure 3.4) including:

1) Heating from room temperature to 100 °C with a heating rate 3 °C/min to prevent the compacts from cracking.
2) Holding this temperature (100 °C) for 10 minutes (any moisture in the sample will be burned out at this step).
3) Increasing the temperature from 100 °C to 550 °C at a rate of 3 °C/min.
4) Holding this temperature for 15 minutes.
5) Increasing the temperature from 1250 °C at a rate of 3 °C/min.
6) Holding this temperature for 2 hours.
7) Cooling the furnace down to room temperature.

The sintered ceramic targets were then removed from the furnace after it had cooled down.

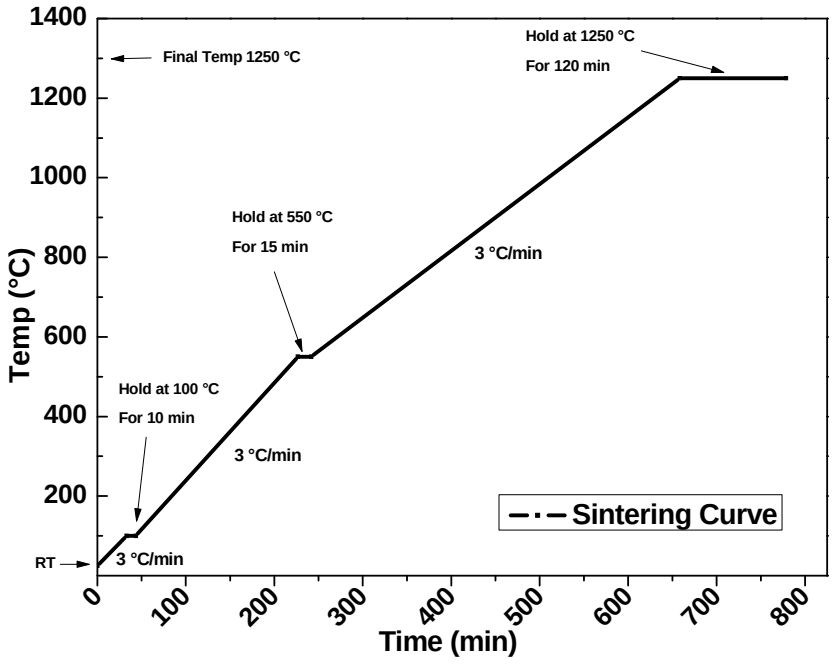

Figure 3.4 β -TCP sintering curve schematic.

The following section describes the method used to measure the shrinkage and densification that resulted from this sintering process.

3.2.2 Density measurements. Bulk densities for green and sintered samples were measured for all compositions. Compositions that showed poor densification when the dopant percentage additions were varied, were not used for the remainder of the research, only the compositions that showed the highest densification were used for dopant combinations and mechanical and biological characterization.

Table 3.1 shows the combination of dopant used for this research based on the highest densifications recorded. Commercial ceramics usually use sintering additives as a measure to increase densification. For this research no additives were used simply because we wanted to identify the specific effects of the dopants being added.

Table 3.1

Weight percent and combination of dopants

Compositions	Weight (%)
TCP	N/A
TiO_2	1
MgO	1
ZnO	0.5
TiO_2+MgO+ZnO	1 + 1 + 0.5

The dense compact targets were used in the pulsed laser deposition to coat the magnesium and its alloy. In the following section the equipment and deposition parameters are stated.

3.3 Deposition Parameters

The experimental set-up consists of a KrF excimer laser (Lambda Physik LPX200) and a stainless steel vacuum chamber in which the target and substrate were placed (Figure 3.5).

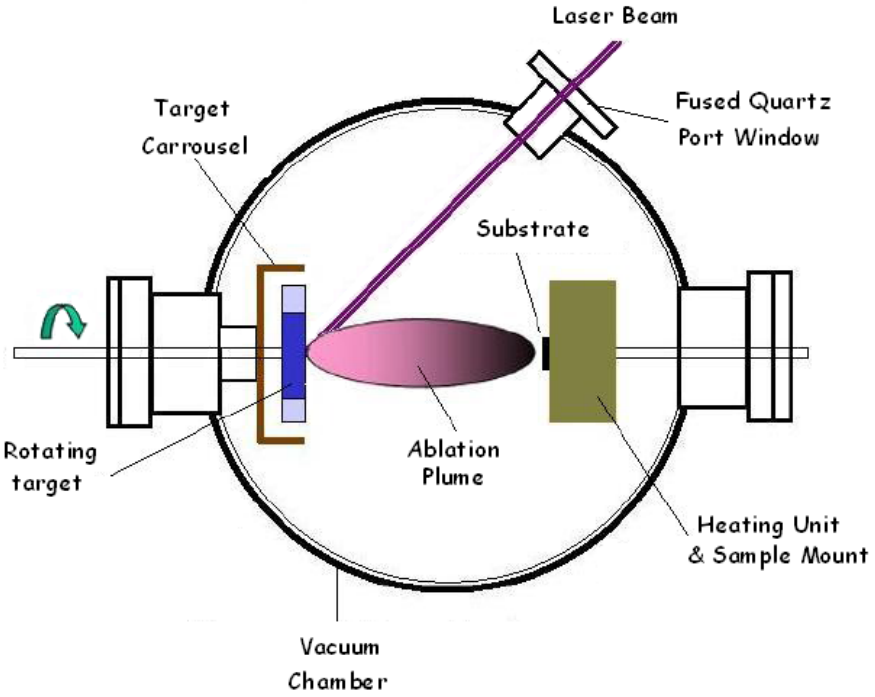

Figure 3.5 Schematic diagram of multi-target PLD method (Technology).

The target is mounted onto the target holder using silver paste. The laser beam (pulse duration, 30 ns; repetition rate, 10 Hz; input energy, 300 mJ/pulse) was focused on the target through high-quality quartz optics (focal length, 20 cm) at an angle of 45°. The target was kept rotating during deposition to avoid deep crater formation. Prior to each deposition targets were polished to eliminate uneven interaction with the ablated surface. The magnesium substrates were polished using isopropyl alcohol for lubricant, followed by sonic cleaning in acetone for 10 minutes. The magnesium substrate was placed directly onto the stainless steel holder and was connected to the holder using double-sided copper tape for room temperature deposition. The substrate heater-target distance was set to 4.5 cm. A turbomolecular pump pumped the vacuum

chamber to a pressure of 10^{-7} mbar before introducing argon ambient gas at 3×10^{-1} mbar for deposition.

After all the samples were prepared structural characterization using X-ray diffraction (XRD) and scanning electron microscopy (SEM) was conducted. XRD was used to test if there were any significant changes to the phases of β-TCP deposited film after the introduction of dopants compared to β-TCP processed under the same conditions and SEM was used to visualize the microstructure of sintered β-TCP structures with various dopant additions and to compare them with that of sintered undoped β -TCP compact. These sintered compacts were then used for PLD deposition and to conduct biological studies.

3.4 Structural Characterization

3.4.1 X-ray diffraction analysis. English physicists Sir W.H. Bragg and his son Sir W.L. Bragg developed a relationship in 1913 to explain why the cleavage faces of crystals appear to reflect X-ray beams at certain angles of incidence (theta, θ) (Bragg & Bragg, 1913). Bragg's Law refers to the simple equation:

$$n\lambda = 2d \sin\theta \qquad (1)$$

The variable d is the distance between atomic layers in a crystal, and the variable lambda λ is the wavelength of the incident X-ray beam; n is an integer. This observation is an example of X-ray wave interference, commonly known as X-ray diffraction, and was direct evidence for the periodic atomic structure of crystals assumed for several centuries. Although Bragg's law was used to explain the interference pattern of X-rays scattered by crystals, diffraction has been developed to study the structure of all states of matter with any beam, e.g., ions, electrons, neutrons, and protons, with a wavelength similar to the distance between the atomic or molecular structures of interest. XRD is used to measure the average spacing between layers or rows of

atoms, to determine the orientation of a single crystal or grain, and to find the crystal structure of an unknown material. It is also used to measure the size, shape and internal stress of small crystalline regions.

To eliminate the peaks for the magnesium substrate the films were deposited on Glass, then placed in a specimen holder, individually and analyzed using a Bruker® AXS D8 discover diffractometer tube consisting of a copper anode generating the characteristic Cukα radiative source with a wavelength of 1.54 Å and equipped with a couple of 0.2 mm slits on both the source and detector. Operating parameters for the tube are 40 kV at 40 mA.

A *Z*-scan was done using a point detector to align the sample to the path of the X-ray beam. Area detector was then used to run a locked couple scan (θ - 2θ scan) on all the samples. Diffraction patterns are collected by the detector while the sample is rotated through 2θ = 20° to 80°. An X-ray detector (point detector) is placed at an angle to satisfy the geometry such that the angle between the incoming rays and the reflected rays is 2θ, as shown in Figure 3.6.

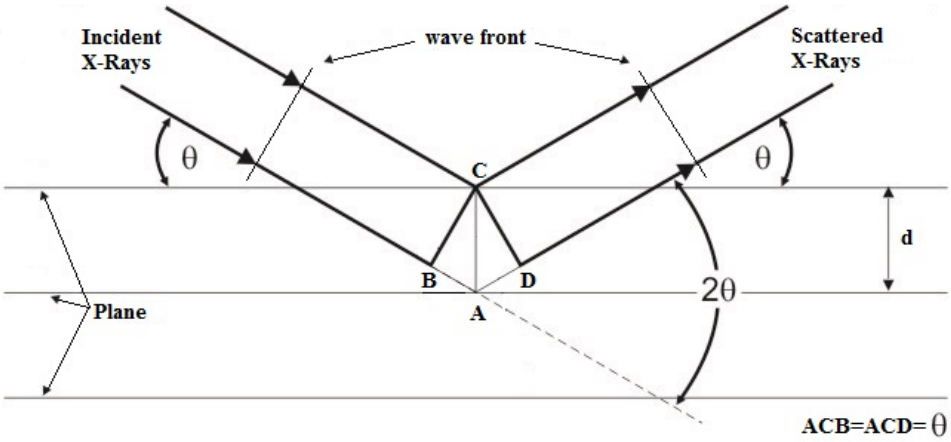

Figure 3.6 Schematic of the diffraction geometry.

3.4.2 Scanning electron microscopy. A scanning electron microscope uses beams of electrons to create magnified images of samples, as opposed to beams of light that a traditional microscope uses (Lausmaa et al.). Because the scanning electron microscope can magnify a

sample up to 500,000 times it has a wide range of applications. They are used for quality control in both the pharmaceutical and semiconductor industries, sample comparisons in forensics, diagnostics in medical labs, and in research labs to determine the composition of samples treated in different ways. Scanning electron microscopes have different kinds of signal detectors available that include back-scattered electrons (for imaging), characteristic X-rays (for determining types and amounts of elements present in the sample), transmitted electrons, and cathode-luminescence. Other variations in different scanning electron microscopes include availability of low or high vacuum mode and imaging options for bright field samples and/or dark field samples. Scanning electron microscope is the most widely employed thin film and coating characterization instrument (Lausmaa et al.; Ohring, 2002).

Hitachi® SEM SU8000 was used to visualize the fabricated samples used in these experiments. Depending on the particular sample, appropriate voltage and current were selected to capture high quality images. Elemental compositions of the ceramics and films were also evaluated using the attached energy dispersive X-ray analyzer to verify stoichiometric transfer from the target to the PLD deposited films.

Triple detector system offers a variety of signal collection. Top detector can detect high angle BSE (HA-BSE), which has pure Z-number contrast with less topographical information. The upper detector collects either the SE signal for surface topography/ voltage contrast, or user-selectable low angle BSE (LA-BSE), for both topographical information and compositional contrast. Both signals can also be mixed. The Lower detector is used for longer working distance SE imaging of surface topography. Table 3.2 illustrates a list of upper and lower triple detectors' signal information.

Table 3.2

SEM detectors and signal information

Signal name	Detector	Signal information
HA-BSE	Top	Compositional/Crystal information
LA-BSE	Upper	Compositional/Topographic information
SE	Upper	Surface information (Including voltage contrast)
Lower	Lower	Topographic contrast

Several models SEM's are available on the market; a schematic of a variety of signal detecting system for visualizing absolute surface information is shown in Figure 3.7.

All compositions were observed under SEM to study the effect of dopants on the microstructure of β-TCP. Ceramic targets that were subjected to a biological study were also observed under the SEM for all compositions and all time durations (2, 4, 6, 8, 10 weeks).

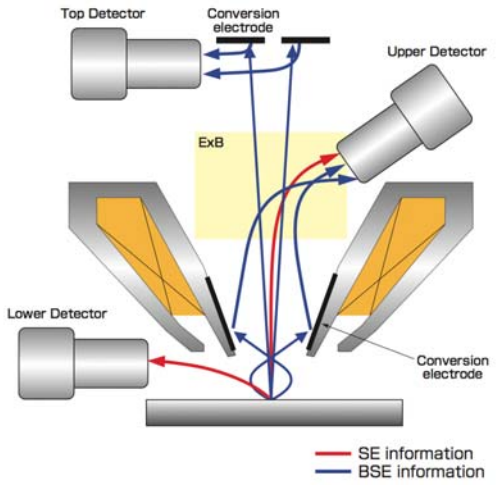

Figure 3.7 Scanning electron microscope (High-Tech).

Nanoindentation tests and corrosion analysis were conducted on the samples to give an idea of the mechanical characteristics. The following section describes the equipment used and the science behind the procedures.

3.5 Mechanical Characterization

3.5.1 Nanoindentation tests. Indentation techniques are most frequently used to measure two important mechanical properties the hardness (H) and the elastic modulus (E). As the indenter is pressed into the sample, both elastic and plastic deformation occurs, which results in the formation of a hardness impression conforming to the shape of the indenter. During indenter withdrawal, only the elastic portion of the displacement is recovered, which facilitates the use of an elastic solution in modeling the contact process.

A typical load–displacement curve and the deformation pattern of an elastic–plastic sample during and after indentation are shown in Figure 4.8 (a) and (b) (Oliver & Pharr, 1992).

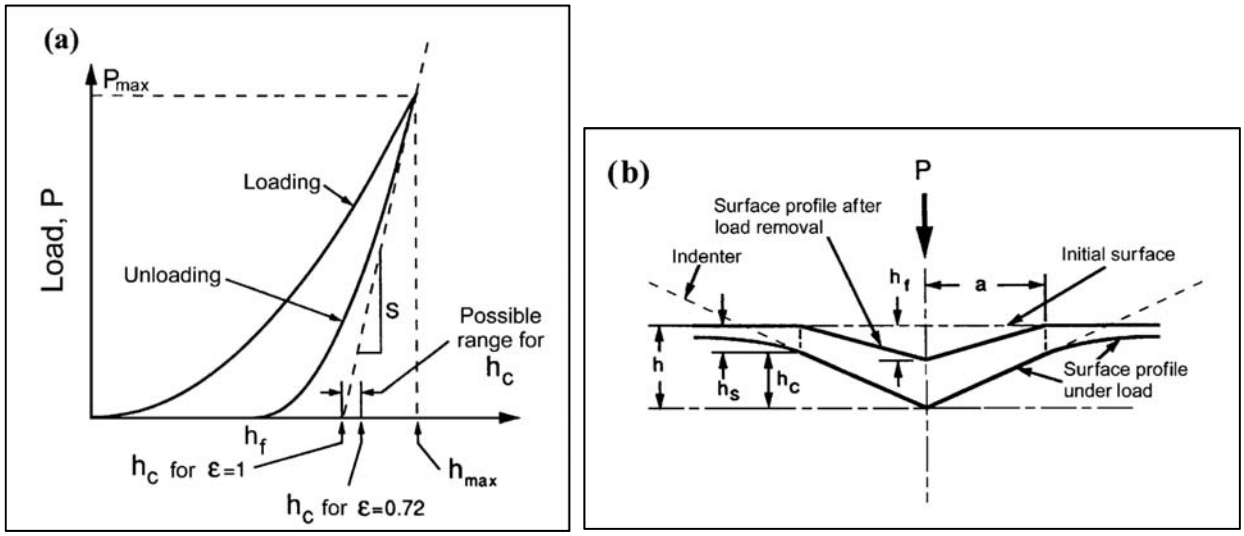

Figure 3.8 (a) A typical load-displacement curve (b) The deformation pattern of an elastic-plastic sample during and after indentation.

where

- P represents the applied force.

- h denotes the indenter displacement.
- h_{max} represents the displacement at the peak load, P_{max}.
- h_c is the contact depth and is defined as the depth of the indenter in contact with the sample under load.
- h_f is the final displacement after complete unloading.
- h_r is the plastic deformation after load removal.
- h_s represents the surface displacement at the contact perimeter.
- S is the initial unloading contact stiffness.

Nanoindentation is the mean pressure that a material can support under load and hardness is defined as the indentation load divided by the projected contact area of the indentation. From the load–displacement curve, hardness can be obtained at the peak load as

$$H = \frac{P_{max}}{A} \qquad (2)$$

where A is the projected contact area. Measurement of the projected contact area from a load-displacement curve requires the contact depth, h_c.

The elastic modulus of the indented sample can be derived from the slope of the initial portion of the unloading curve, i.e. the initial unloading contact stiffness, S = dP/dh. Based on relationships developed by Sneddon for the indentation, S can be derived as follows

$$S = 2\beta\sqrt{\frac{A}{\pi}}E_r \qquad (3)$$

where β is a constant that depends on the geometry of the indenter and E_r is the reduced elastic modulus, which accounts for the fact that elastic deformation occurs in both the sample and the indenter (Sneddon, 1965). E_r is given by

$$E_r = \frac{1-\nu^2}{E} + \frac{1-\nu_i^2}{E_i} \qquad (4)$$

where E and ν are the elastic modulus and Poisson's ratio for the sample, respectively, and E_i and ν_i for the indenter. For diamond, E_i = 1141 GPa and ν_i = 0.07 (Oliver & Pharr, 1992; Tabor, 1951).

The contact stiffness and the projected contact area need to be determined from the load–displacement curve to calculate elastic modulus, E, from Eqns. (3) and (4). Oliver and Pharr found that the unloading curve is usually not linear as suggested by Doerner, but is better described by a power law:

$$P = B\left(h - h_f\right)^m \qquad (5)$$

where B and m are empirically determined fitting parameters (Oliver & Pharr, 1992) (Doerner & Nix, 1986). The unloading stiffness, S, is then established by differentiating Eq. (5) at the maximum depth of penetration, h = h_{max} (i.e., Eq. (6))

$$S = \left(\frac{dP}{dh}\right)_{h=h_{max}} = Bm\left(h_{max} - h_f\right)^{m-1} \qquad (6)$$

For an indenter with a known geometry, the projected contact area is a function of the contact depth. The area function for a perfect Berkovich indenter is given by

$$A_c = 24.56h_c^2 \qquad (7)$$

Indenters used in practical nanoindentation testing are not ideally sharp. Therefore, tip geometry calibration or area function calibration is needed. A series of indentations is made on fused quartz at depths of interest. A plot of A versus h_c can be curve fit according to the following functional form (Eq. (8)):

$$A_c = 24.56h_c^2 + C_1h_c^1 + C_2h_c^{1/2} + C_3h_c^{1/4} + \cdots C_8h_c^{1/128} \qquad (8)$$

where C_1 through C_8 are constants. The lead term describes a perfect Berkovich indenter, the others describe deviations from the Berkovich geometry due to blunting of the tip (Oliver & Pharr, 1992).

The contact depth can be estimated from the load–displacement data using Eq. (9):

$$h_c = h_{max} - \varepsilon \frac{P_{max}}{S} \qquad (9)$$

where ε is a constant that depends on the indenter geometry (ε = 0.75 for a Berkovich indenter) (Oliver & Pharr, 1992).

The nanoindentation analysis was performed using the Nano Indenter® XP system (MTS Systems Corporation). This instrument has a maximum applied load is 500 mN, indenter load resolution of 50 nN, and displacement resolution of < 0.02 nm. It provides the possibility to obtain reliable characterization data for thin films and individual grains. Testworks 4 software is used for analysis of collected data. A Berkovich diamond indenter was used for all the experiments. A schematic representation of the nanoindenter is shown in Figure 3.9.

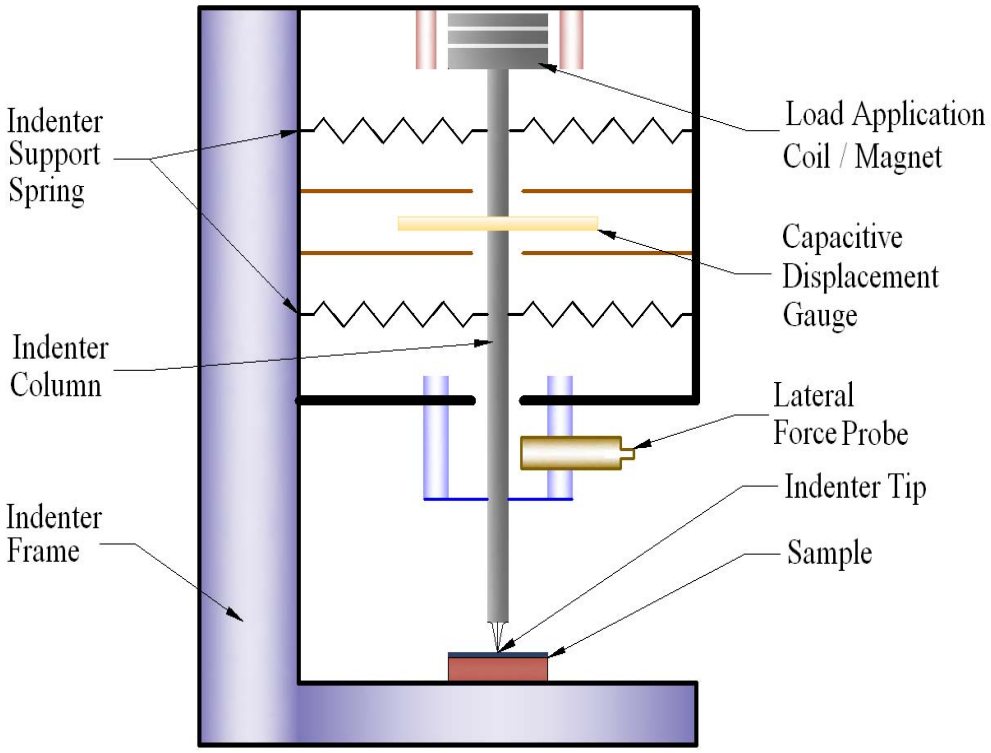

Figure 3.9 Schematic representation of the nanoindenter setup (Mensah-Darkwa, 2012).

3.5.2 Corrosion tests. Predicting the corrosion behavior of magnesium is very challenging, because it does not follow the normal corrosion behavior as other materials. Typically, anodic and cathodic reactions model the behavior of all electrochemical corrosion processes. The anodic and cathodic reactions are usually inversely related. As the applied potential (E_{appl}) or current density increases, the anodic reaction rate increases and the cathodic reaction rate decreases. An anodic increase of applied potential causes an increase in the anodic dissolution rate, while the cathodic site decreases in hydrogen evolution.

In this section, the primary electrochemical methods used for determining the corrosion rate of the coated magnesium and magnesium alloy used in this research are addressed.

Potentiodynamic polarization over a potential range about $\pm$ 200 - 250 mV from the open circuit potential results in a polarization curve that can be analyzed for corrosion rate, provided that the rates of other anodic reactions are small in comparison, which is a requirement of all electrochemical assessments of corrosion rate. Typically presented in a semi-logarithmic plot, polarization curves provide corrosion rate by extrapolation of the linear cathodic and/or anodic regions to the corrosion potential or by fitting to the following equation (Frankel & Rohwerder, 2003; Jones, 1996; R. G. Kelly, Scully, Shoesmith, & Buchheit, 2003):

$$I_{net} = i_{corr}\left(\exp\left[\frac{2.3(E-E_{corr})}{\beta_a}\right] - \exp\left[\frac{-2.3(E-E_{corr})}{|\beta_c|}\right]\right) \qquad (10)$$

where:

I_{net} is the current measured as a function of applied potential E,

E_{corr} is the corrosion potential,

i_{corr} is the corrosion current density,

and β_a and β_c are the anodic and cathodic Tafel slopes, respectively.

The equation represents an idealized form of the electrochemical data for the case of a

mixed electrode in which there is only one anodic and one cathodic reaction taking place on the corroding surface. Both reactions must be controlled by activation polarization and E_{corr} must be far from both reversible potentials. Most commercial corrosion analysis software packages contain the capability to fit data to this equation.

Potentiodynamic polarization over a wide range of potential generates more information about the system than just the corrosion rate. For instance, information can be obtained about the proximity of the open circuit potential to regions of passivity or localized corrosion susceptibility. Potentiodynamic polarization is a tool for laboratory investigations, not corrosion rate monitoring, as it involves perturbation of the potential relatively far from the steady-state corrosion potential.

The corrosion rate also can be determined from the polarization resistance (R_P) using the Stearn-Geary equation provided that the polarization resistance is similar to the charge transfer resistance and if the Tafel slopes are known (Mansfeld, 1976; Scully, 2000; Stern & Geary, 1957).

$$R_p = \frac{B}{I_{corr}} = \frac{(\Delta E)}{(\Delta i)_{\Delta E \to 0}} \qquad (11)$$

where:

- R_p is the polarization resistance
- I_{corr} the corrosion current

The proportionality constant, B, for a particular system can be determined empirically (calibrated from separate weight loss measurements) or, as shown by (Stern & Geary, 1957), can be calculated from β_a and β_c, the slopes of the anodic and cathodic Tafel.

$$B = \frac{\beta_a \cdot \beta_c}{2.3(\beta_a + \beta_c)} \qquad (12)$$

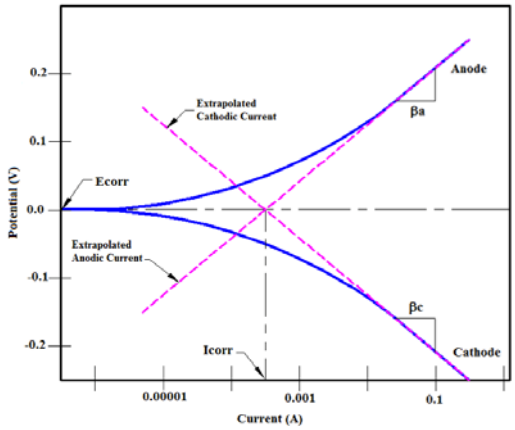

Figure 3.10 Polarization plot showing intersection of anodic and cathodic Tafel.

At low overvoltage values, deviations from Tafel behavior for a non-corroding electrode are due primarily to the reverse reaction of the oxidation-reduction system, and at high over-voltages to concentration and/or resistance polarization. The most common way to determine R_P is by the linear polarization resistance method, in which the potential is scanned about $\pm 5 - 10$ mV relative to the corrosion potential. The slope (dE/di), at the zero current potential is a measure of R_P (Ramirez & Lei, 1996). These simplified analyses assume that the polarization response is perfectly linear, and error will result if there is any deviation from linearity. The linear polarization resistance method has been put to considerable use in corrosion monitoring as it involves relatively little potential agitation.

The potentiodynamic polarization studies were carried out using a Gamry® R600 Potentiostat (Gamry Instruments). All DC potentiodynamic polarization measurements were performed in at room temperature in Hench simulated body fluid solution (SBF) buffered at a pH = 7.4. The scan rate was set at 5 mV/s spanning a scan range of ± 0.3 V vs open circuit potential (E_{oc}). A 50 ml electrochemical cell with a standard three-electrode configuration consisting of the sample acting as the working electrode and the standard Ag/AgCl electrode and platinum wire used as the reference and counter electrodes, respectively. The samples were immersed in

the test solution for 15 min until steady state conditions before running the tests. Fresh solution was used for each experiment. Figure 3.11 illustrates the experimental setup used in this research.

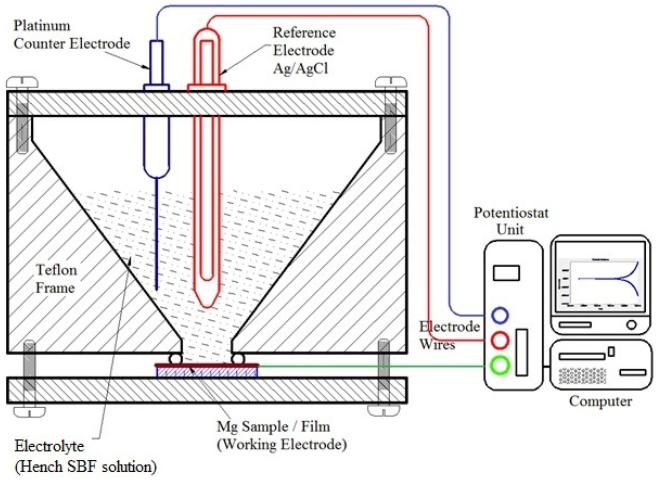

Figure 3.11 Experimental setup for electrochemical corrosion testing.

After fabricating the samples and conducting structural and mechanical analysis, it is necessary to test for biocompatibility, dissolution rate, and surface apatite formation ability. The following section describes the methods used to test for bio mineralization ability as well as cytotoxicity of the materials being studied in this research.

3.6 Biological Studies

3.6.1 Mineralization studies. SBF was used to replicate the human body's natural physiological environment. Experiments were conducted for durations of 2, 4, 6, 8, and 10 weeks for all compositions.

Preparation

Following the standard procedure to make Hench's simulated body fluid (L.L. Hench & Wilson, 1993) SBF was prepared, the procedure calls for the preparation of 1 liter of solution. First a solution of 1 normal hydrochloric acid at 100 mL was made by adding 8.26 mL of

concentrated HCL and 91.74 mL of de-ionized distilled water and mixing with a magnetic stirring rod. Then the 500 mL beaker to be used was washed with approximately 4 mL of N HCL and de-ionized water and dried. The beaker was filled with 500 mL of de-ionized water and poured into a 1 L glass flask with a magnetic stirring rod. Next, the reagent salts were added in the order specified by Hench, and made sure each one was completely dissolved before adding the next. After all reagents were added, the pH of the solution was measured and adjusted to approximately 7.40 by stirring the solution and adding 1N-HCl solution in. Finally the volume was adjusted by adding de-ionized water to make 1 liter of SBF.

Table 3.3

Reagent preparation for simulated body fluid (L.L. Hench & Wilson, 1993)

Order	Reagent	Purity	Amount (g)
1	NaCl	99.5 %	7.996
2	$NaHCO_3$	99.5 %	0.350
3	KCl	99.5 %	0.244
4	$K_2HPO_4.3H_2O$	99 %	0.171
5	$MgCl_2.6H_2O$	98 %	0.305
6	1N-HCl	-	40 ml
7	$CaCl_2.2H_2O$	95 %	0.368
8	$Na_2SO_4.10H_2O$	99 %	0.161
9	$NH_2C(CH_2OH)_3$	99.9 %	6.057

Procedure

All sintered targets and coated samples were placed in a 24 well plate. The wells were filled with 2 ml of SBF solution via pipetting from larger flask containing the previously made

SBF. This procedure was conducted in a bench hood. All samples were placed in an incubator at a regulated temperature of 37 °C to simulate the human body's internal temperature.

Following conclusion of the biological experiment, all targets and films were removed from the wells and gently washed by repeated dipping in de-ionized water. All samples were then left to dry for approximately 48 hours. After the drying process ended, samples were then weighed for change due to any apatite formation or dissolution occurrence. Weight measurements were recorded for each composition and time duration. In general, if there was any Ca-P based apatite such as hydroxycarbonate apatite (HCA) formation, then that would result in weight increase, however, if there is any dissolution of sample occurring then there is a loss in weight.

Owing to its inherent biocompatibility, synthetic beta-tricalcium phosphate forms a strong bond with human bone and is thus very attractive for use as an implant material. β-TCP coatings also enhance the cell response of surrounding bone tissue to a metallic or ceramic implant. The rapidly increasing popularity of Ca-P coatings is due to accumulating evidence that an implant coated with a material chemically similar to natural bone should result in a more desirable tissue response. Since ceramic β-TCP is brittle, and thus not suitable for load-bearing applications, metal oxide reinforced β-TCP coatings are applied to dental and medical implant materials to combine the superior mechanical properties of the implant metals with the biocompatibility of β-TCP.

To be most effective, Ca-P coatings should remain on the implant metal surface and stimulate bone in-growth until sufficient bone regenerates at the implant-bone interface. Unfortunately, both the presence of additional phases in the coating can cause excessive dissolution in a physiological environment and consequently reduce the coating integrity of the

implants. To decrease the solubility of the β-TCP coatings the film needed to be crystalline, historically making post-deposition annealing a requirement. However, annealing is time consuming, and, more important, is detrimental to the thermo-stability of the underlying implant metal and is often the main cause of crack formation and the degradation in adhesion of the coating to the substrate. Therefore the challenge has been to develop an approach capable of producing phase-pure, β-TCP coatings on various implant materials.

3.6.2 Cell viability tests. The materials used in conducting this test included a 24-well Corning/ Costar plate, MC3T3-E1 pre-osteoblastic mouse calvaria-derived cells; alpha minimum essential medium (α-MEM) supplemented with 10 % fetal bovine serum (FBS) and 1 % penicillin-streptomycin solution; phosphate buffered saline (PBS); 70 % ethanol; Trypsin – 0.53 mM EDTA solution; and Live/Dead reagent stock solutions (Calcein AM and Ethidium Homodimer (EthD-1)).

Frozen cells were removed from liquid nitrogen and thawed in a water bath at 37 °C. Cells were pipetted into a 50 ml centrifuge tube containing 9 ml of growth media pre-warmed to 37 °C. The cells were centrifuged in a hemocytometer at 500 rpm for 5 minutes. Growth media was aspirated off the top of the cells and cells are cultured in T75 Corning cell culture flasks in the prepared α-MEM media solution at 37 °C under 5 % CO_2 and passaged every 7 days. MC3T3-E1 cells were kept in the α-MEM media and every 2 to 3 days the media in the flasks was aspirated and fresh media added to avoid excessive alkalinity of the medium during culturing. After 7 days, the cells were the washed with PBS, to remove all traces of serum, which contains trypsin inhibitor. Cells are passaged with 1 ml of 0.25 % Trypsin, which was added to the flask swirled gently and incubated at 37 °C for 3 minutes to detach the cells from the bottom of the flask. Special care should be taken not to agitate the flask to avoid clumping. Cells are

then observed in an inverted microscope to ensure cell layer is dispersed. 9 ml of fresh growth media was added to the flasks and the resulting cell suspension was transferred into a new 50 ml vial. The appropriate aliquots of the cells suspension were split and seeded into two separate flasks, usually at a subcultivation ratio of 1:6 and incubated at 37 °C under 5 % CO_2. This process was performed for each group of cells at each time point to obtain the desired amount of cells. Cells at passage numbers 21–23 were used in the experiments.

Live-dead assay tests

For the experiments, all samples were sterilized by autoclaving under a UV light for 30 min on each side, and then placed in a separate well of a 24-well plate. Before harvesting cells for the experiment, 80 % confluence of the cell must be ensured. Part of the cell suspension 1:3 was diluted in complete media by adding 3 µL cells to 7 µL complete media. 1 µL of this diluted cell suspension containing 50,000 cells/well was then seeded into each of the test wells on the corning plates. When seeding, the cells were mixed gently and often to prevent settling of the cells. The cells were place in an incubator overnight to ensure that the cells firmly attach to the surface. After 24 h incubation, the samples were rinsed with PBS to remove non-adherent cells and stained with the Live/Dead Viability/Cytotoxicity Kit. To prepare the dye the Live/Dead reagent stock solutions was removed from the freezer and allowed to warm to room temperature. 2 µl of the supplied 4 mM EthD-1 stock solution was added to 20 ml sterile PBS in 50 ml centrifuge tube and 0.5 µl of the 2 mM calcein AM stock solution was added to the EthD-1 solution and vortexed to ensure mixing, the resulting solution was then stored in foil wrap. To stain with the live/dead reagent, media was aspirated form the wells and the wells were rinsed with 1ml of PBS using a micropipette, swished lightly and aspirated using a glass Pasteur pipet. When adding the PBS to the wells, the liquid was squirted on the sidewall of the well where

there are no attached cells. 200 µl PBS and 10 µl dye were added to each of the wells. The plate was then covered with foil and incubated for 30 min.

All viable cells fluoresced green and all dead/dying cells fluoresced red. The cells were then visualized using an EVOS digital inverted fluorescent microscope equipped with a UV light source and an accompanying UV filters set, Figure 3.12. Stained cells were visualized using a 4×. Magnification on an inverted fluorescence microscope (EVOS) equipped with a Sony ICX285AL CCD camera. Pictures were taken with the appropriate filter block. The operating features of the microscope are a mechanical glide stage**:** X-Y axis fine-positioning controls; 69 mm (2.7-in) per rotation; 110 mm × 110 mm (4.3-in × 4.3-in) range of motion; Z-axis focusing controls, 480 µm/rotation; interchangeable vessel holders available for most common shapes and sizes.

Figure 3.12 AMG EVOS digital inverted fluorescence microscope (EVOS).

CHAPTER 4

Results and Discussions

This chapter presents the results of the mechanical and biological tests and discusses these in light of the suitability of the improved coated metallic material for application in bone tissue engineering.

4.1 Densification Measurements

To improve mechanical properties of ceramic compacts, it is necessary to achieve good densification. To prepare the green ceramics they were pressed manually via uniaxial pressing for various compositions of tricalcium phosphate with the selected dopant. Polyvinyl alcohol was used to process the green compacts. The use of this binding agent prevented samples from sticking to the mold and cracking during processing.

After preparing the green compacts, all samples were sintered in a muffle furnace for 2 hours at 1250 °C. This temperature and sintering time was based on literature review (Caroff et al., 1998; Itatani et al., 2002; X. L. Wang et al., 2005). High alumina setter plates were used to place these samples inside the furnace. It is well known that β-TCP has the best densification between 1200 – 1300 °C; above 1300 °C there is high possibility of β-TCP transforming to α-TCP phase, this also changes the resorption properties and bioactivity characteristics (Ando, 1958). Good densification is important to improve mechanical and physical properties of β-TCP. Green and sintered densities were measured and were normalized with respect to the theoretical density of TCP (3.07 g/cm^3). Average green and sintered densities for each of these compositions were calculated and represented separately. The shrinkage of undoped β-TCP samples is shown in Figure 4.1.

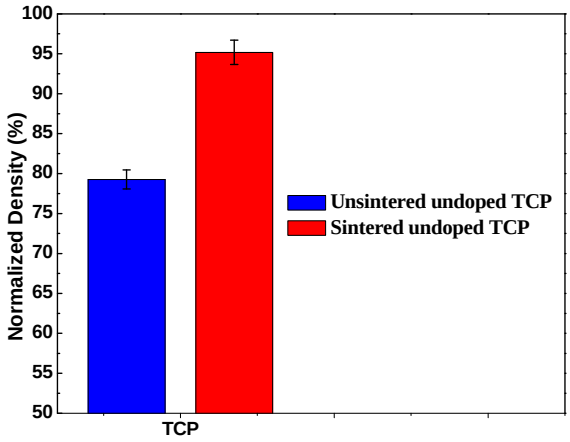

Figure 4.1 Densification of undoped TCP.

In the preliminary stage of this project the main objective was to determine the ratio of dopant to be added to TCP. The amount of each dopant was kept minimal to preserve the β-TCP structure and eliminate any unwanted phase formation.

Based on literature review, a decision was made to use (0.25, 0.5, and 1 wt %). Figure 4.2 shows the effect of MgO on densification based on 0.25 wt %, 0.5 wt %, and 1 wt %.

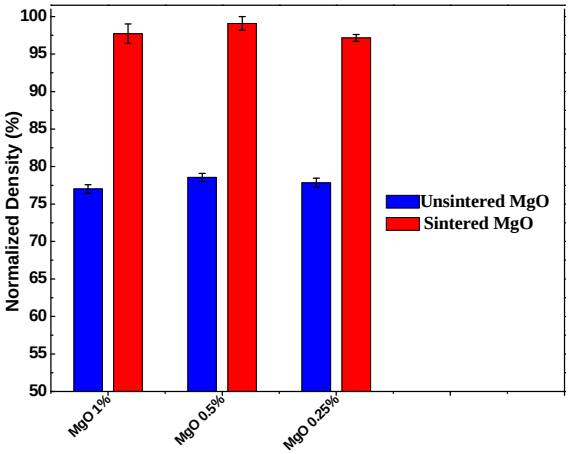

Figure 4.2 Densification of TCP doped with 1 %, 0.5 % and 0.25 % MgO.

It was observed that MgO influenced a slightly higher densification to TCP at 1 wt % addition compared to 0.25 wt % and 0.5 wt %. In Figure 4.3 the highest density for TCP-ZnO compacts were present at 0.5 wt % addition.

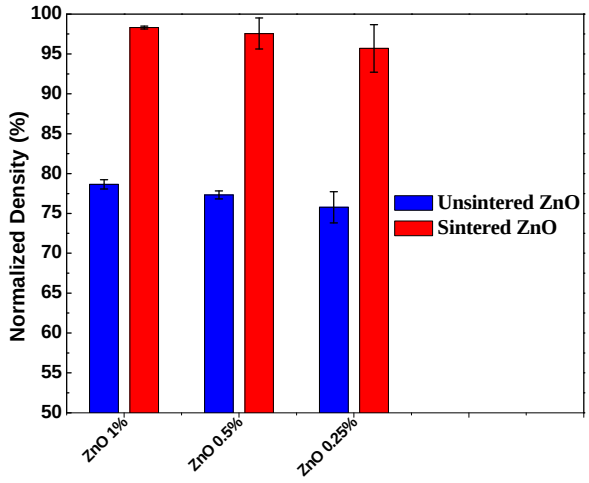

Figure 4.3 Densification of TCP doped with 1 %, 0.5 % and 0.25 % ZnO.

It was determined based on trends in densification that by using 1 wt % of TiO_2 added to TCP it was possible to obtain the maximum densification, as seen in Figure 4.4.

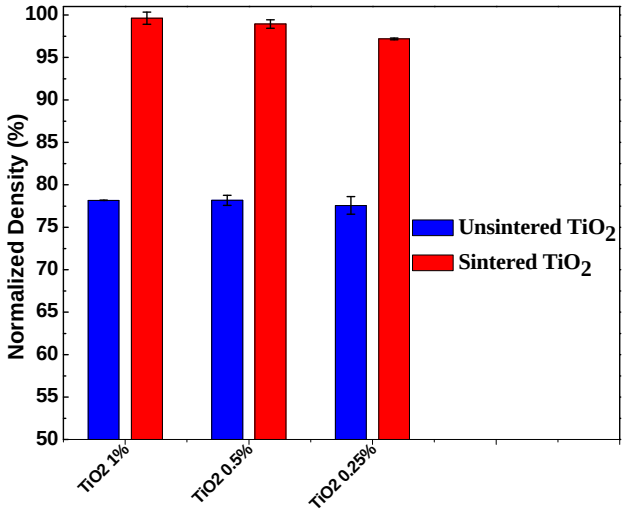

Figure 4.4 Densification of TCP doped with 1 %, 0.5 % and 0.25 % TiO_2.

Based on this observation we decided to optimize the density of TCP by using these compositions and ratios of dopants for the remainder of the research.

4.1.1 Single dopant system. Density was measured and normalized with respect to theoretical density for the disk compacts. TCP-MgO (1 wt %) showed around 21 % densification increase for the sintered targets as shown in Figure 4.5.

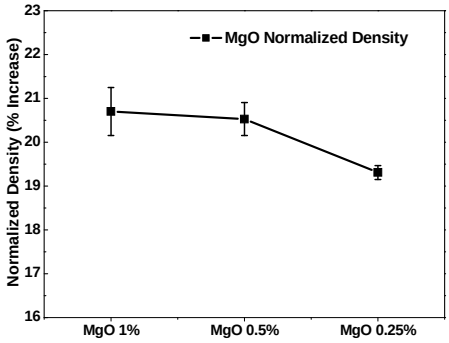

Figure 4.5 Densification % increase due to MgO doping.

TCP-ZnO (0.5 wt %) demonstrated a positive effect on densification for disk compacts by increasing the density from 77 to 98 % as shown in Figure 4.6.

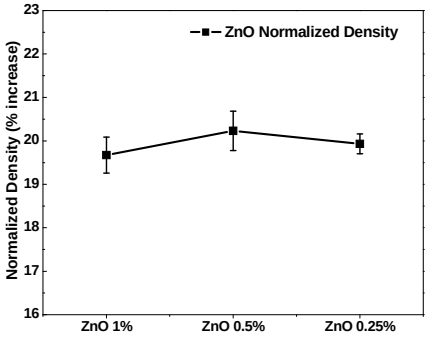

Figure 4.6 Densification % increase due to ZnO doping.

The effect of titanium dioxide on sintered density was positive on all three compositions. 1 wt % addition shows the highest densification, it showed an increase in densification of 21 % as shown in Figure 4.7.

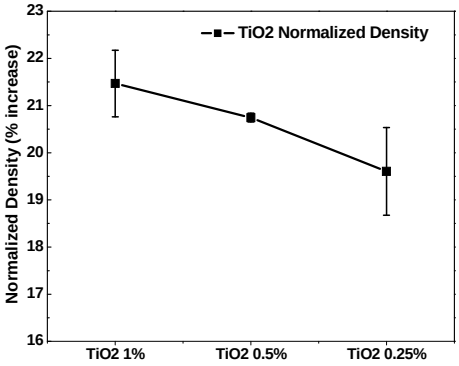

Figure 4.7 Densification % increase due to TiO_2 doping.

4.1.2 Ternary dopant system [TCP + TiO2(1 wt %) + MgO(1 wt %) + ZnO (0.5 wt %)]. The highest densification was recorded for the ternary compound targets. For the sintered target there was a 22 % increase in density as shown in Figure 4.8. The ternary compound densification analysis confirms that the combined effect of these dopants on TCP is more pronounced than in the single dopant compositions.

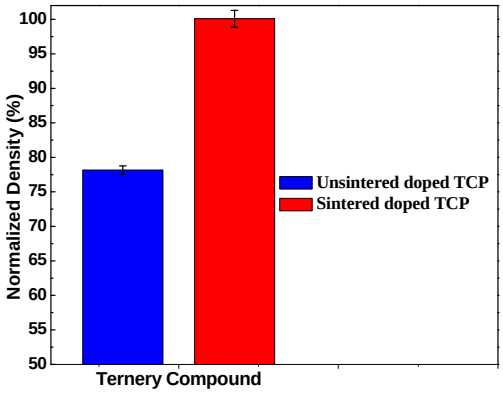

Figure 4.8 Densification of TCP doped with 1 % MgO, 1 % TiO_2 and 0.5 % ZnO.

4.2 Effect of Sintering

In general, sintering controls both densification and grain growth. The sintering process provides the energy to encourage the individual powder particles to bond or sinter together to remove the porosity present from the compaction stages. During densification the samples become denser and grain growth commences, this is the process of grain boundary motion to increase the average grain size. It can be seen as a competition between two thermally activated phenomena that proceed by solid-state diffusion of matter: densification and grain growth.

Usually, the objective is to promote the first and prevent the second. The size of the grain as well as the high relative density of sintered samples can benefit many properties, such as; mechanical strength and electrical breakdown strength, thus, being able to control these properties during processing is of great importance. In general, the strength for ceramics is proportional to the inverse square root of the grain size (Carter & Norton, 2007), similar to the

relationship of metals.

As the resorbability of a biomaterial depends principally on its dissolution rate (Hoppe, Gueldal, & Boccaccini, 2011; Sainz, Pena, Serena, & Caballero, 2010), which depends on microstructure (phase assemblage, porosity, surface roughness, etc.) conditioning the mechanical performance of implanted materials in the body, the understanding and the control of these parameters must be taken into serious account. Therefore, due to the complexity of calcium phosphate based biomaterials, further optimization of these materials is still required. For this reason, in the last decades, a new approach has been considered in order to optimize synthesis, phase compatibility, microstructure, dissolution rate, mechanical resistance and osteogenesis of tricalcium phosphate based biomaterials; enhancing not only bone formation but also tissue regeneration. It consists of doping TCP with trace elements that do not break biocompatibility. Some of the chemical components which can be used as additives (CO_3^{2-}, SiO_4^{2-}, Mg^{2+}, Zn^{2+}, F^-, Cl^-, Na^+ and K^+) are restricted to elements contained in natural bone (Carrodeguas, De Aza, García□Páez, De Aza, & Pena, 2010; Douard et al., 2011).

Figure 4.9 shows the effect of sintering on the green compacts. It can be seen that the grains coalesce and grains grow to an average size of ~10 μm.

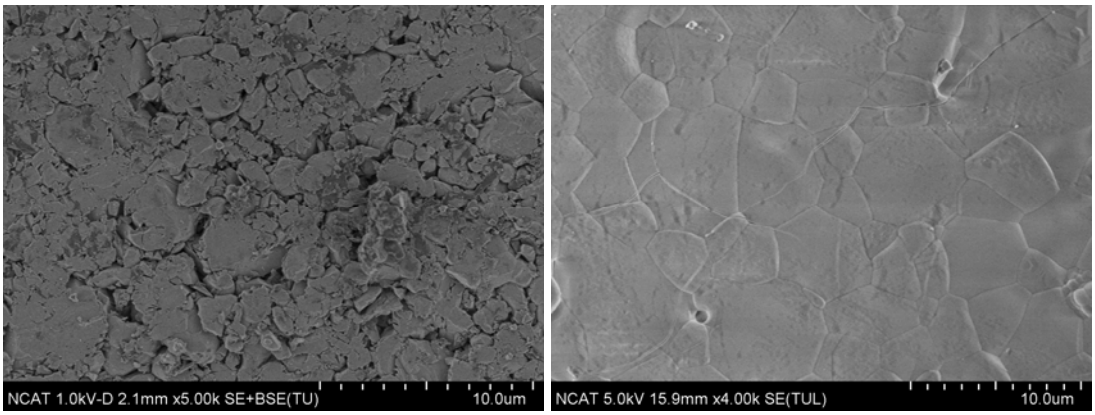

Figure 4.9 Surface structure of undoped TCP, before and after sintering.

Ando et al. found that a small amount of magnesia contained in tricalcium phosphate stabilizes β modification of the phosphate (Ando, 1958). However, a new compound $Ca_3Mg_3(PO_4)_4$ is formed below 1175 °C when more than 0.6 mol. of MgO to 1 mol. of P_2O_5 is introduced into the phosphate. Furthermore, when studying the effect of MgO substitution in β-TCP, Banjerjee et al. and Enderle et al., have shown that MgO can influence the mechanical and biological properties of β-TCP. Incorporation of Mg^{2+} in the crystal structure of β-TCP suppressed β to α phase (Ando, 1958; Banerjee et al., 2010; Enderle, Götz-Neunhoeffer, Göbbels, Müller, & Greil, 2005).

Figure 4.10 illustrates the densification effect based on the addition of 1 % MgO to TCP, defined grain boundaries with an average grain size of about 5 μm were formed as a result of the sintering.

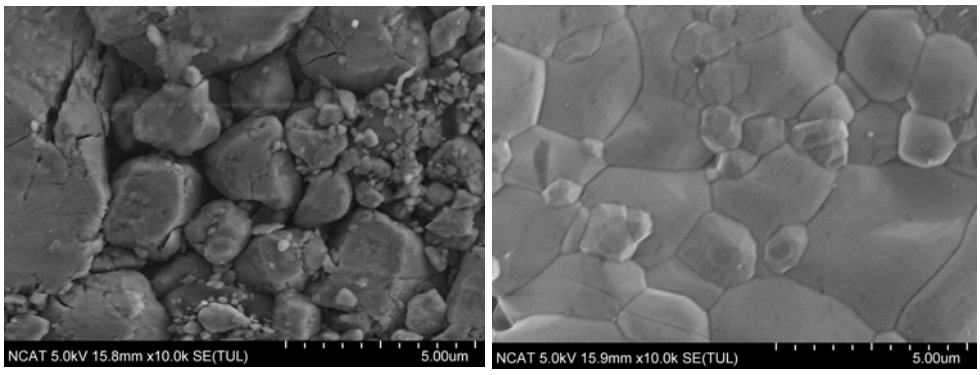

Figure 4.10 Surface structure of 1 % MgO doped TCP, before and after sintering.

Bandyopadhyay et al. studied TCP compositions containing ZnO and showed that addition of ZnO had significant effects on the grain size of the material. It was found that ZnO increases densification of TCP ceramics. Grain size for TCP ceramics dropped from 9 to 2 μm for samples sintered at 1250 °C. An increase in microhardness was also observed; highest microhardness value was observed for 2.5 % ZnO composition sintered at 1250 °C. Cell materials interactions were studied using an osteo precursor cell line, OPC1. These studies

showed that the substrates were non-toxic, however, increasing ZnO content decreased cell spreading and cell–cell interactions in the TCP samples (Bandyopadhyay et al., 2007).

The sintering of TCP doped with 0.5 % ZnO can be seen in Figure 4.11. The grain size formed as a result of this composition was in the range of 2 to 3 μm.

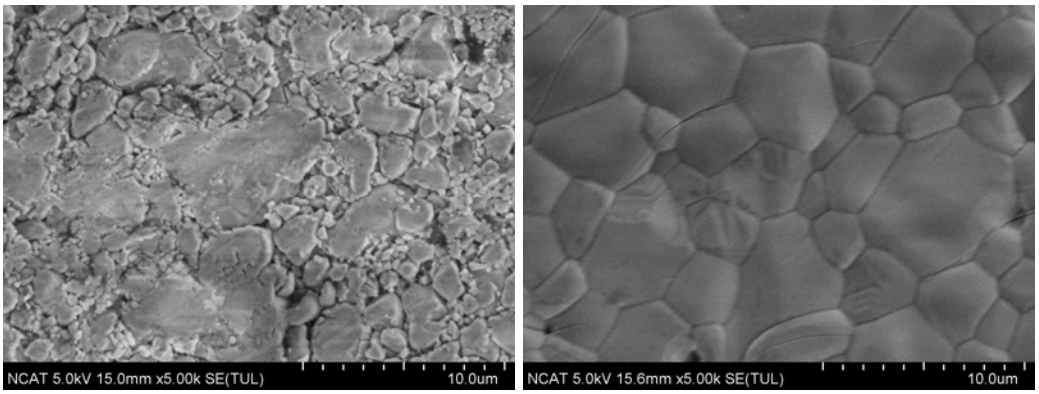

Figure 4.11 Surface structure of 0.5 % ZnO doped TCP, before and after sintering.

Seeley et al. doped tricalcium phosphate with 1.0 wt % TiO_2. Influence of this dopant on physical, mechanical, and biological properties was studied in comparison with undoped TCP. Results show that there is potential for improving these properties with the addition of this metal oxide without hindering the excellent biocompatibility of TCP. The addition of TiO_2 significantly increased the densification of undoped TCP, and ultimate compression strength increased from 70 (625) to 145 (640) MPa with the addition of TiO_2 in TCP (Seeley et al., 2007). Density and compression strength displayed a direct relationship. In vitro cell culture test showed that this composition was nontoxic and OPC1 cells attached and proliferated well on the TCP ceramics. Strength degradation in TCP began after 32 days in SBF, but for the doped composition, no noticeable degradation was noticed up to 96 days (Seeley et al., 2007).

Wolff et al. showed that the addition of TiO_2 show that only β phase was found in XRD analysis until 1250 °C, and the amount of TiO_2 added was sufficient to increase the phase transition temperature of β-TCP. Maximum values of relative density 92 % (TiO_2-TCP) until

1200 °C were found (Wolff et al., 2006).

Influence of addition of 1 % TiO_2 to TCP can be seen in Figure 4.12, an average grain size of 5 to 7 μm was seen as a result of the addition of the dopant.

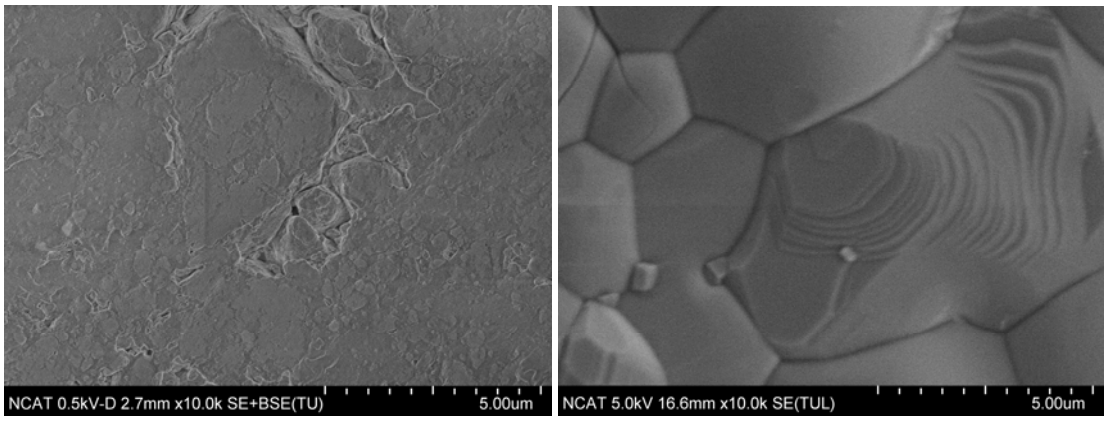

Figure 4.12 Surface structure of 1 % TiO_2 doped TCP, before and after sintering.

Figure 4.13 illustrates the result of doping TCP with the ternary compound [1 % MgO, 0.5 % ZnO, and 1 % TiO_2]. From the figure it can be seen that the grains coalesce and form distinct grain boundaries in the range of 2 to 3 μm. The addition of all three dopants produced samples with smaller grain size than the undoped TCP, thus, producing a compact ceramic with higher strength more resistant to degradation.

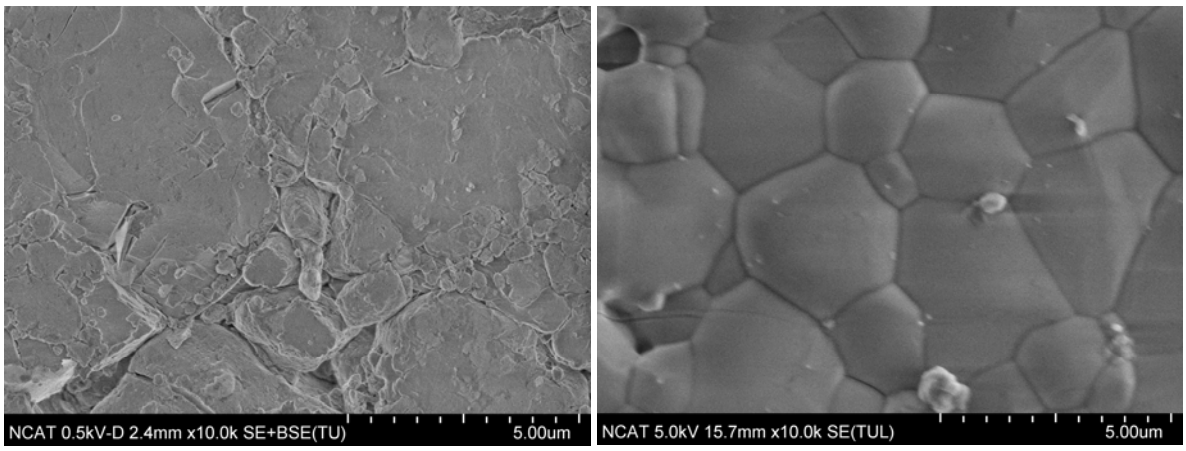

Figure 4.13 Surface structure of the ternary compound doped TCP, before and after sintering.

4.3 PLD Deposition Parameters

TCP ceramics reinforced with compositions of TiO_2 and MgO and ZnO were processed into target shapes via uniaxial powder compression. The compositions were prepared using high purity starting powders; which included synthetic β-TCP ($Ca_3(PO_4)_2$) (Berkely Advanced Biomaterials, CA), titanium dioxide (TiO_2), zinc oxide (ZnO), and magnesium oxide (MgO) (Sigma-Aldrich, St. Louis, MO). Dopant powders were mixed with the TCP in amounts of 1 wt % TiO_2, 0.5 wt % ZnO, and 1 wt % MgO. Two different targets were created from these powders, undoped TCP and the ternary composition of TCP with the three different dopants.

Calcium phosphate films were deposited in a vacuum chamber by utilizing a pulsed KrF laser (Eximer) operating at a repetition rate of 10 Hz with a wavelength of 248 nm and 300 mJ/pulse of energy. The laser beam was focused on a rotating target at an angle of 45°. The films were deposited at room temperature with various pressures of argon inside the chamber. The argon pressure was controlled in the range from 1×10^{-1} to 3×10^{-1} mbar. Magnesium and Mg2ZnO0.3Ca alloy were used as the substrates, and the calcium phosphate film was deposited exclusively on a circular area by utilizing a shadow mask.

The focused laser beam was scanned across the rotating and rastering target surface to avoid deep crater formation. Substrates were fixed at a distance of 4.5 cm from the target. The laser fluence at the target was varied from 6 to 20 J/cm^2 by varying the laser energy between 300 to 400 mJ and the use of an aperture at the site of the laser exit from no aperture to 10×4 mm. By using these parameters, the laser fluence and spot size were calculated, and experiments were conducted to find the growth rate, porosity and roughness of the deposited films. Scanning electron microscopy was used to give a visualization of the films. Table 4.1 and Table 4.2 represent the average of the results of the spot size and fluence rate acquired based on varying

these parameters.

Table 4.1

Spot size calculation based on varying the aperture at the site of the laser exit

Aperture		1st reading (mm)		2nd reading (mm)		3rd reading (mm)		Average reading (mm)		Apt area (mm^2)	Spot area (mm^2)
No aperture		3.26	1.59	3.3	1.69	3.11	1.74	3.22	1.67	N/A	5.39
20	10	3.13	1.44	3.24	1.24	3.1	1.43	3.16	1.37	200	4.32
15	6	3.11	1.05	2.98	1.11	3.09	0.93	3.06	1.03	90	3.15
12	6	3.05	0.98	3.01	1.05	2.76	0.9	2.94	1.00	72	2.94
12	4	2.86	0.97	2.47	1.18	2.45	0.88	2.59	1.01	48	2.62
10	4	2.77	0.83	2.46	0.89	2.15	0.85	2.29	0.86	40	1.96

Table 4.2

Laser fluence based on aperture and input laser energy

Aperture		Laser Energy (mJ)	Laser Fluence (J/cm^2)	Laser Energy (mJ)	Laser Fluence (J/cm^2)
No Aperture		300	6.0	400	8.0
20	10	300	7.5	400	10.0
15	6	300	10.0	400	13.3
12	6	300	10.0	400	13.3
12	4	300	10.0	400	13.3
10	4	300	15.0	400	20.0

Applying laser energy of 400 mJ and using no aperture, depositions were conducted under room temperature in vacuum. The films produced under these conditions were rough and there was a significant loss in phosphate with a Ca/P ratio of over 3. Introducing argon as a background gas resolved the issue of the Ca/P ratio back to around 1.5, which is the theoretical value expected for tricalcium phosphate, however, the resulting film was porous and rough as seen in Figure 4.14 through Figure 4.17. The optimized stoichiometry can be seen in Figure 4.18.

Since the objective of the current research is to produce dense films with good stoichiometry equivalent to that of the target material, varying these parameters and optimizing the deposition process we were able to ultimately find the optimum parameters to achieve the desired results. The smoothest film was achieved at room temperature, input laser energy of 300 mJ, introducing argon as a background gas at 3×10^{-1} mbar, the use of 20×10 aperture and a fluence of 7.5 J/cm^2.

Figure 4.14 through Figure 4.17 illustrate the SEM visualization of the ternary compound ceramic deposited on magnesium and magnesium alloy substrates.

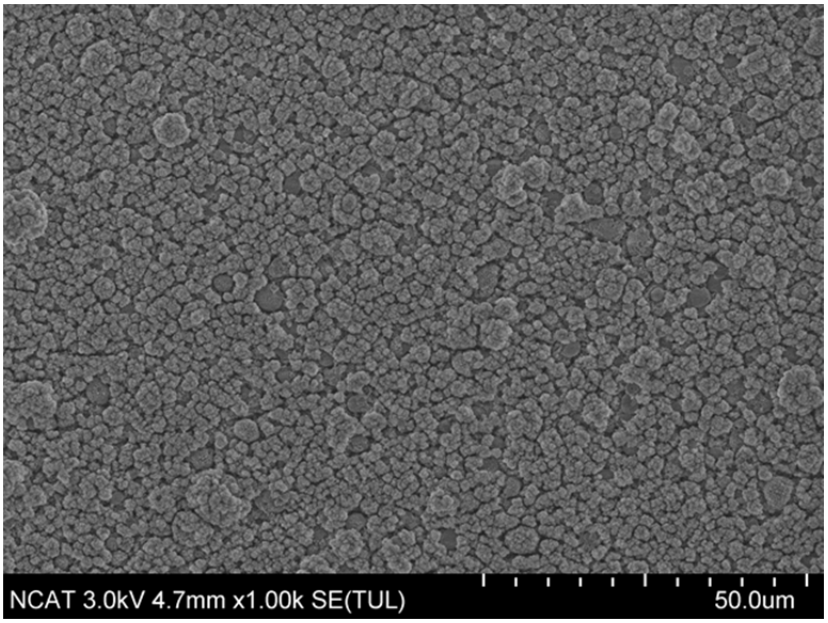

Figure 4.14 Magnesium substrate coated with doped TCP film, before optimization.

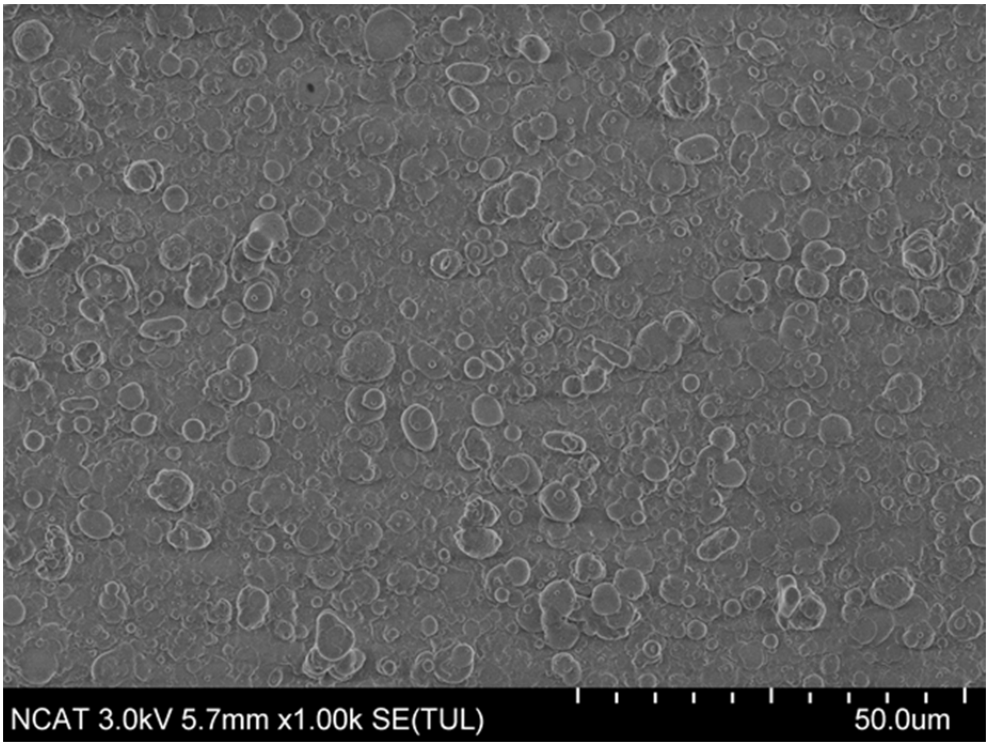

Figure 4.15 Magnesium substrate coated with doped TCP film, after optimization.

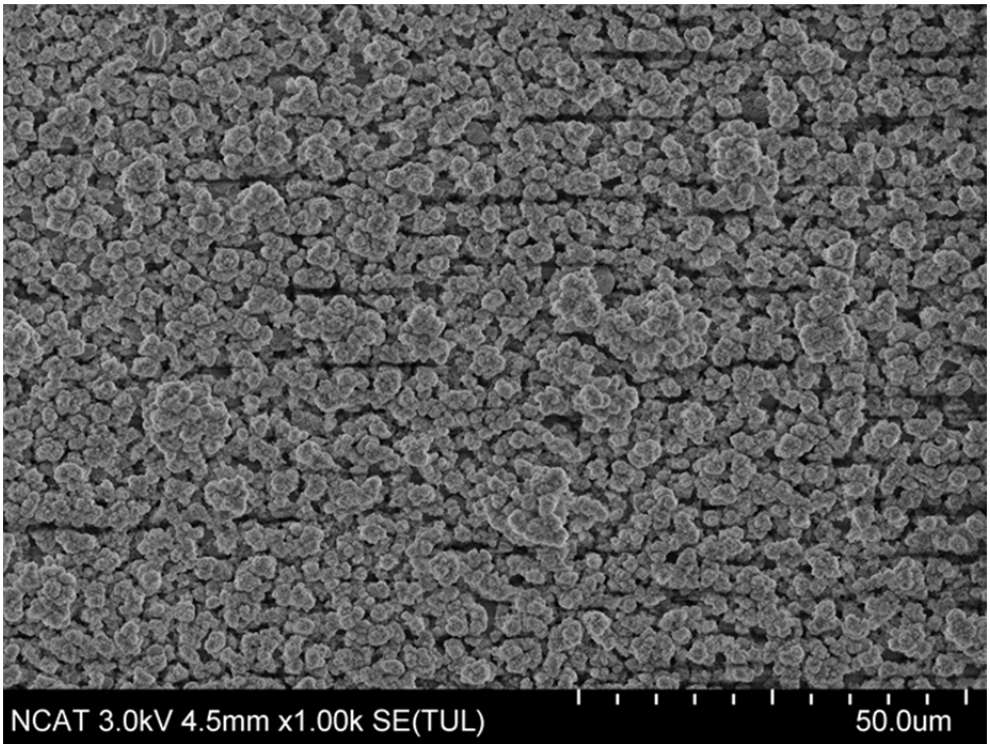

Figure 4.16 Magnesium alloy substrate coated with doped TCP film, before optimization.

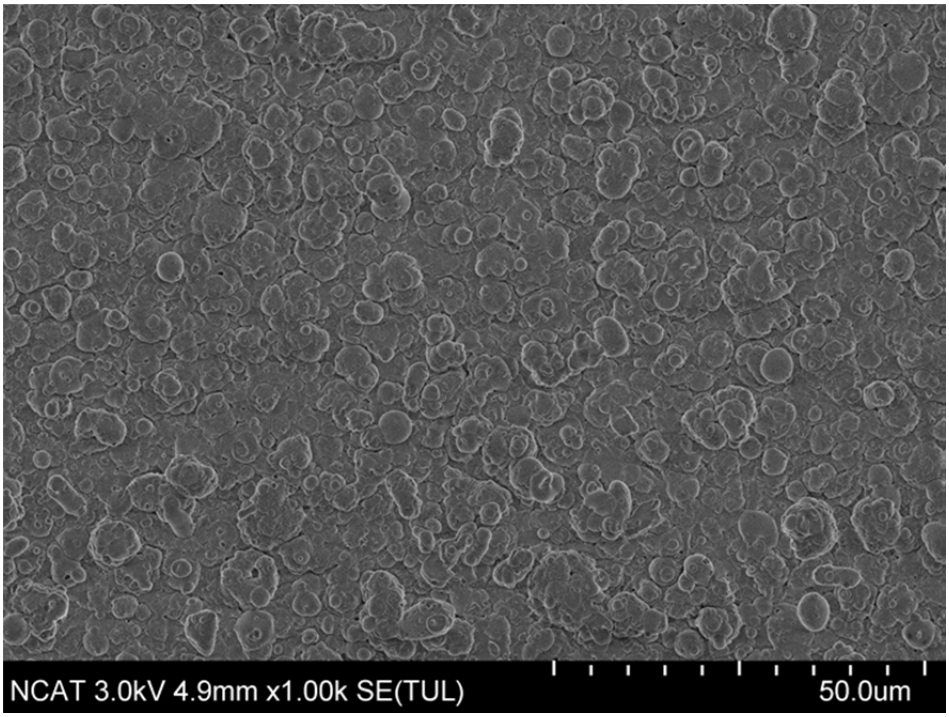

Figure 4.17 Magnesium alloy substrate coated with doped TCP film, after optimization.

4.3.1 Film growth. In order to determine the deposition rate of PLD films, we measured the thickness of the deposited film by using a stylus electromagnetic sensor (KLA Tencor Alpha-Step IQ®). The stylus profilometer is capable of measuring the step height (film thickness) and the surface roughness of the film. Masking the substrate during the deposition created a step height difference between the substrate and the deposited film. The film's average thickness was measured by tracing the surface of the sample; vertical displacements denote the change on the surface topography. From the observed average film thickness, the deposition rate of each sample was estimated using the following equation:

$$\text{Depositon rate} = \frac{\text{Film thickness}}{\text{Number of pulses}}$$

By default, the stylus profilometer is set to scan in the range of 20 μm/1.19 pm and the stylus force is set at 13 mg. For this study the stylus was set to scan over an area of 600 μm across a step with a scan speed of 20 μm/s and sampling rate of 50 Hz. The film thickness was

measured at more than 10 positions over the entire deposited/masked area on the sample. The average film thickness was estimated using two zones leveling technique.

The growth rate slightly increased with introduction of argon background gas, which means that the total amount of material delivered from the target to the substrate was almost constant over a wide range of argon pressures. By applying 50,000 pulses, the deposited rate of TCP coatings was found to be 4 nm/pulse, resulting typically on a film thickness in the range of 1 – 1.5 μm.

4.3.2 Ca/P ratio. The PLD process generally has a very energetic deposition flux. The particles in the flux have kinetic energies comparable to the bond strengths in the growing film. These energies promote surface diffusion on the growing film, resulting in high-quality films at lower substrate temperatures as compared with other thermal deposition techniques (Chrisey & Hubler, 1994). It has shown that particles with energies above 50 eV can cause material to be re-sputtered from the film surface (Willmott, 2004). This not only reduces the effective deposition rate but can also lead to a change in the stoichiometry of multi-elemental films by preferential resputtering. By introducing a background gas, such as argon in the present work, the entire kinetic-energy distribution can be shifted to lower values (Willmott, Timm, & Huber, 1997). The decrease in calcium deposition can be explained by a scattering of the plume with the background gas. Regarding phosphorus, however, the phosphorus deposition increased with the argon pressure despite plume scattering. The preferential resputtering phenomenon is likely to be more important than plume scattering for determining the amount of deposited phosphorus. A preferential resputtering of phosphorus from a calcium phosphate film was observed during the deposition of the calcium phosphate films, and an increase in the background argon pressure resulted in a better stoichiometry (lower Ca/P ratio) of the film (Koch et al., 2007). This is in

good agreement with the relationship between the Ca/P ratio of the ceramic and that of the film obtained through the PLD process under argon pressure in present work.

The chemical composition and the constituting phases of the films were analyzed using the EDX and the XRD techniques. Figure 4.18 shows the Ca/P ratios of the films determined by using EDX. The Ca/P ratio decreased from ~ 3.2 to ~ 1.5 with the introduction of argon background gas.

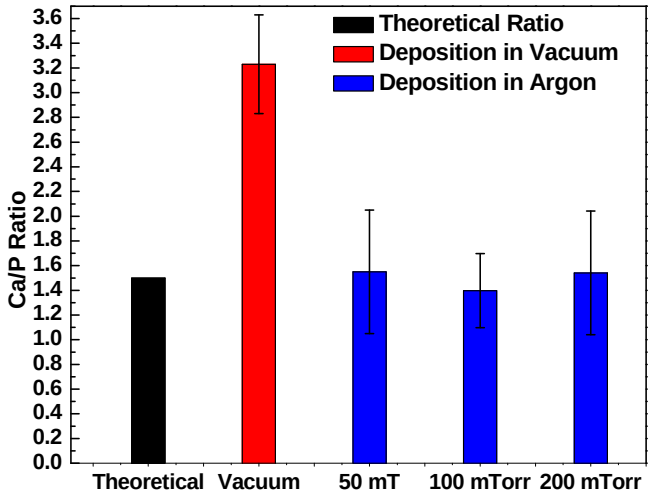

Figure 4.18 Ca-P ratio under different argon pressures.

4.4 X-Ray Diffraction

X-ray diffraction is a versatile, non-destructive technique that reveals detailed information about the chemical composition and crystallographic structure of natural and manufactured materials. A crystal lattice is a regular three-dimensional distribution (cubic, rhombic, etc.) of atoms in space. These are arranged so that they form a series of parallel planes separated from one another by a distance *d*, which varies according to the nature of the material. For any crystal, planes exist in a number of different orientations - each with its own specific d-spacing. When a monochromatic X-ray beam with wavelength λ is projected onto a crystalline material at an angle θ, diffraction occurs only when the distance traveled by the rays reflected

from successive planes differs by a complete number n of wavelengths.

Bragg's Law

By varying the angle θ, the Bragg's Law conditions are satisfied by different d-spacing in polycrystalline materials. Plotting the angular positions and intensities of the resultant diffracted peaks of radiation produces a pattern, which is characteristic of the sample. Where a mixture of different phases is present, the resultant diffractogram is formed by addition of the individual patterns.

Based on the principle of X-ray diffraction, a wealth of structural, physical and chemical information about the material investigated can be obtained. A host of application techniques for various material classes is available, each revealing its own specific details of the sample studied. X-ray diffraction at grazing incidence with a Cu Kα source was employed in order to detect crystalline phases at the interface. The X-ray diffractions at different incident grazing angles of the sample are shown in Figure 4.19.

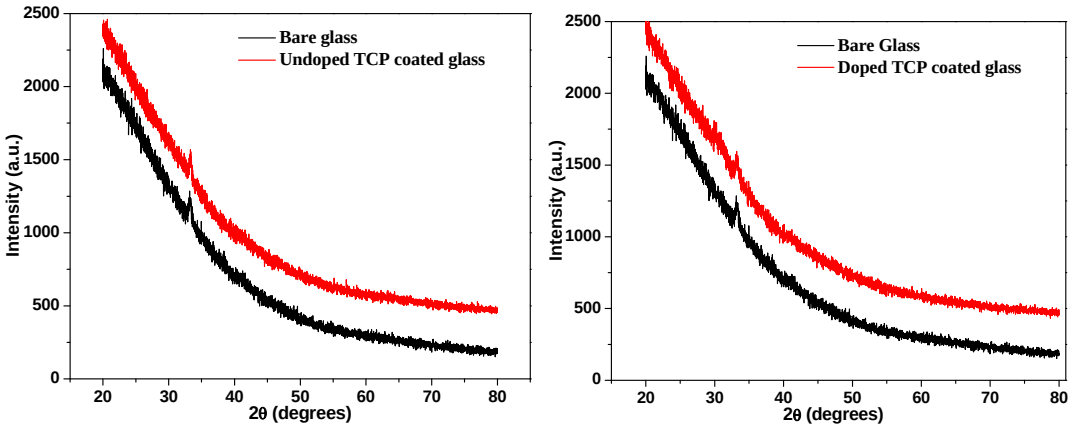

Figure 4.19 XRD pattern of the (a) undoped TCP coating on glass, (b) doped TCP coating on glass.

From the diffractograms obtained Figure 4.19 it seems that there is no crystalline film formation in the samples. From a physicochemical perspective, amorphous forms tend to be

more soluble in certain solvents due to their increased surface energy; a direct result of their less-ordered structures as compared to specific crystal structure in crystalline form, Figure 4.20 (Holmes & Bridges, 2004). The increase in surface energy allows for greater molecular interaction between different materials. Since the aim of this research is to develop biodegradable materials, it is desirable to have the films in amorphous form.

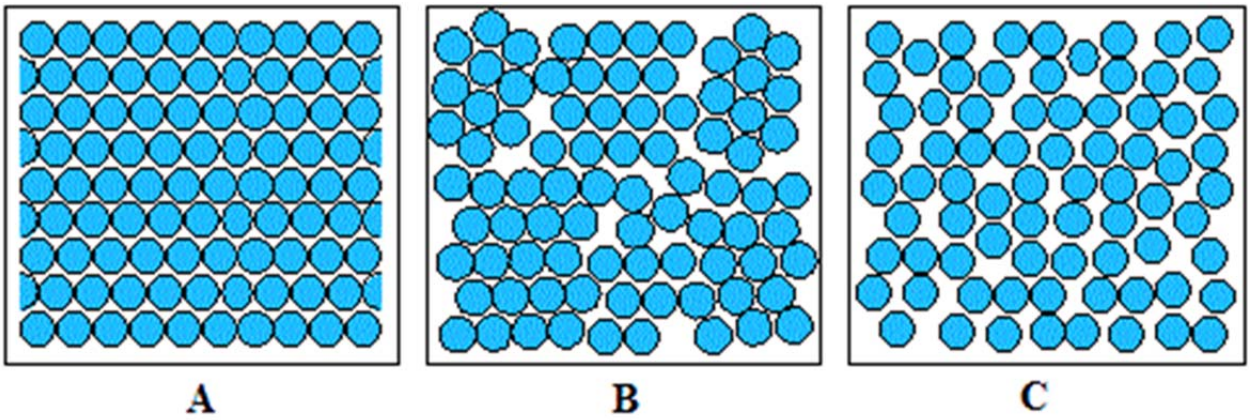

Figure 4.20 Aggregate of atomic arrangement (A) single crystal, (B) polycrystal, and (C) amorphous solid.

4.5 Mechanical Characterization

4.5.1 Nanoindentation tests. The mechanical property of hardness refers to a material's resistance to indentation either by a ball (Brinell test) or by a pyramidal diamond (Vickers test). Indentation hardness tests involve the measurement of the size of a residual plastic impression in the specimen as a function of the indenter load to provide a measure of the area of contact for a given indenter load, elastic modulus and hardness of the sample material from load-displacement measurements i.e. the depth of penetration beneath the specimen surface is measured as the load is applied to the indenter. The modulus of the sample material is then obtained from a measurement of the stiffness of the contact, that is, the rate of change of load and depth, and knowing the geometry of the indenter allows the size of the area of contact to be determined by

calculations. Depth and area of indentation are related to applied load, with high values reflecting hard materials and low values, soft materials.

The measurement of hardness is important, particularly when combining various materials for bearing or wear conditions. Nanoindentation has high accuracy and can be used for analyzing small sample areas, e.g.: Different grains/orientations. Real time measurements are possible when using nanoindentation testing and no optical measurements are required. Different indenter tips can be used depending on the application (Area function needs to be created). Stress-Strain curves can be generated with the same testing method. Creep and fatigue measurements are possible when using this instrument.

Mechanical properties of the dopant combination incorporated into TCP structure were evaluated via nanoindentation testing, using a Nano Indenter® XP system (MTS Systems Corporation). A Berkovich indenter (a three-sided pyramid with a face angle of 65.3°) was used. Depth sensing indentation tests were carried out on a reference sample of fused silica with a Poisson ratio of 0.17. Fused silica is usually chosen as a reference sample since its modulus is load independent. First, nanoindentation was performed to check the effect of dopant addition to the ceramic compact samples with average diameter of 1.3 mm and average height of 0.15 mm, and then the test was conducted on the corresponding material used as a coating on both the magnesium and its alloy substrates.

Structures with 1 wt % TiO_2, 1 wt % MgO and 0.5 wt % ZnO were tested for their elastic strength and compared with undoped TCP structures processed under the same conditions. Nine indentations were made on each sample. The results are an average of these nine indentations with controlled depths from 50 up to a maximum of 1500 nm. Other conditions were the same as for the reference. In each test run, the indenter was driven into the specimen surface (loading

half-cycle) under a load gradually increased to the predetermined peak value, unloaded gradually to 10 % of the peak load (unloading half-cycle) after being held at peak load for 30 s, and then driven again into the specimen surface to a higher value of the peak load. Such a procedure repeated for nine times with increasing peak loads and resulted in a load–displacement curve containing nine loading/unloading. Four samples of each composition were tested and results from the indentation testing were recorded.

The load–displacement curves obtained for the ceramic targets and deposited films are shown in figure 4.21 and Figure 4.22. For each material, averages of four measurements are given in this plot. For the ceramics in bulk form, the load-displacement curves from all the five measurements overlap with each other, indicating a high level of reproducibility. For the ceramics coated substrates, slight scatters exist among the different load–displacement curves. These scatters may be attributed to the softness or roughness of these amorphous ceramics deposited coating.

(a) Doped TCP **(b) Undoped TCP**

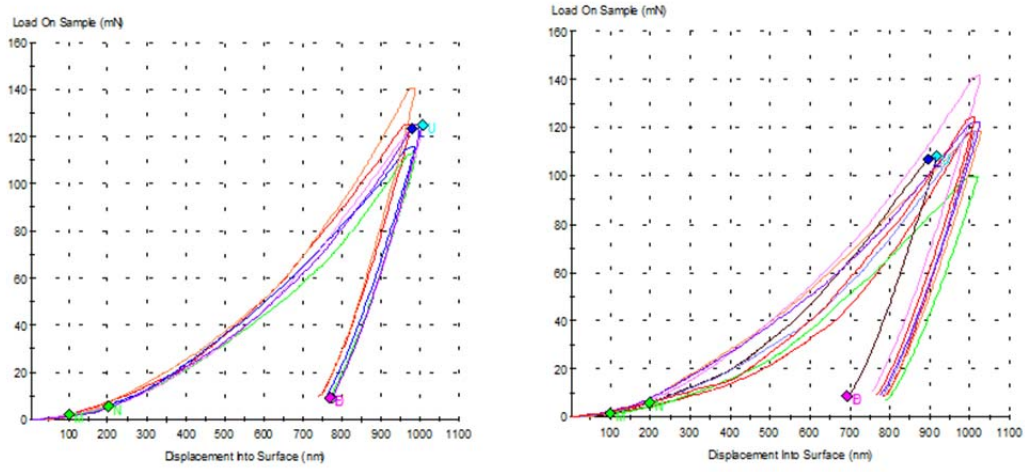

Figure 4.21 Load vs displacement curves for the ceramic compacts.

(a) Undoped TCP-on-Mg

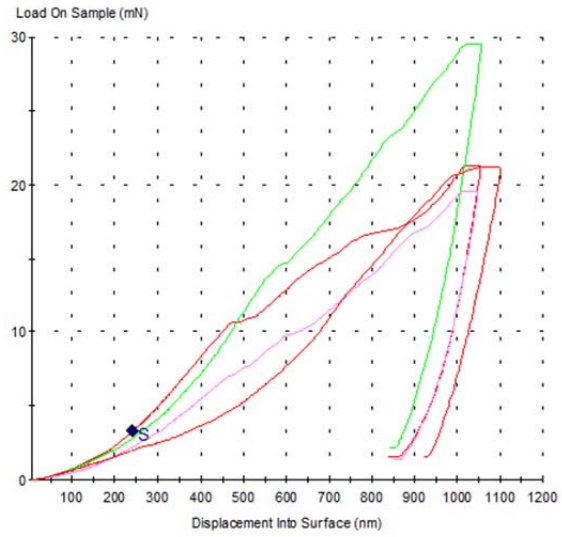

(b) Undoped TCP-on-Alloy

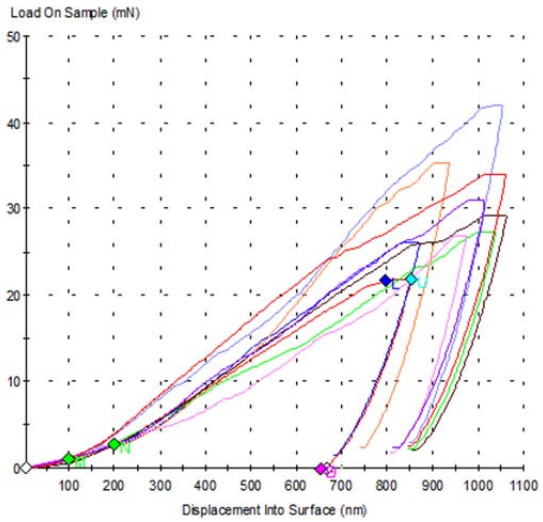

(c) Doped TCP -on-Alloy

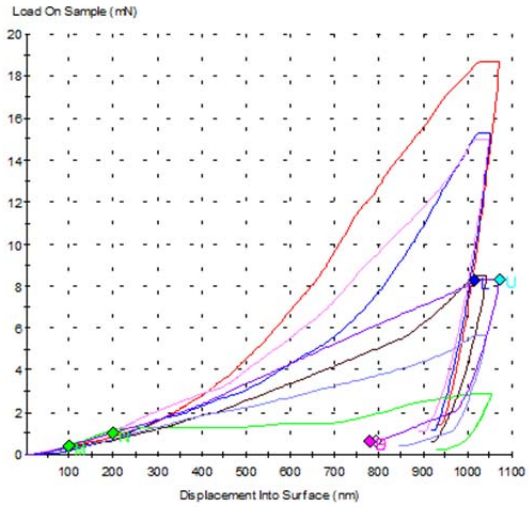

(d) Doped TCP -on-Mg

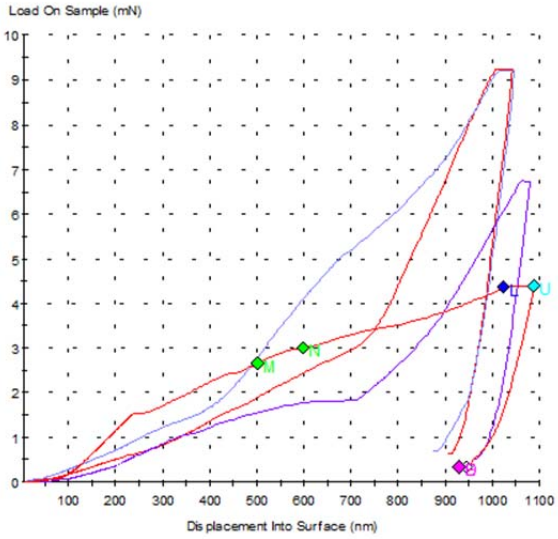

Figure 4.22 Load vs displacement for the coated samples.

Table 4.3

Hardness and modulus of elasticity resulting from nanoindentation

Sample	Hardness (GPa)	Modulus (GPa)
TCP	6.500	114.70
TC	6.950	132.70
TCP on Alloy	0.145	7.460
Doped TCP on Alloy	1.200	21.840
TCP on Mg	0.092	4.825
Doped TCP on Mg	0.840	21.400

A representation of the results obtained from the indentation tests performed on the ceramic targets and the deposited films are illustrated in Figure 4.23 through Figure 4.25.

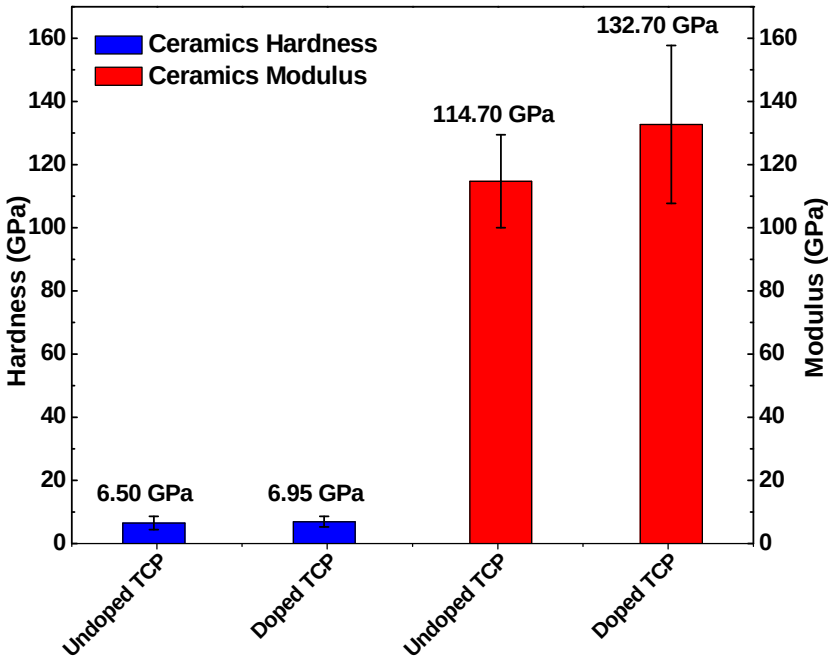

Figure 4.23 Hardness and modulus of the ceramic targets.

Nanoindentation test performed on the bulk ceramic targets revealed an increase in both

hardness and modulus as a result of dopant addition. Doping with the ternary compound increased the hardness slightly, by 6.92 %, and the modulus of elasticity by 15.69 %.

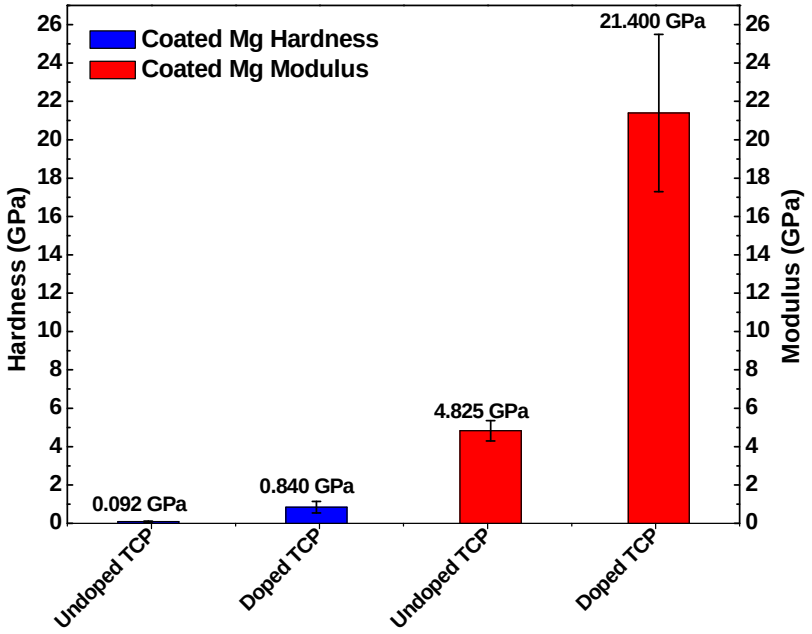

Figure 4.24 Hardness and modulus of TCP and doped TCP coated magnesium substrates.

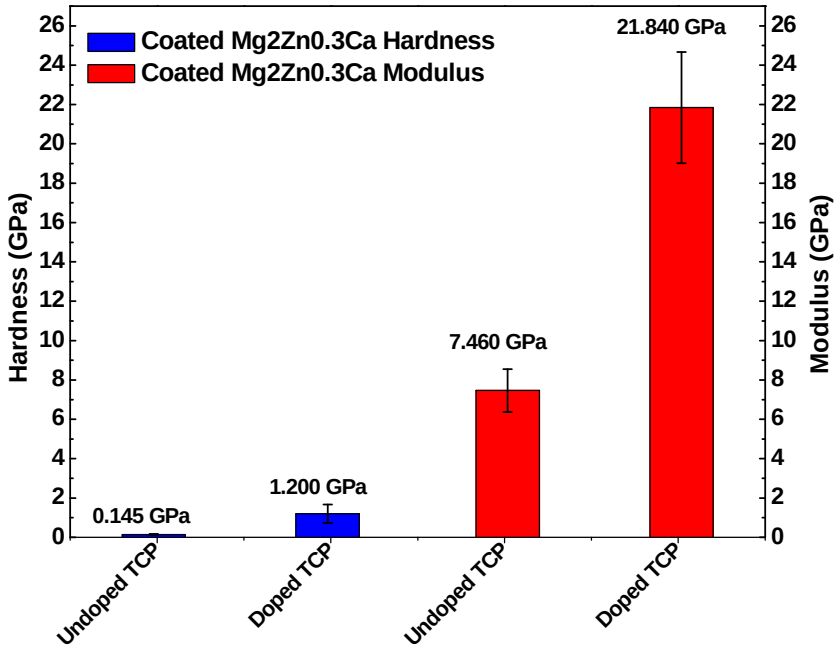

Figure 4.25 Hardness and modulus of TCP and doped TCP coated alloy substrates.

As inferred from Figure 4.25, doped TCP doped magnesium alloys have higher hardness

values than its counterpart coated with undoped TCP and the magnesium coated with both compositions, Figure 2.5. TCP coated magnesium is the softest, with a hardness of only 0.092 GPa, followed by TCP coated on the magnesium alloy, with a hardness of 0.145 GPa. Doped TCP coated on the magnesium alloy has the highest hardness of 1.2 GPa and doped TCP coated on the magnesium alloy is next at 4.1 GPa.

The elastic moduli of the four substrates are listed in Table 4.3. Similarly the doped TCP coating on the magnesium alloys exhibits the highest modulus of 21.84 GPa and doped TCP coating on magnesium is next with a modulus of 21.4 GPa. TCP coated on magnesium shows the minimum modulus of 4.83 GPa, followed by the undoped TCP coated magnesium substrate, with a modulus of 7.46 GPa. The somewhat lower modulus of deposited films, relative to bulk form (which is 114.7 and 132.7 GPa), is due to the fact that the TCP layers deposited by physical vapor deposition are amorphous.

From these results it can deduced that the addition of dopants to TCP resulted in an increase in both hardness and modulus of elasticity, thus, improving the mechanical properties of these materials to be used as load bearing implant materials.

4.5.2 Potentiodynamic polarization measurement. Electrochemical test was conducted in the SBF solution at room temperature. A three-electrode cell was used for the electrochemical measurements. The counter electrode made of platinum and a standard Ag/AgCl electrode was used as the reference electrode. The sample with an exposed area of 0.18 cm^2 was taken as the working electrode. The polarization scan was started from 300 mV below the anode corrosion potential at a constant voltage scan rate of 0.5 mV/s. Figure 4.26 through Figure 4.29 show the potentiodynamic polarization of the bare substrates and undoped TCP and doped TCP coated samples in SBF.

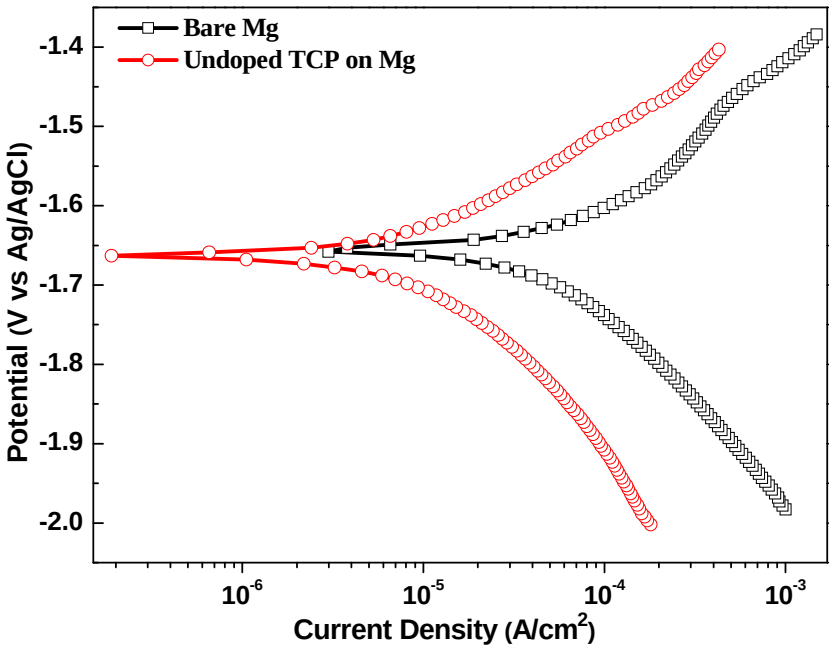

Figure 4.26 Potentiodynamic polarization curves for TCP coated magnesium samples in SBF solution.

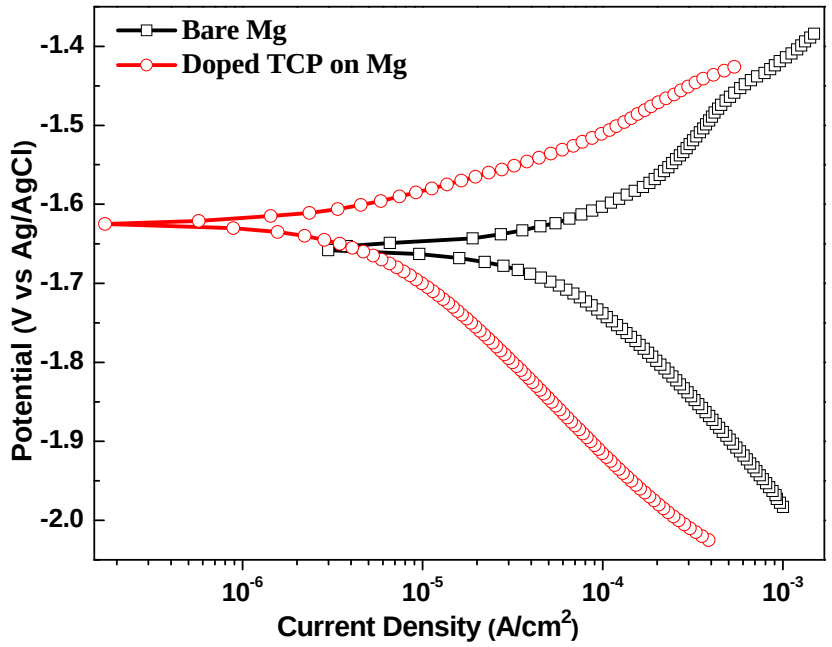

Figure 4.27 Potentiodynamic polarization curves for doped TCP coated magnesium samples in SBF solution.

The corrosion potential (E_{corr}) and corrosion current density (i_{corr}) obtained from these

curves are listed in Table 4.4. Coating the bare substrate with TCP showed a shifted toward to positive current by 0.3126 mA/cm^2, while the corrosion potential showed no change. These results are in agreement with results found in literature (Y. W. Song et al., 2008) who showed that coating metal implants with Ca-P inhibits the corrosion. When the magnesium substrate was coated with the doped TCP an improvement of 0.031 mA/cm^2 was seen in the current density as well a positive shift of 0.04 V in the corrosion potential when compared to that coated with the undoped TCP, so the addition of dopants would be beneficial since our results indicated that coating with the doped TCP will inhibit the degradation of magnesium in SBF.

Table 4.4

Corrosion current density (i_{corr}) and corrosion potential (E_{corr}) of coated magnesium substrates

Element	E_{corr} (V)	i_{corr} (A/cm^2)
Bare Mg	-1.66	3.66E-04
TCP on Mg	-1.66	5.34E-05

Element	E_{corr} (V)	i_{corr} (A/cm^2)
Bare Mg	-1.66	3.66E-04
Doped TCP on Mg	-1.62	2.27E-05

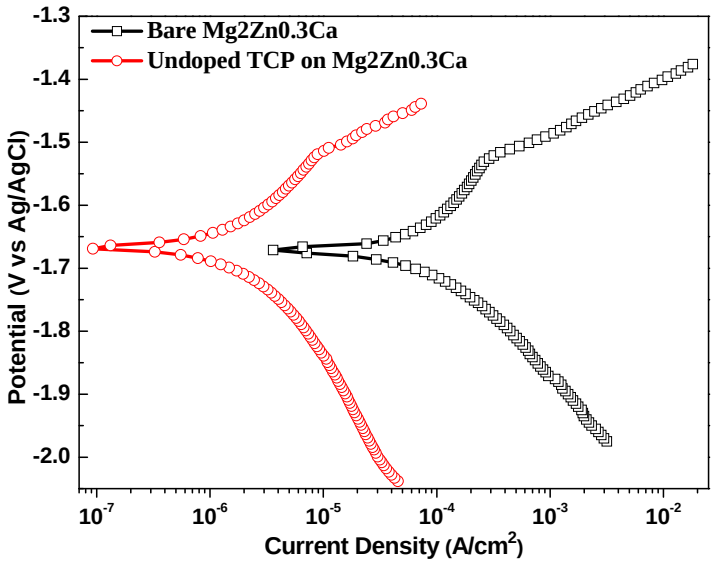

Figure 4.28 Potentiodynamic polarization curves for TCP coated alloy samples in SBF solution.

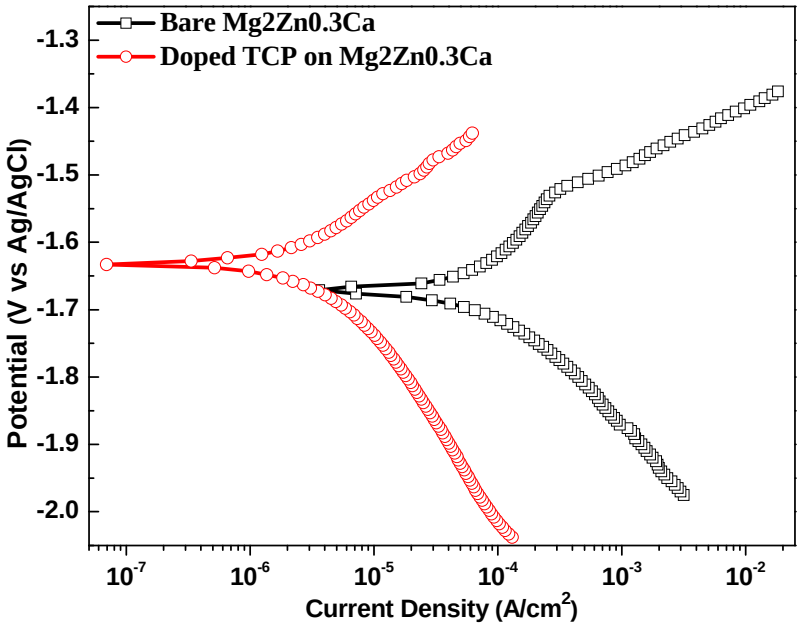

Figure 4.29 Potentiodynamic polarization curves for doped TCP coated alloy samples in SBF solution.

Similar trends can be seen on the magnesium alloy substrate as those seen on the magnesium substrates. The corrosion current density of the coated alloy is shifted toward to positive potential by 0.4596 mA/cm^2 when coated with TCP and 0.4523 mA/cm^2 when coated with doped TCP. Furthermore, coating with the doped TCP showed a positive shift in the values of the corrosion potential of the coated magnesium alloy, confirming that the corrosion resistance of the coated magnesium alloy should be enhanced. This is because the cathodic hydrogen evolution reaction is reduced after the magnesium alloy substrate is covered with doped β-TCP coating (Y. W. Song et al., 2008). The polarization analysis indicates that the coating can prevent the penetration of solution and effectively protect the magnesium and magnesium alloy from corrosion in physiological environment, thus coatings magnesium with the doped TCP can very well inhibit the anodic dissolution, indicating that the corrosion should be more difficult to happen on the coated substrates in the same medium. Table 4.5 summarizes the reduction in

corrosion rates of the magnesium alloys with different coatings.

Table 4.5

Corrosion current density (i_{corr}) and corrosion potential (E_{corr}) of coated magnesium alloy

Element	E_{corr} (V)	i_{corr} (A/cm^2)
Bare Alloy	-1.67	4.76E-04
TCP on Alloy	-1.67	1.64E-05

Element	E_{corr} (V)	i_{corr} (A/cm^2)
Bare Alloy	-1.67	4.76E-04
Doped TCP on Alloy	-1.63	2.37E-05

4.6 Biological Characterization

4.6.1 Mineralization studies. The formation of a bone like apatite layer on biomaterials is thought to promote osteo-conductivity, inducing bone formation on the biomaterials (van Blitterswijk et al., 2008). Bioactivity of bioceramics relies on their ability to induce hydroxyapatite formation in simulated body fluid (SBF). This ability is an indication of bioactivity for bioceramics (Ramila & Vallet-Regi, 2001). Beside the formation of HA other phases of calcium phosphate may be formed in the physiological environment (W. E. Brown, Eidelman, & Tomazic, 1987). Other forms of calcium phosphate phases may be present as a result of exposure to SBF. Such calcium phosphates may consist of octacalcium phosphate (OCP) and dicalcium phosphate dehydrate (DCPD), these ceramics are considered as a precursor phase of HA formation (J. Elliot, 1994; Leng, Chen, & Qu, 2003). Because OCP and DCPD are the kinetically more favorable phases, the stable thermodynamic structure of apatite does not ensure that the most favorable precipitation phase from the calcium and phosphorous solutions is HA (Berland, Boistelle, & Olmer, 1990). Theoretical analysis based on nucleation kinetics indicated that the OCP nucleation rates could be much faster than that of HA in the physiological environment (Lu & Leng, 2005).

For this research, characterization of the apatite formation was not done due to the

complications of the process; however, we concluded that the apatite is more favorable to be HCA or OCP, based on literature. The apatites found in this experiment had different morphologies; further research is needed to pinpoint what calcium phosphate phase each morphology represents.

Films were fabricated on silicon wafers to determine the mineralization on the surface and to remove the effect of magnesium corrosion when studying the properties of the deposited films. All disk samples were subjected to biological study in simulated body fluid up to 10 weeks and the films were exposed to SBF for 4 weeks. Scanning electron micrographs were recorded at the 0, 2, 4, 8, and 10 weeks points of the experiment for the ceramics and at the 2, 3, 4, 7, 14, and 21 days points for the films. Figure 4.30 through Figure 4.35 illustrate the apatite growth on the ceramic compacts after soaking in SBF for ten weeks, and those of the deposited films after soaking for three weeks.

At each time point, samples of each composition were taken out, washed with distilled water, and then dried for two days. Once dried, the weight of each sample was carefully recorded and compared with their dry weight before immersion. Surface microstructures of the samples were observed using SEM to determine the morphology of the apatite layers. Some samples revealed formation of an apatite layer on the surface, which is good for cell adhesion and provides sites for exceptional implant-tissue interfacial bonding.

Undoped TCP as shown in Figure 4.30 was used as control in the SBF solution to visualize the effect of the dopants in reference to the undoped compacts.

TCP exhibited less ability to induce calcium phosphate apatite formation on its surface than the doped samples; Xin has also reported similar trends with TCP in SBF (Xin, Leng, Chen, & Zhang, 2005). Kotani et al. investigated the bone bonding ability to β-TCP and showed that

there's a strong bond despite the lack of apatite formation on the surface (Kotani et al., 1991).

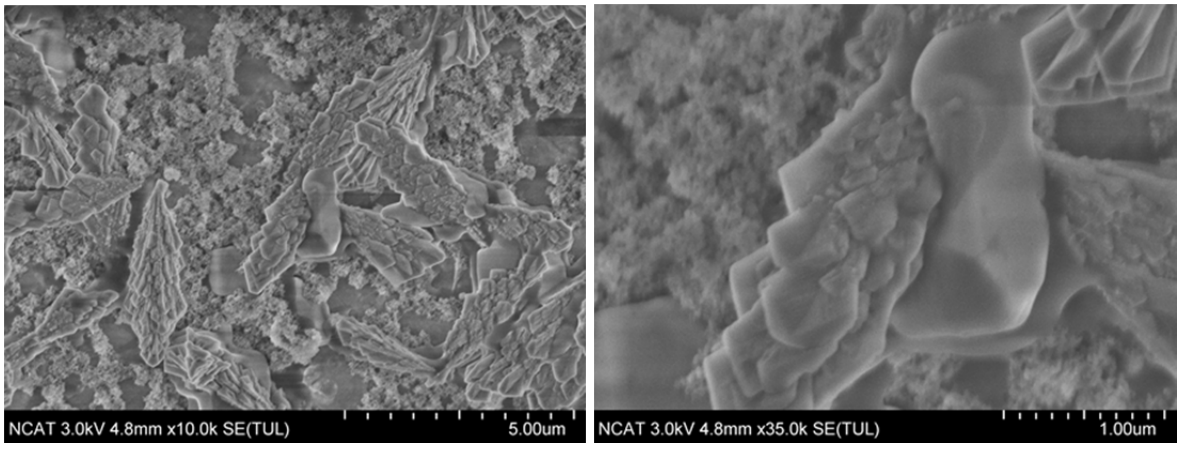

Figure 4.30 Apatite growth on undoped TCP compacts in SBF for 10 weeks, high and low magnification.

After ten weeks the samples were filled with apatite. The apatite formation may have been due to the local release of calcium and phosphorous, which may be more favorable to promote apatite growth. We can conclude that apatite formation was actively occurring in the TCP ceramics over the ten week SBF treatment.

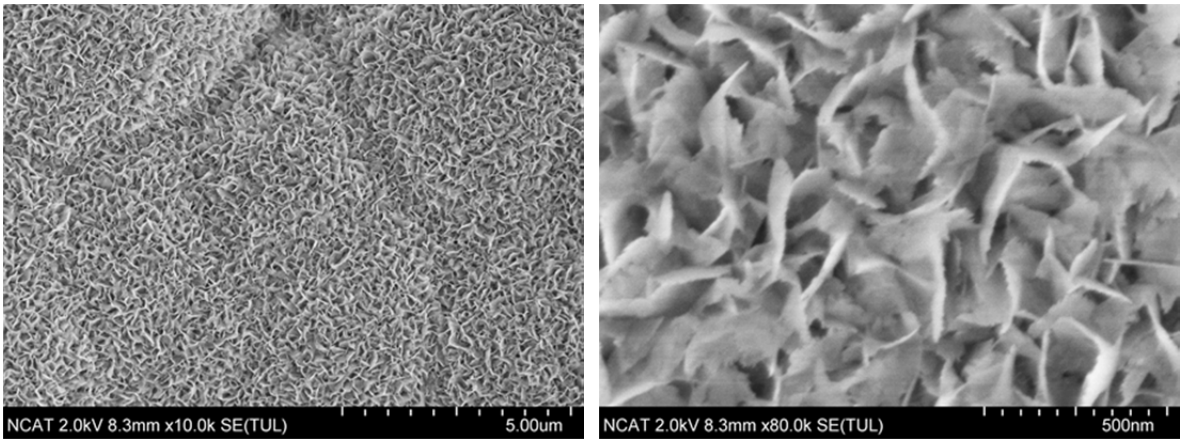

Figure 4.31 Apatite growth of TCP - 1 % TiO_2 compacts in SBF for ten weeks, high and low magnification.

Beginning at the two weeks point there is growth of apatite layer on the surface of the compacts; due to significant apatite growth the grain structure could hardly be seen. A flake-like

apatite layer was formed on the surface of these samples; we believe that the phase of this bone-like apatite is either HCA or OCP. There was enough apatite formation to cover the entire surface of the sample. We concluded that the presence of TiO_2 (1 wt %) increased the bioactivity of TCP due to the increased amount of apatite on the surface after soaking for 10 weeks in SBF, as shown in Figure 4.31. This layer would be ideal for osteoblast cell adhesion, thus, providing good cell-material interfacial bonding.

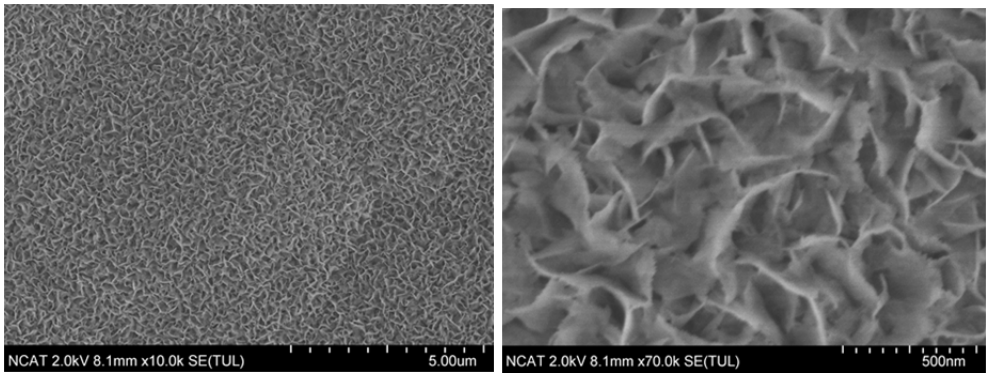

Figure 4.32 Apatite growth of TCP - 0.5 % ZnO in SBF for ten weeks, high and low magnification.

In Figure 4.32 the surface microstructure of TCP-ZnO composition showed changes as well throughout the experiment. There was no visible degradation of the grain boundaries. There was also an apatite layer formation and no significant increase in surface porosity.

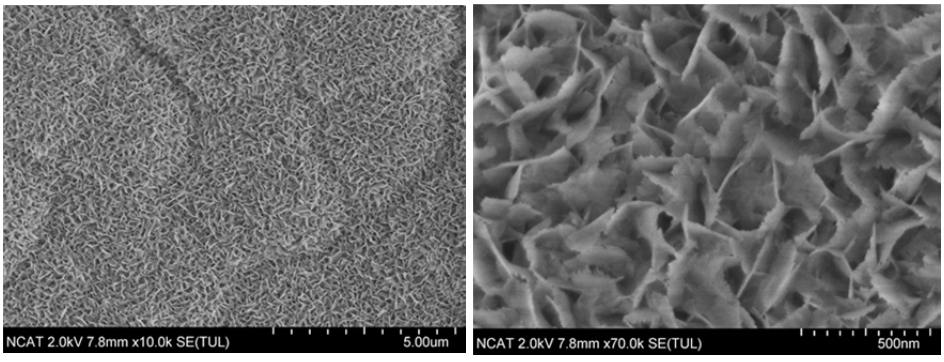

Figure 4.33 Apatite growth of TCP - 1 % MgO in SBF for ten weeks, high and low magnification.

In the case of the TCP-MgO composition, as shown in Figure 4.33 we observed very distinct apatite growth on the grain boundaries. We also observed very unique crystal-like apatite formation on the surface microstructure up to 10 weeks. These crystals are similar to the OCP crystals found by the electrochemical method (E. Zhang et al., 2005).

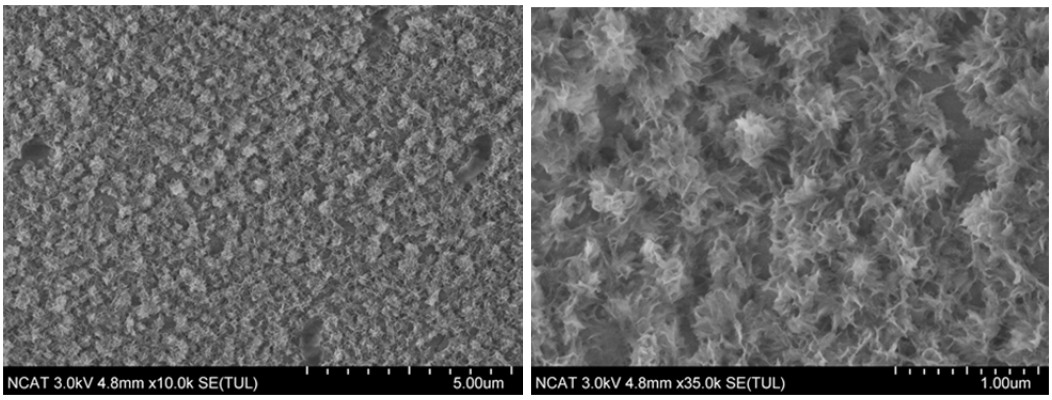

Figure 4.34 Apatite growth on the ternary compound doped TCP in SBF for ten weeks, high and low magnification.

The TCP-ternary composition in Figure 4.34 showed a significant ability to promote apatite formation on the surface, apatite was found to confluence and cover the surface of the ceramic compact where the grain boundaries were no longer visible. The increase in weight after ten weeks of soaking in SBF correlates the apatite growth on the surface in this combination of dopants.

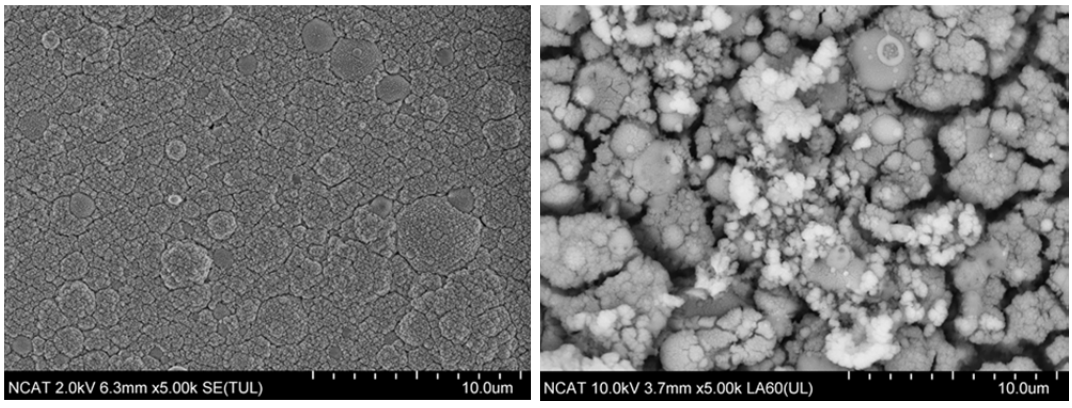

Figure 4.35 (a) TCP film before SBF exposure, (b) Apatite growth after 3 weeks in SBF.

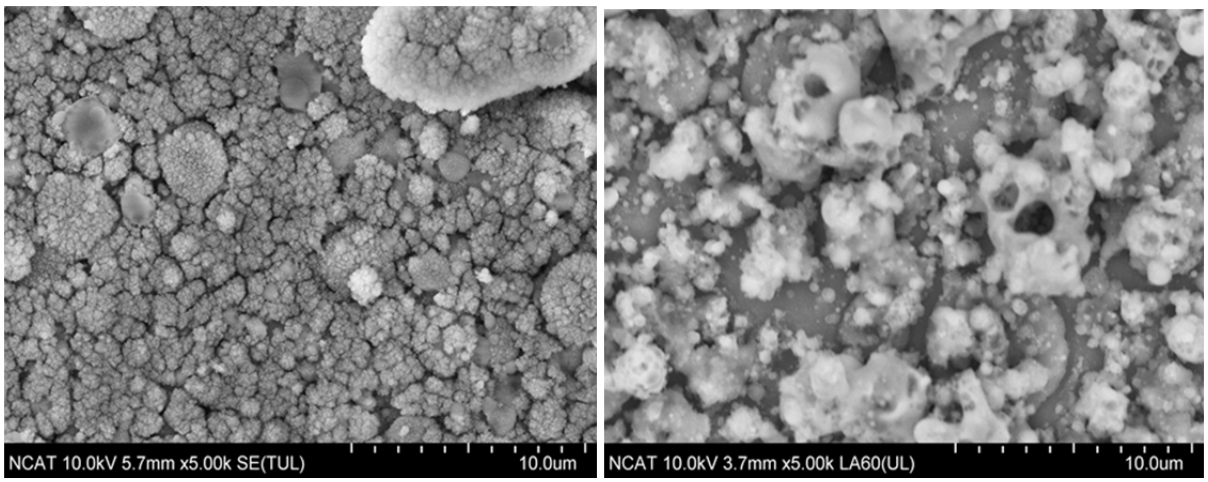

Figure 4.36 (a) doped TCP films before SBF exposure, (b) Apatite growth after 3 weeks in SBF.

Figure 4.35 and Figure 4.36 show SEM images of the coated Si before and after immersion in the SBF solution for 23 days. It can be seen from Figure 4.35 (a) and (b) that the morphology is obviously different than that of the coating before immersion. After 21 days immersion, a bulk-structure phase is formed on the surface shown in Figure 4.36 (a) and (b).

4.6.2 Weight change. In this experiment weight change was used to determine apatite formation and/or degradation of TCP/ doped TCP ceramics. The data collected was the weight change of the post SBF compression compacts. An initial weight was measured before SBF treatment and compared to the final weight after treatment. Weight loss is a sign of occurring dissolution because ions are being released from the ceramic compacts causing a slight decrease in bulk sample weight; however, when these Ca-P ions react with other ions in the SBF solution it is possible to form a calcium phosphate apatite layer on the surface or inside the sample; when this happens the apatite formation has a greater effect on the weight property of the ceramic than does the dissolution effect.

As expected, the samples that showed an increase in weight also showed apatite formation on the surface and inside the samples. Similarly, samples that revealed no significant change in weight also did not show apatite formation.

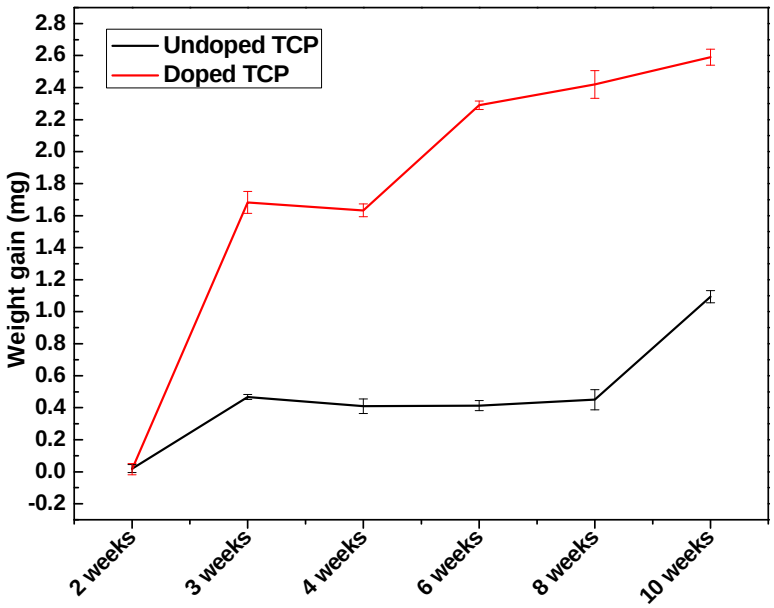

Figure 4.37 Weight gain of ceramic compacts as a result of exposure to SBF for 10 weeks.

Figure 4.37 shows the effects of weight change on TCP versus the various combination of doped TCP. All samples showed an increase in weight up until week 8, where the undoped TCP showed a decrease due to the dissolution of the ceramic in the physiological environment.

4.6.3 Cell viability tests. Cell culture was done using osteoblast precursor cell line (MC3T3-E1) to determine if there were any toxic effects caused by the addition of dopants into TCP. It is important that the dopants do not compromise the biocompatibility of TCP by causing any cytotoxicity. If the osteoblast cells are not affected by the dopants then they would tend to spread out and occupy as much surface area as possible, thus, having a more flattened structure. However, if there were some toxicity on the surface of the material; the cells would rather adhere to themselves than the material's surface therefore; they form a sort of ball structure that would have the least amount of interaction with the surface. This cell culture experiment was done at two intervals, 1 day for the films and 5 days for the ceramics.

Pre-osteoblastic mouse calvaria-derived cells (MC3T3-E1) were used to study the cell–material interactions. All samples were sterilized by autoclaving under a UV light for 30 min.

Cells were seeded onto the disk compacts, bare metals, and ceramic coated metals placed in 24 well plates. The base medium for this cell line is α-MEM supplemented with 10 % fetal bovine serum (FBS) and 1 % penicillin-streptomycin solution (without phenol red). Cultures were maintained at 37 °C under an atmosphere of 5 % CO_2.

Cell viability

To determine the cell viability after seeding onto different substrates, the cultures were incubated with calcein-AM and ethidium homodimer for 30 min and monitored under a fluorescence microscope at each stage of cell culture. Figure 4.38 through Figure 4.40 show the overlapping green and red fluorescence observed when the living cells were incubated with the dye mixture. Ethidium homodimer penetrates dead/permeable cells and gives a red fluorescence, while calceine fluorescence green. In our experiments we found the red fluorescence was negligible on the bulk ceramics and the coated metals, while the bare metals showed a significant number of dead cells, suggesting that most of the cells attached to the ceramics and coated metals were healthy and evolved continuously.

Since magnesium is very well known to have high dissolution rates and the solubility of apatite is inversely related to its crystallinity, it was expected that all the doped coatings, being amorphous, would not endure a 5-day test, thus, the tests for the coated and uncoated metals was conducted for 1 day, while the ceramics were cultured for 5. The stability of the TCP coating is crucial in the early stage of the bone mineralization process. If the TCP coating dissolves too rapidly in vivo, osteoblast contact with the implant surface is likely to be reduced. In contrast, an excessively crystalline coating will inhibit cell proliferation.

Samples tested for osteoblast viability included: (A) Magnesium substrates, (B) Mg2Zn0.3Ca substrates, (C) β-TCP coated on both (A) and (B) substrates, and (D) doped β-TCP

coated on both metal substrates. All coated samples statistically increased osteoblast adhesion above that for the uncoated metals.

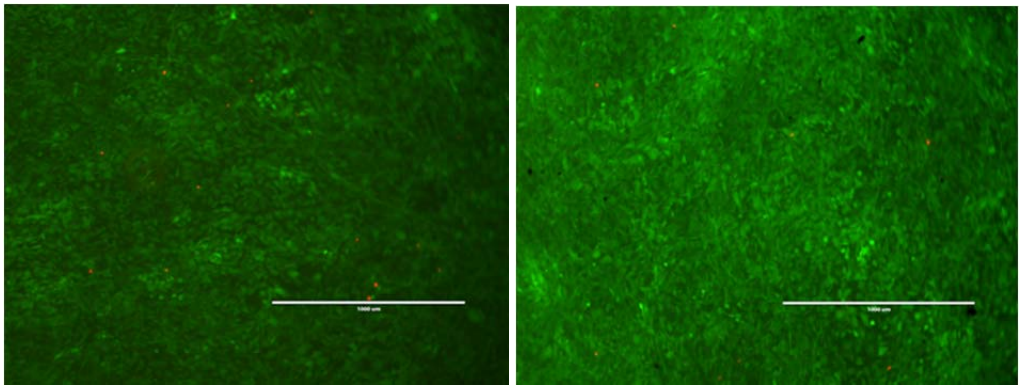

(a) Undoped TCP ceramic (b) Doped TCP ceramic

Figure 4.38 Live-dead fluorescence images of the ceramic compacts after 5 days cell seeding.

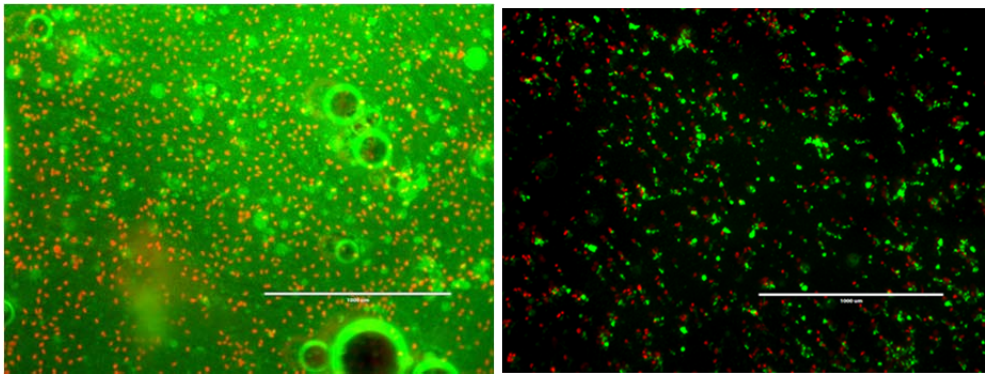

(a) Undoped TCP on Mg (b) Undoped TCP on alloy

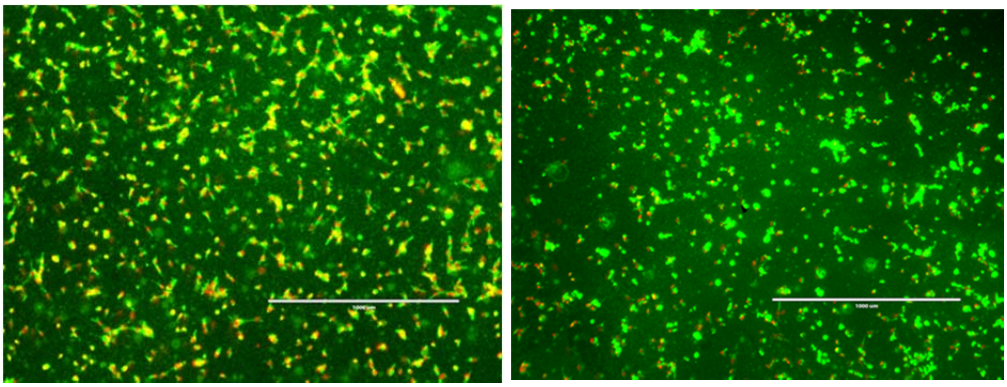

(c) Doped TCP on Mg (d) Doped TCP on alloy

Figure 4.39 Live-dead fluorescence images of the coated metals after 1 day cell seeding.

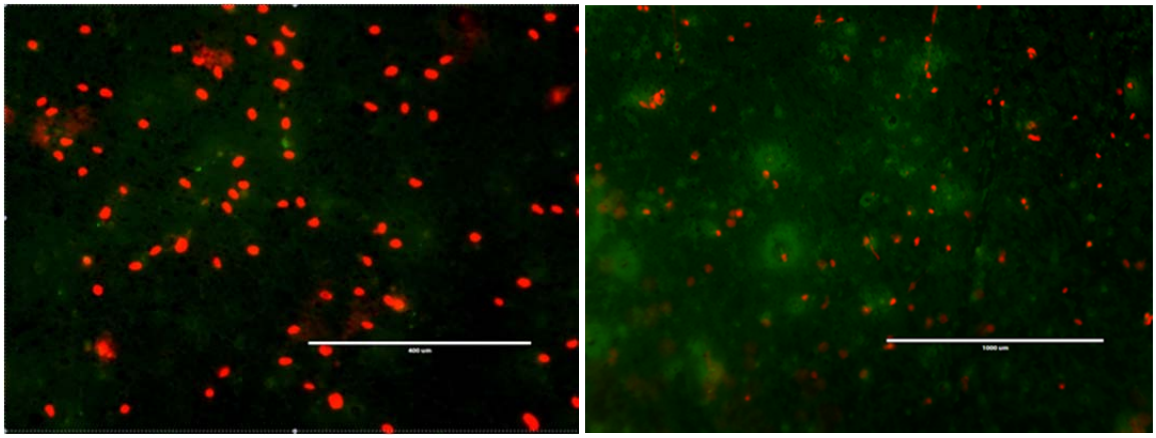

(a) bare Mg (b) bare alloy

Figure 4.40 Live-dead fluorescence images of the bare metals after 1 day cell seeding.

After 5 days of culture, cells showed spreading on the surfaces of both undoped and doped β-TCP ceramic compacts as shown in Figure 4.38 (a) and (b), most cells fluoresced green indicating that most remained alive and there was a negligible amount of red fluorescence indicating dead cells. On both samples, cells formed a well-flattened confluent layer covering the entire surface. For the coated metals, the amount of live cells was more pronounced on the samples coated with the doped β-TCP when compared with bare substrates and those coated with β-TCP as shown in Figure 4.39 (a) though (d). Figure 4.40 show the fluorescent images of cells seeded on bare substrates and cultured for 1 day as inferred from the images, there was barely any cell attachment.

It is presumed that such improvements in osteoblast adhesion may be attributed to the surface chemistry and grain size, which are the major difference between the TCP coating and the bare metals tested. The TCP coating has an average grain size of 2 to 3 μm, compared to those for the blank substrates. This translates into increased surface area and more defects/artifacts, which may be an important mechanism to enhance the interaction between osteoblasts and the coating. Also, the surface of the doped and undoped TCP coatings are

bioactive and well mimic the natural chemical environment in the bone tissue, which may also be favorable for cell attachment and growth. Therefore, reinforced TCP may be the most desirable coating to encourage cell attachment, because it is degradable and can stimulate bone in-growth as it dissolves gradually in the physiological environment.

CHAPTER 5

Conclusions and Future Work

5.1 Conclusions

The objective of this research was to develop biodegradable Ca–P coatings mainly consisting of β-TCP, on magnesium and magnesium alloy substrates by pulsed laser deposition. To achieve this objective, a number of key steps were taken throughout the project. The first key step was to develop and fabricate a ceramic compound using β-TCP. The second key step was to dope β-TCP with metal oxides consisting of MgO, ZnO, and TiO_2 to improve the sintering effect.

The third step was to fabricate β-TCP coating by pulsed laser deposition technique. Following that, the samples were structurally, mechanically, and biologically characterized to investigate the effect of dopant addition. It was found that the doped calcium phosphate ceramics were the most favorable materials to be used as a coating to improve the corrosion properties of the magnesium alloys. Cell culture was also conducted to study the bioactivity of the β-TCP coated scaffolds.

A number of conclusions can be drawn from this project:

- The method of fabricating the β-TCP target was explored by doping with three metal oxides: MgO, ZnO, and TiO_2. By varying the amount of dopant added into the β-TCP powder, it was discovered that the most favorable combination for making the TCP target was when 1 wt % MgO, 0.5 wt % ZnO, and 1 wt % TiO_2 were added and sintered at 1250 °C for 2 hours. This conclusion was supported by the relevant tests conducted throughout the project.
- In order to improve the mechanical and corrosion properties of the implant, a magnesium

alloy Mg2Zn0.3Ca was used. Magnesium alloyed with zinc (Zn) and calcium (Ca) is known to improve on the corrosive nature of the material and inhibit hydrogen gas evolution during degradation.

- To optimize the PLD deposition parameters, the laser fluence at the target was varied from 6 to 20 J/cm^2 by varying the laser energy between 300 to 400 mJ and the use of an aperture at the site of the laser exit from no aperture to 10 × 4 mm. By using these parameters, the laser fluence and spot size were calculated, and experiments were conducted to find the growth rate and roughness of the deposited films. The optimum smoothest film was achieved at room temperature, by introducing argon as a background gas at 3×10^{-1} mbar, the use of 20×10 aperture, and input laser energy of 300 mJ producing a fluence of 7.5 J/cm^2.
- Two types of coatings were investigated, undoped β-TCP and β-TCP doped with ternary compound [1 wt % MgO, 0.5 wt % ZnO, and 1 wt % TiO_2] used for enhancing the mechanical and corrosion properties. It was discovered that the magnesium substrate coated with the doped β-TCP had higher hardness (4.825 GPa) and modulus of elasticity (21.4 GPa) than the one coated with undoped β-TCP (0.092 GPa) and (0.84 GPa). Similarly, coatings on the magnesium alloy showed the ternary compound doped TCP to have a hardness of (21.84 GPa) and modulus of elasticity of (7.46 GPa), while the undoped TCP coatings had a hardness of (0.145 GPa) and a modulus of (1.2 GPa). Therefore, these devices could be potentially used as implant materials for bone formation.
- One of the primary concerns about surface coating of magnesium alloys is their effectiveness in corrosion resistance. It can be seen that β-TCP ceramic coatings can

reduce the corrosion rate of the magnesium alloy substrate by approximately 88 %. In comparison, ternary compound coated samples showed more than 95 % reduction in corrosion rate could be obtained.

- In terms of analyzing the bioactivity of the β-TCP coatings, the first major study was to evaluate the mineralization ability by soaking the samples in simulated body fluid and studying the resulting apatite formation on the surface, the weight gain as a result of the apatite formation, and investigation of any dissolution resulting from the exposure to the physiological environment over a period of ten weeks. It was found that the addition of dopants to β-TCP promoted apatite formation on all the samples studied in the present research.
- The second major biological study was to determine the cell viability on the coated samples by utilizing live-dead assay and visualizing under a fluorescence microscope. Cell adhesion, proliferation and differentiation behavior are significantly improved for the doped TCP coated alloy compared with bare magnesium substrates, indicating that the β-TCP and ternary compound doped TCP coated samples offer a biologically favorable environment. Therefore applying β-TCP and ternary compound coatings on the surface of the magnesium alloy has shown that it is biocompatible, does not introduce any toxic element. In addition, the improved biological response to the doped TCP coated alloy is believed to be closely related to its corrosion resistance, since normally the cytotoxicity of magnesium alloys is due to the high corrosion rate resulting in gas pockets next to the implant site.

In summary, coating with oxide-reinforced β-TCP might be promising for the surface treatment of magnesium alloys that exhibited good corrosion resistance and

surface biocompatibility.

5.2 Recommendations for Future Work

It is recommended that the findings of this study be utilized to help enhance the bone formation process. In future work, there are a few aspects that can be improved. In terms of fabrication, PLD being a very versatile method, offers great benefits for fabricating multicomponent thin films, however, there are several obstacles that must be overcome to improve and control the composition of the films over the selected substrate surface such as optimizing the fluence of the laser on the target, high energy input leads to splashing of the deposited species while low energy input leads to low deposition rates. In addition, new techniques have to be developed for fabricating films with better uniformity and improved stoichiometry. The impact of PLD coating on implant fabrication will be greatly enhanced with the development of new techniques that allow for coating of holes, grooves, and curved surfaces.

Based on the promising results obtained from the current research arises the possibility of investigating the use of alternative dopants in TCP or combinations such as SrO, SiO_2, Ag_2O, NaF, and CaO to produce coatings that will promote bioactivity and improve on the mechanical properties, the TCP sintering process and enhance the corrosion resistance of the metal implants. Although attempts have been made to develop advanced engineering ceramic materials with improved or novel properties through the incorporation of the aforementioned oxides, no studies have been conducted to investigate their combined properties when applied as thin film coatings. It is expected that the inclusion of these metal oxides in a ceramic matrix will produce composites possessing high stiffness and improved mechanical properties compared with a single-phase ceramic material.

The results showed that incorporating metal oxides into TCP ceramic material induced

improved mechanical properties and enhanced osteogenesis within the implants in in vitro testing. In future work different metal oxide components could be added into the TCP coating to help the promote bone formation and in vivo testing should be conducted to verify the results for clinical applications.

References

A.D.A.M., I. (2006). Fracture Fixation Devices. from http://health.allrefer.com/about/adam.html

Abidin, N. I. Z., Martin, D., & Atrens, A. (2011). Corrosion of high purity Mg, AZ91, ZE41 and Mg2Zn0.2Mn in Hank's solution at room temperature. *Corrosion Science, 53*(3), 862-872. doi: 10.1016/j.corsci.2010.10.008

Agna, J. W., Knowles, H. C., Jr., & Alverson, G. (1958). The mineral content of normal human bone. *J Clin Invest, 37*(10), 1357-1361. doi: 10.1172/jci103725

Ahn, J. S., Cha, J. O., Shin, C. H., Yeo, S. J., Im, H. J., Sakai, J., . . . Nam, T. H. (2007). Effect of ambient Ar gas on the composition control and crystalline properties of TiNi thin films fabricated by using pulsed laser deposition. *Journal of the Korean Physical Society, 50*(6), 1750-1754.

Akao, M., Aoki, H., Kato, K., & Sato, A. (1982). Dense polycrystalline beta-tricalcium phosphate for prosthetic applications. *Journal of Materials Science, 17*, 343-346.

Al-Abdullat, Y., Tsutsumi, S., Nakajima, N., Ohta, M., Kuwahara, H., & Ikeuchi, K. Surface modification of magnesium by NaHCO3 and corrosion behavior in Hank's solution for new biomaterial applications. *MATERIALS TRANSACTIONS, 42*(8), 1777 - 1780.

Altieri, C., Flores, J., Gonzalez, V., & Rodríguez, A. Biomechanics of Orthopaedic Fixations.

Ando, J. (1958). Phase Diagrams of Ca3(PO4)2-Mg3(PO4)2 and Ca3(PO4)2-CaNaPO4 Systems. *Bulletin of the Chemical Society of Japan, 31*(2), 201-205.

Antunes, R. A., & de Oliveira, M. C. L. (2009). Corrosion processes of physical vapor deposition-coated metallic implants. *Critical reviews in biomedical engineering, 37*(6), 425-460.

Avedesian, M. M., Baker, H., & Committee, A. I. H. (1999). *Magnesium and Magnesium Alloys*: Asm International.

Averbuch-Pouchot, T., & Durif, A. (1996). *Topics in Phosphate Chemistry*: World Scientific.

Azevedo, C. R. F. (2003). Failure analysis of a commercially pure titanium plate for osteosynthesis. *Engineering Failure Analysis, 10*(2), 153-164. doi: 10.1016/s1350-6307(02)00067-5

Baker, H., & Committee, A. I. H. (1999). *Magnesium and magnesium alloys*: ASM International.

Bandyopadhyay, A., Withey, E. A., Moore, J., & Bose, S. (2007). Influence of ZnO doping in calcium phosphate ceramics. *Materials Science & Engineering C-Biomimetic and Supramolecular Systems, 27*(1), 14-17. doi: 10.1016/j.msec.2005.11.004

Banerjee, S. S., Tarafder, S., Davies, N. M., Bandyopadhyay, A., & Bose, S. (2010). Understanding the influence of MgO and SrO binary doping on the mechanical and biological properties of beta-TCP ceramics. *Acta Biomater, 6*(10), 4167-4174. doi: 10.1016/j.actbio.2010.05.012

Barralet, J. E., Gbureck, U., Grover, L. M., & Thull, R. (2004). Mechanically induced phase transformation of alpha- and beta-tricalcium phosphate. In M. A. Barbosa, F. J. Monteiro, R. Correia & B. Leon (Eds.), *Bioceramics, Vol 16* (Vol. 254-2, pp. 277-280).

Barrère, F., Mahmood, T. A., de Groot, K., & van Blitterswijk, C. A. (2008). Advanced biomaterials for skeletal tissue regeneration: Instructive and smart functions. *Materials Science and Engineering: R: Reports, 59*(1–6), 38-71. doi: http://dx.doi.org/10.1016/j.mser.2007.12.001

Basting, D., & Stamm, U. (2001). The development of excimer laser technology - History and future prospects. *Zeitschrift Fur Physikalische Chemie-International Journal of Research*

in Physical Chemistry & Chemical Physics, 215, 1575-1599. doi: 10.1524/zpch.2001.215.12.1575

Bauer, S., Schmuki, P., von der Mark, K., & Park, J. (2013). Engineering biocompatible implant surfaces: Part I: Materials and surfaces. *Progress in Materials Science, 58*(3), 261-326. doi: http://dx.doi.org/10.1016/j.pmatsci.2012.09.001

Ben-Hamu, G., Eliezer, D., Dietzel, W., & Shin, K. S. (2008). Stress corrosion cracking of new Mg–Zn–Mn wrought alloys containing Si. *Corrosion Science, 50*(5), 1505-1517. doi: http://dx.doi.org/10.1016/j.corsci.2008.02.012

Berland, Y., Boistelle, R., & Olmer, M. (1990). Urinary supersaturation with respect to brushite in patients suffering calcium oxalate lithiasis. *Nephrol Dial Transplant, 5*(3), 179-184.

Bettger, W. J., & Odell, B. L. (1993). Physiological roles of zinc in the plasma-membrane of mammalian-cells. *Journal of Nutritional Biochemistry, 4*(4), 194-207. doi: 10.1016/0955-2863(93)90052-x

Bigi, A., Fini, M., Bracci, B., Boanini, E., Torricelli, P., GiavareSi, G., . . . Giardino, R. (2008). The response of bone to nanocrystalline hydroxyapatite-coated Ti13Nb11Zr alloy in an animal model. *Biomaterials, 29*(11), 1730-1736. doi: 10.1016/j.biomaterials.2007.12.011

Black, J., & Hastings, G. (1998). *Handbook of Biomaterial Properties*. London.

Bloyer, D. R., McNaney, J. M., Cannon, R. M., Saiz, E., Tomsia, A. P., & Ritchie, R. O. (2007). Stress–corrosion crack growth of Si–Na–K–Mg–Ca–P–O bioactive glasses in simulated human physiological environment. *Biomaterials, 28*(33), 4901-4911. doi: http://dx.doi.org/10.1016/j.biomaterials.2007.08.005

Blum, J., Eckert, K. L., Schroeder, A., Petitmermet, M., Ha, S. W., & Wintermantel, E. (1996). *In vitro testing of porous titanium dioxide ceramics*. Otsu, Japan: Pergamon.

Bobby Kannan, M., Singh Raman, R. K., Witte, F., Blawert, C., & Dietzel, W. (2011). Influence of circumferential notch and fatigue crack on the mechanical integrity of biodegradable magnesium-based alloy in simulated body fluid. *Journal of biomedical materials research. Part B, Applied biomaterials, 96*(2), 303-309. doi: 10.1002/jbm.b.31766

Bobyn JD, S. G., Hacking SA, Tanzer M, Krygier JJ. (1999). Characteristics of bone ingrowth and interface mechanics of a new porous tantalum biomaterial. *J Bone Joint Surg Br., 81*(5), 907-914.

Bone, C., & Expressed, P. (1976). Protection from stress in bone and its effects.

Bonfield, W. (1999). Developing New Materials for Replacement Surgery. *Parliamentary and Scientific Committee Lecture, 4*(56).

Bonfield, W., Grynpas, M. D., Tully, A. E., Bowman, J., & Abram, J. (1981). Hydroxyapatite reinforced plyethylen - A mechanically compatible implant material for bone-replacement. *Biomaterials, 2*(3), 185-186. doi: 10.1016/0142-9612(81)90050-8

Böstman, O., & Pihlajamäki, H. (2000). Clinical biocompatibility of biodegradable orthopaedic implants for internal fixation: a review. *Biomaterials, 21*(24), 2615-2621. doi: http://dx.doi.org/10.1016/S0142-9612(00)00129-0

Bragg, W., & Bragg, W. (1913). The reflection of X-rays by crystals. *Proceedings of the Royal Society of London. Series A, 88*(605), 428-438.

Brown, M., & Farrar, D. (2008). Development of bioresorbable polymers in orthopaedics. *Plastics, Rubber and Composites, 37*(2-4), 2-4.

Brown, P., & Hocker, N. (1991). Variations in solution chemistry during the low-temperature formation of HA. *J Am Ceram Soc, 74*(8), 1848-1854.

Brown, P. W., & Fulmer, M. (2005). Kinetics of hydroxyapatite formation at low temperature. *Journal of the American Ceramic Society, 74*(5), 934-940.

Brown, W. E., Eidelman, N., & Tomazic, B. (1987). Octacalcium phosphate as a precursor in biomineral formation. *Adv Dent Res, 1*(2), 306-313.

Brown, W. E., Mathew, M., & Tung, M. S. (1981). Crystal-chemistry of octacalcium phosphate. *Progress in Crystal Growth and Characterization of Materials, 4*(1-2), 59-87. doi: 10.1016/0146-3535(81)90048-4

Bulgakov, A. V., & Bulgakova, N. M. (1995). Dynamics of laser-induced plume expansion into an ambient gas during film deposition. *Journal of Physics D-Applied Physics, 28*(8), 1710-1718. doi: 10.1088/0022-3727/28/8/022

Bulgakov, A. V., & Bulgakova, N. M. (1998). Gas-dynamic effects of the interaction between a pulsed laser-ablation plume and the ambient gas: analogy with an underexpanded jet. *Journal of Physics D-Applied Physics, 31*(6), 693-703. doi: 10.1088/0022-3727/31/6/017

Calderin, L., Xilin, Y., Stott, M. J., & Sayer, M. (2002). Density functional study of structural, electronic and vibrational properties of Mg- and Zn-doped tricalcium phosphate biomaterials. *Biomaterials, 23*(20), 4155-4163. doi: 10.1016/S0142-9612(02)00199-0

Cao, W., & Hench, L. L. (1996). Bioactive materials. *Ceramics International, 22*(6), 493-507.

Carbajal, L., Caballero, A., & Sainz, M. A. (2012). Design and processing of ZnO doped tricalcium phosphate based materials: Influence of β/α polymorph phase assemblage on microstructural evolution. *Journal of the European Ceramic Society, 32*(3), 569-577. doi: http://dx.doi.org/10.1016/j.jeurceramsoc.2011.09.025

Caroff, F., Oh, K. S., Famery, R., & Boch, P. (1998). Sintering of TCP-TiO2 biocomposites: influence of secondary phases. *Biomaterials, 19*(16), 1451-1454.

Carrodeguas, R. G., De Aza, A. H., García-Páez, I., De Aza, S., & Pena, P. (2010). Revisiting the Phase-Equilibrium Diagram of the Ca3 (PO4) 2–CaMg (SiO3) 2 System. *Journal of the American Ceramic Society, 93*(2), 561-569.

Carter, C. B., & Norton, G. (2007). *Ceramic Materials: Science and Engineering*: Springer Science+Business Media, LLC.

Chao, J., & López, V. (2007). Failure analysis of a Ti6Al4V cementless HIP prosthesis. *Engineering Failure Analysis, 14*(5), 822-830. doi: 10.1016/j.engfailanal.2006.11.003

Chen, X.-C., Yin, T.-A., He, J.-S., Ma, Q.-Y., Han, Z.-M., & Li, L.-X. (1985). Low levels of zinc in hair and blood, pica, anorexia, and poor growth in Chinese preschool children. *The American journal of clinical nutrition, 42*(4), 694-700.

Chiu, K. Y., Wong, M. H., Cheng, F. T., & Man, H. C. (2007). Characterization and corrosion studies of fluoride conversion coating on degradable Mg implants. *Surface and Coatings Technology, 202*(3), 590-598. doi: http://dx.doi.org/10.1016/j.surfcoat.2007.06.035

Choi, J. W., Kong, Y. M., Kim, H. E., & Lee, I. S. (1998). Reinforcement of hydroxyapatite bioceramic by addition of Ni3Al and Al2O3. *Journal of the American Ceramic Society, 81*(7), 1743-1748.

Chrisey, D. B., & Hubler, G. K. (1994). *Pulsed Laser Deposition of Thin Films*: John Wiley & Sons.

Christel, P., Meunier, A., Dorlot, J. M., Crolet, J. M., Witvoet, J., Sedel, L., & Boutin, P. (1988). Biomechanical Compatibility and Design of Ceramic Implants for Orthopedic Surgery. *Annals of the New York Academy of Sciences, 523*(1), 234-256. doi: 10.1111/j.1749-6632.1988.tb38516.x

Christen, H. M., & Eres, G. (2008). Recent advances in pulsed-laser deposition of complex oxides. *Journal of Physics-Condensed Matter, 20*(26). doi: 10.1088/0953-8984/20/26/264005

Claes, L., Heitemeyer, U., Krischak, G., Braun, H., & Hierholzer, G. (1999). Fixation technique influences osteogenesis of comminuted fractures. *Clin Orthop Relat Res*(365), 221-229.

Clèries L, F.-P. J., Morenza JL. (2000). Behavior in simulated body fluid of calcium phosphate coatings obtained by laser ablation. *Biomaterials., 21*(18), 1861-1865.

Damron, T. A. (2008). *Oncology And Basic Science*: Wolters Kluwer Health/Lippincott, Williams & Wilkins.

de Groot, K. Effect of porosity and physicochemical properties on the stability, resorption and strength of calcium phosphate ceramics. *6*, 227-234.

Dean, C. (2012). Dietary Magnesium and Stroke Prevention. *Natural Medicine Journal*.

DeGarmo, E. P., Black, J. T., & Kohser, R. A. (1997). *Materials and processes in manufacturing*: Prentice Hall.

Dickens, B., Schroeder, L. W., & Brown, W. E. (1974). Crystallographic studies of the role of Mg as a stabilizing impurity in β-Ca3(PO4)2. The crystal structure of pure β-Ca3(PO4)2. *Journal of Solid State Chemistry, 10*(3), 232-248. doi: http://dx.doi.org/10.1016/0022-4596(74)90030-9

Disegi, J., & Wyss, H. (1989). Implant materials for fracture fixation: a clinical perspective. *Orthopedics, 12*(1), 75-79.

Doerner, M., & Nix, W. (1986). A method for interpreting the data from depth-sensing indentation ins t rurnen ts. *J. Mater. Res, 1*(4).

Douard, N., Detsch, R., Chotard-Ghodsnia, R., Damia, C., Deisinger, U., & Champion, E. (2011). Processing, physico-chemical characterisation and in vitro evaluation of silicon containing β-tricalcium phosphate ceramics. *Materials Science and Engineering: C, 31*(3), 531-539.

Driessens, F. C. M., & Verbeeck, R. M. H. (1990). *Biominerals*: CRC-Pr.

Ducheyne, P., Hench, L., Kagen, A., Martens, M., Bursens, A., & Mulier, J. (1980). *J. Biomed. Mater., 225*(14).

Ducheyne, P., & Qiu, Q. (1999). Bioactive ceramics: the effect of surface reactivity on bone formation and bone cell function. *Biomaterials, 20*(23), 2287-2303.

Eason, R. (2006). *Pulsed laser deposition of thin films: applications-led growth of functional materials*: Wiley-Interscience.

El-Rahman, S. S. A. (2003). Neuropathology of aluminum toxicity in rats (glutamate and GABA impairment). *Pharmacological research : the official journal of the Italian Pharmacological Society, 47*(3), 189-194. doi: 10.1016/s1043-6618(02)00336-5

Ellingsen, J. E. (1991). A study on the mechanism of protein adsorption to TiO2. *Biomaterials, 12*(6), 593-596. doi: http://dx.doi.org/10.1016/0142-9612(91)90057-H

Elliot, J. (1994). *Structure and Chemistry of the Apatites and Other Calcium Orthophosphates*. Amsterdam.

Elliot, J. C. (1994). *Structure and Chemistry of the Apatites and Other Calcium Orthophosphates*: Elsevier Science Limited.

Ellis Iii, E. (1993). Rigid skeletal fixation of fractures. *Journal of Oral and Maxillofacial Surgery, 51*(2), 163-173. doi: http://dx.doi.org/10.1016/S0278-2391(10)80016-3

Enderle, R., Götz-Neunhoeffer, F., Göbbels, M., Müller, F. A., & Greil, P. (2005). Influence of magnesium doping on the phase transformation temperature of β-TCP ceramics examined by Rietveld refinement. *Biomaterials, 26*(17), 3379-3384. doi: http://dx.doi.org/10.1016/j.biomaterials.2004.09.017

Evans, F. G. (1976). Mechanical properties and histology of cortical bone from younger and older men. *Anat Rec, 185*(1), 1-11. doi: 10.1002/ar.1091850102

EVOS, A. from http://amgmicro.com/products/microscopes/evos-fl/

Famery, R., Richard, N., & Boch, P. (1994). Preparation of α- and β-tricalcium phosphate ceramics, with and without magnesium addition. *Ceramics International, 20*(5), 327-336. doi: http://dx.doi.org/10.1016/0272-8842(94)90050-7

Farlex, I. (2013). Immobilization.

Feng, A., & Han, Y. (2010). The microstructure, mechanical and corrosion properties of calcium polyphosphate reinforced ZK60A magnesium alloy composites. *Journal of Alloys and Compounds, 504*(2), 585-593. doi: http://dx.doi.org/10.1016/j.jallcom.2010.06.013

Fielding, G. A., Bandyopadhyay, A., & Bose, S. (2012). Effects of silica and zinc oxide doping on mechanical and biological properties of 3D printed tricalcium phosphate tissue engineering scaffolds. *Dent. Mater., 28*(2), 113-122. doi: 10.1016/j.dental.2011.09.010

Fleck, C., & Eifler, D. (2010). Corrosion, fatigue and corrosion fatigue behaviour of metal implant materials, especially titanium alloys. *International Journal of Fatigue, 32*(6), 929-935. doi: 10.1016/j.ijfatigue.2009.09.009

Frankel, G. S., & Rohwerder, M. (2003). Experimental Techniques for Corrosion. In M. S. a. G. S. Frankel (Ed.), *Corrosion and Oxide Films* (Vol. 4). Weinheim, Germany: Wiley-VCH.

Gao, H. (2006). Application of Fracture Mechanics Concepts to Hierarchical Biomechanics of Bone and Bone-like Materials. *International Journal of Fracture, 138*(1-4), 101-137. doi: 10.1007/s10704-006-7156-4

Geiohegan, D. B. (1994). Pulsed laser deposition of thin films. In D. B. C. a. G. K. Hubler (Ed.), (pp. 115-165). New York: John Wiely & Sons, Inc.

Geng, F., Tan, L., Zhang, B., Wu, C., He, Y., Yang, J., & Yang, K. (2009). Study on β-TCP coated porous Mg as a bone tissue engineering scaffold material. *J. Mater. Sci. Technol., 25*(1).

Geng, F., Tan, L. L., Jin, X. X., Yang, J. Y., & Yang, K. (2009). The preparation, cytocompatibility, and in vitro biodegradation study of pure beta-TCP on magnesium. *Journal of Materials Science-Materials in Medicine, 20*(5), 1149-1157. doi: 10.1007/s10856-008-3669-x

Geohegan, D. B., Puretzky, A. A., Duscher, G., & Pennycook, S. J. (1998). Photoluminescence from gas-suspended SiOx nanoparticles synthesized by laser ablation. *Applied Physics Letters, 73*(4), 438-440. doi: 10.1063/1.121892

Geohegan, D. B., Puretzky, A. A., & Rader, D. J. (1999). Gas-phase nanoparticle formation and transport during pulsed laser deposition of YBa2Cu3O7 - d. *Applied Physics Letters, 74*(25), 3788-3790.

Gibson, I., Akao, M., Best, S., & Boneield, W. (1996). Bioceramics. *173*(9).

Gibson, L. J., & Ashby, M. F. (1999). *Cellular Solids*: Cambridge University Press.

Giordani, E., Guimarães, V., Pinto, T., & Ferreira, I. (2004). Effect of precipitates on the corrosion fatigue crack initiation of ISSO 5832–9 stainless steel biomaterial. *Int J Fatigue*(26), 1129-1136.

Giori, N. J. (2010). Unexpected finding of a fractured metal prosthetic femoral head in a nonmodular implant during revision total hip arthroplasty. *The Journal of Arthroplasty, 25*(4), 659.e613-655.

Giovanni Iazzetti, E. R. (2002). Atlas of Human Anatomy. *Diane Pub Co.*

Goodman, S. B., Ma, T., Chiu, R., Ramachandran, R., & Lane Smith, R. (2006). Effects of orthopaedic wear particles on osteoprogenitor cells. *Biomaterials, 27*(36), 6096-6101. doi: 10.1016/j.biomaterials.2006.08.023

Goodwin, T. J., Leppert, V. J., Risbud, S. H., Kennedy, I. M., & Lee, H. W. H. (1997). Synthesis of gallium nitride quantum dots through reactive laser ablation. *Applied Physics Letters, 70*(23), 3122-3124.

Gray-Munro, J. E., & Strong, M. (2009). The mechanism of deposition of calcium phosphate coatings from solution onto magnesium alloy AZ31. *Journal of Biomedical Materials Research Part A, 90A*(2), 339-350. doi: 10.1002/jbm.a.32107

Gu, X., Zheng, Y., Cheng, Y., Zhong, S., & Xi, T. (2009). In vitro corrosion and biocompatibility of binary magnesium alloys. *Biomaterials, 30*(4), 484-498. doi: 10.1016/j.biomaterials.2008.10.021

Gu, X. N., Li, N., Zhou, W. R., Zheng, Y. F., Zhao, X., Cai, Q. Z., & Ruan, L. (2011). Corrosion resistance and surface biocompatibility of a microarc oxidation coating on a Mg-Ca alloy. *Acta Biomaterialia, 7*(4), 1880-1889. doi: 10.1016/j.actbio.2010.11.034

Gupta, R. K., Mensah-Darkwa, K., & Kumar, D. (2013). Effect of Post Heat Treatment on Corrosion Resistance of Phytic Acid Conversion Coated Magnesium. *Journal of Materials Science & Technology, 29*(2), 180-186. doi: http://dx.doi.org/10.1016/j.jmst.2012.12.014

Habibovic, P., Barrere, F., van Blitterswijk, C. A., de Groot, K., & Layrolle, P. (2002). Biomimetic hydroxyapatite coating on metal implants. *Journal of the American Ceramic Society, 85*(3), 517-522.

Hanabusa, M. (1993). Paper presented at the Mater. Res. Soc. Symp. Proc.

Harandi, S. E., Idris, M. H., & Jafari, H. (2011). Effect of forging process on microstructure, mechanical and corrosion properties of biodegradable Mg-1Ca alloy. *Materials & Design, 32*(5), 2596-2603. doi: 10.1016/j.matdes.2011.01.042

Harilal, S. S. (2001). Expansion dynamics of laser ablated carbon plasma plume in helium ambient. *Applied Surface Science, 172*(1-2), 103-109. doi: 10.1016/s0169-4332(00)00837-0

Harilal, S. S., Bindhu, C. V., Nampoori, V. P. N., & Vallabhan, C. P. G. (1998). Influence of ambient gas on the temperature and density of laser produced carbon plasma. *Applied Physics Letters, 72*(2), 167-169. doi: 10.1063/1.120602

Hartwig, A. (2001). Role of magnesium in genomic stability. *Mutation Research-Fundamental and Molecular Mechanisms of Mutagenesis, 475*(1-2), 113-121. doi: 10.1016/s0027-5107(01)00074-4

Hayes, J. S., & Richards, R. G. (2010). The use of titanium and stainless steel in fracture fixation. *Expert Rev Med Devices, 7*(6), 843-853. doi: 10.1586/erd.10.53

Hench, L. L. (1998). Bioceramics. *Journal of the American Ceramic Society, 81*(7), 1705-1728.

Hench, L. L., & Polak, J. M. (2002). Third-Generation Biomedical Materials. *Science, 295*(5557), 1014-1017. doi: 10.1126/science.1067404

Hench, L. L., & Wilson, J. (1993). *An Introduction to Bioceramics*: World Scientific Publishing C. Pte. Limited.

Hermawan, H. (2012). Introduction to Metallic Biomaterials. *Biodegradable Metals*, 1-11.

Hermawan, H., & Mantovani, D. (2009). Degradable metallic biomaterials: the concept, current developments and future directions. *Minerva Biotecnologica, 21*(4), 207-216.

High-Tech, H. SU8000 Series.

Hing, K., Best, S., & Bonfield, W. (1999). Characterization of porous hydroxyapatite. *Journal of Materials Science: Materials in Medicine, 10*(3), 135-145.

Holmes, D., & Bridges, A. (2004). Atomic Scale Structure of Materials. from http://www.doitpoms.ac.uk/tlplib/atomic-scale-structure/printall.php

Hoppe, A., Gueldal, N. S., & Boccaccini, A. R. (2011). A review of the biological response to ionic dissolution products from bioactive glasses and glass-ceramics. *Biomaterials, 32*(11), 2757-2774. doi: 10.1016/j.biomaterials.2011.01.004

Huang, J., Best, S. M., Bonfield, W., & Buckland, T. (2010). Development and characterization of titanium-containing hydroxyapatite for medical applications. *Acta Biomaterialia, 6*(1), 241-249. doi: http://dx.doi.org/10.1016/j.actbio.2009.06.032

Hulbert, S., Bokros, J., Hench, L., Wilson, J., & Heimke, G. (1987). *Ceramics in Clinical Applications: Past, Present and Future*.

Hutmacher, D., Hurzeler, M. B., & Schliephake, H. (1996). A review of material properties of biodegradable and bioresorbable polymers and devices for GTR and GBR applications. *The International journal of oral & maxillofacial implants, 11*(5), 667-678.

Hyun Seung Yu, K. S. H., Hwan Kim, Dong Ho Lee, Choon Ki Lee, Bong Soon Chang, Deug Joong Kim, Jun Hyuk Seo, Jae Hyup Lee, Ki Soo Park. (2003). US Patent No. US7582310.

Itatani, K., Takahashi, M., Howell, F. S., & Aizawa, M. (2002). Effect of metal-oxide addition on the sintering of β-calcium orthophosphate. *Journal of Materials Science: Materials in Medicine, 13*(7), 707-713.

Iwasaki, A., Torres, C., Ohashi, P. S., Robinson, H. L., & Barber, B. H. (1997). The dominant role of bone marrow-derived cells in CTL induction following plasmid DNA immunization at different sites. *The Journal of Immunology, 159*(1), 11-14.

Jacobs, J., Hallab, N., Skipor, A., & Urban, R. (2003). Metal degradation products: a cause for concern in metal-metal bearings? *Clin Orthop Relat Res., 417*, 139-147.

Jacobs, J. J., Skipor, A. K., Patterson, L. M., Hallab, N. J., Paprosky, W. G., Black, J., & Galante, J. O. (1998). Metal release in patients who have had a primary total hip arthroplasty. A prospective, controlled, longitudinal study. *J Bone Joint Surg Am., 80*(10), 1447-1458.

Jamesh, M., Kumar, S., & Narayanan, T. S. N. S. (2011). Corrosion behavior of commercially pure Mg and ZM21 Mg alloy in Ringer's solution - Long term evaluation by EIS. *Corrosion Science, 53*(2), 645-654. doi: 10.1016/j.corsci.2010.10.011

Jarcho, M. (1985). Calcium phosphate ceramics as hard tissue prosthetics. *Clin. Orthop. Relat. Res., 157*, 259.

Jarcho, M., Salsbury, R., Thomas, M., & Doremus, R. (1979). Synthesis and fabrication of beta-TCP (Whitlockite) ceramics for potential prosthetic applications. *J. Mater. Sci., 14*, 142-150.

Jarco, M., Kay, J., Gumaer, K., & Doremus, R. (1977). *J. Bioeng., 79*(1).

Jardim, P. M., Solorzano, G., & Vander Sande, J. B. (2004). Second phase formation in melt-spun Mg-Ca-Zn alloys. *Materials Science and Engineering a-Structural Materials*

Properties Microstructure and Processing, 381(1-2), 196-205. doi: 10.1016/j.msea.2004.04.043

Jay, E. E., Mallinson, P. M., Fong, S. K., Metcalfe, B. L., & Grimes, R. W. (2011). Partitioning of dopant cations between @b-tricalcium phosphate and fluorapatite. *JNM, 414*(3), 7-7. doi: 10.1016/j.jnucmat.2011.05.003

Jennifer, W., & Michael, P. (2003). Osteoblast response to pure titanium and titanium alloy *Bio-Implant Interface*: CRC Press.

JJ., J., JL., G., & RM., U. (1998). Corrosion of metal orthopaedic implants. *J Bone Joint Surg Am., 80*(2), 268-282.

Jones, D. A. (1996). *Principles and Prevention of Corrosion 2nd Ed.* Upper Saddle River, NJ.

Kalita, S. J., Bhardwaj, A., & Bhatt, H. A. (2007). Nanocrystalline calcium phosphate ceramics in biomedical engineering. *Materials Science and Engineering: C, 27*(3), 441-449.

Kasuga, T., Kondo, H., & Nogami, M. (2002). Apatite formation on TiO2 in simulated body fluid. *Journal of Crystal Growth, 235*(1-4), 235-240. doi: 10.1016/s0022-0248(01)01782-1

Kawamura, H., Ito, A., Miyakawa, S., Layrolle, P., Ojima, K., Ichinose, N., & Tateishi, T. (2000). Stimulatory effect of zinc-releasing calcium phosphate implant on bone formation in rabbit femora. *Journal of Biomedical Materials Research, 50*(2), 184-190. doi: 10.1002/(SICI)1097-4636(200005)50:2<184::AID-JBM13>3.0.CO;2-3

Kelly, R., & Miotello, A. (1996). *Comments on explosive mechanisms of laser sputtering.* Paper presented at the Laser Ablation. Symposium F: Third International Symposium on Laser Ablation (COLA'95) 1995 E-MRS Spring Conference, 22-26 May 1995, Netherlands.

Kelly, R. G., Scully, J. R., Shoesmith, D. W., & Buchheit, R. G. (2003). *Electrochemical Techniques in Corrosion Science and Engineering*. New York.

Koch, C. F., Johnson, S., Kumar, D., Jelinek, M., Chrisey, D. B., Doraiswamy, A., . . . Mihailescu, I. N. (2007). Pulsed laser deposition of hydroxyapatite thin films. *Materials Science and Engineering: C, 27*(3), 484-494. doi: http://dx.doi.org/10.1016/j.msec.2006.05.025

Koh, Y.-H., Lee, E.-J., Yoon, B.-H., Song, J.-H., Kim, H.-E., & Kim, H.-W. (2006). Effect of polystyrene addition on freeze casting of ceramic/camphene slurry for ultra-high porosity ceramics with aligned pore channels. *Journal of the American Ceramic Society, 89*(12), 3646-3653. doi: 10.1111/j.1551-2916.2006.01311.x

Kotani, S., Fujita, Y., Kitsugi, T., Nakamura, T., Yamamuro, T., Ohtsuki, C., & Kokubo, T. (1991). Bone bonding mechanism of β-tricalcium phosphate. *Journal of Biomedical Materials Research, 25*(10), 1303-1315. doi: 10.1002/jbm.820251010

Kroto, H. W., Heath, J. R., O'Brien, S. C., Curl, R. F., & Smalley, R. E. (1985). C60: Buckminsterfullerene. *Nature, 318*(6042), 162-163.

Kruth, J.-P., Wang, X., Laoui, T., & Froyen, L. (2003). Lasers and materials in selective laser sintering. *Assembly Automation, 23*(4), 357-371.

Ku, C. H., Piolettli, D. P., Browne, M., & Gregson, P. J. (2002). Effect of different Ti-6A1-4V surface treatments on osteoblasts behaviour. *Biomaterials, 23*(6), 1447-1454. doi: 10.1016/s0142-9612(01)00266-6

Lacefield, W. R. (1998). Current status of ceramic coatings for dental implants. *Implant Dentistry, 7*(4), 315.

Lahann, J., Klee, D., Thelen, H., Bienert, H., Vorwerk, D., & Hocker, H. (1999). Improvement of haemocompatibility of metallic stents by polymer coating. *Journal of Materials Science-Materials in Medicine, 10*(7), 443-448. doi: 10.1023/a:1008939400812

Lambotte, A. (1909). Technique et indication des prothèses dans le traitement des fractures. *Presse Med, 17*, 132.

Lambotte, A. (1932). L'utilisation du magnesium comme materiel perdu dans l'osteosynthese`. *Bull Me´m Soc Nat Chir, 28*, 1325-1334.

Lane, W. A. (1895). Some remarks on the treatment of fractures. *BMJ, 1*(1790), 861-863. doi: 10.1136/bmj.1.1790.861

Langstaff, S., Sayer, M., Smith, T. J. N., Pugh, S. M., Hesp, S. A. M., & Thompson, W. T. (1999). Resorbable bioceramics based on stabilized calcium phosphates. Part I: rational design, sample preparation and material characterization. *Biomaterials, 20*(18), 1727-1741. doi: http://dx.doi.org/10.1016/S0142-9612(99)00086-1

Larry L. Hench, J. W. (October 1993). An Introduction to Bioceramics Volume One. *World Scientific, London, UK.*

Lausmaa, J., Kasemo, B., & Mattsson, H. (1990). Surface spectroscopic characterization of titanium implant materials. *Applied Surface Science, 44*(2), 133-146. doi: http://dx.doi.org/10.1016/0169-4332(90)90100-E

Lee, D. D., Rey, C., & Aiolova, M. (2000). Bioresorbable ceramic composites: Google Patents.

Lee, W. J., Lee, S. W., Kim, H. L., Kim, D. J., & Han, J. S. (2005). *J. Korean Phys. Soc., 47*, 152.

Lemons, J. (1993). Inorganic and organic composition for treatment of bone lesions: Google Patents.

Leng, Y., Chen, J., & Qu, S. (2003). TEM study of calcium phosphate precipitation on HA/TCP ceramics. *Biomaterials, 24*(13), 2125-2131. doi: http://dx.doi.org/10.1016/S0142-9612(03)00036-X

Lhotka, C., Szekeres, T., Steffan, I., Zhuber, K., & Zweymuller, K. (2003). Four-year study of cobalt and chromium blood levels in patients managed with two different metal-on-metal total hip replacements. *Journal of Orthopaedic Research, 21*(2), 189-195. doi: 10.1016/s0736-0266(02)00152-3

Li, H., Khor, K. A., & Cheang, P. (2002). Titanium dioxide reinforced hydroxyapatite coatings deposited by high velocity oxy-fuel (HVOF) spray. *Biomaterials, 23*(1), 85-91. doi: 10.1016/s0142-9612(01)00082-5

Li, L., Gao, J., & Wang, Y. (2004). Evaluation of cyto-toxicity and corrosion behavior of alkali-heat-treated magnesium in simulated body fluid. *Surface and Coatings Technology, 185*(1), 92-98. doi: http://dx.doi.org/10.1016/j.surfcoat.2004.01.004

Li, Y., Lee, I.-S., Cui, F.-Z., & Choi, S.-H. (2008). The biocompatibility of nanostructured calcium phosphate coated on micro-arc oxidized titanium. *Biomaterials, 29*(13), 2025-2032. doi: http://dx.doi.org/10.1016/j.biomaterials.2008.01.009

Li, Z., Gu, X., Lou, S., & Zheng, Y. (2008). The development of binary Mg-Ca alloys for use as biodegradable materials within bone. *Biomaterials, 29*(10), 1329-1344. doi: 10.1016/j.biomaterials.2007.12.021

Liao, Y. (2006). Practical Electron Microscopy and Database.

Lin, F. H., Lin, C. C., Lu, C. M., Liu, H. C., Sun, J. S., & Wang, C. Y. (1995). Mechanical properties and histological evaluation of sintered beta-Ca2P2O7 with Na4P2O7 center dot 10H2O addition. *Biomaterials, 16*(10), 793-802. doi: 10.1016/0142-9612(95)99642-y

Lindberg, J., Zobitz, M., Poindexter, J., & Pak, C. (1990). Magnesium bioavailability from magnesium citrate and magnesium oxide. *J Am Coll Nutr, 9*(1), 48-55.

Linder, L., Carlsson, A., Marsal, L., Bjursten, L. M., & Branemark, P. I. (1988). Clinical aspects of osseointegration in joint replacement - A histological study of titanium implants. *Journal of Bone and Joint Surgery-British Volume, 70*(4), 550-555.

Lu, X., & Leng, Y. (2005). Theoretical analysis of calcium phosphate precipitation in simulated body fluid. *Biomaterials, 26*(10), 1097-1108. doi: 10.1016/j.biomaterials.2004.05.034

Lusvardi, G., Zaffe, D., Menabue, L., Bertoldi, C., Malavasi, G., & Consolo, U. (2009). In vitro and in vivo behaviour of zinc-doped phosphosilicate glasses. *Acta Biomaterialia, 5*(1), 419-428. doi: 10.1016/j.actbio.2008.07.007

Magnissalis, E. A., Zinelis, S., Karachalios, T., & Hartofilakidis, G. (2003). Failure analysis of two Ti-alloy total hip arthroplasty femoral stems fractured in vivo. *Journal of Biomedical Materials Research Part B-Applied Biomaterials, 66B*(1), 299-305. doi: 10.1002/jbm.b.10003

Mansfeld, F. (1976). The polarization resistance technique for measuring corrosion currents. In M. G. F. a. R. W. Staehle (Ed.), *Advances in Corrosion Science and Technology*. Plenum, New York.

Mao, L., Wang, Y., Wan, Y., He, F., & Huang, Y. (2009). Effects of Zn on microstructure and mechanical properties of biomedical Mg–Ca–Zn alloys. *Heat Treat Metal, 34*(10), 19-22.

Maret, W., & Sandstead, H. H. (2006). Zinc requirements and the risks and benefits of zinc supplementation. *Journal of Trace Elements in Medicine and Biology, 20*(1), 3-18.

Matthews, N. S., Khambay, B. S., Ayoub, A. F., Koppel, D., & Wood, G. (2003). Preliminary assessment of skeletal stability after sagittal split mandibular advancement using a

bioresorbable fixation system. *British Journal of Oral and Maxillofacial Surgery, 41*(3), 179-184. doi: http://dx.doi.org/10.1016/S0266-4356(03)00048-2

Maurus, P. B., & Kaeding, C. C. (2004). Bioabsorbable implant material review. *Operative Techniques in Sports Medicine, 12*(3), 158-160. doi: 10.1053/j.otsm.2004.07.015

McBride, E. D. (1938). Absorbable metal in bone surgery - A further report on the use of magnesium alloys. *Journal of the American Medical Association, 111*(27), 2464-2466.

Mckee, M. D., & Nanci, A. (1996). Osteopontin: an interfacial extracellular matrix protein in mineralized tissues. *Connective tissue research, 35*(1-4), 197-205.

Mensah-Darkwa, K. (2012). Experimental setup for electrochemical corrosion testing.

Metev, S., & Meteva, K. (1989). Nucleation and growth of laser-plasma deposited thin-films. *Applied Surface Science, 43*, 402-408. doi: 10.1016/0169-4332(89)90247-x

Metev, S. M., & Veĭko, V. P. (1994). *Laser-assisted microtechnology*: Springer-Verlag.

Meyer, J., & Fowler, B. (1997). Lattice defects in nonstoichiometric calcium hydroxyapatites. *Inorg Chem, 21*, 3029-3035.

Miao, S., Cheng, K., Weng, W., Du, P., Shen, G., Han, G., . . . Zhang, S. (2008). Fabrication and evaluation of Zn containing fluoridated hydroxyapatite layer with Zn release ability. *Acta Biomaterialia, 4*(2), 441-446. doi: http://dx.doi.org/10.1016/j.actbio.2007.08.013

Monma, H., & Goto, M. (1983). Behavior of the alpha<=>beta phase transformation in tricalcium phosphate. *Yogyo Kyokai Shi, 91*, 473-475.

Moritz, N., Jokinen, M., Peltola, T., Areva, S., & Yli-Urpo, A. (2003). Local induction of calcium phosphate formation on TiO2 coatings on titanium via surface treatment with a CO2 laser. *Journal of Biomedical Materials Research Part A, 65A*(1), 9-16. doi: 10.1002/jbm.a.10434

Morra, M., Cassinelli, C., Meda, L., Fini, M., Giavaresi, G., & Giardino, R. (2005). Surface analysis and effects on interfacial bone microhardness of collagen-coated titanium implants: a rabbit model. *The International journal of oral & maxillofacial implants, 20*(1), 23.

Mow, H. (2005). Basic Orthoaedic Biomechanics and Mechano-Biology. *Biomed Eng Online, 4*(28).

Namiki, A., Kawai, T., & Ichige, K. (1986). Angle-resolved time-of-flight spectra of neutral particles desorbed from laser irradiated CdS. *Surface Science, 166*(1), 129-140. doi: http://dx.doi.org/10.1016/0039-6028(86)90536-4

Navarro, M., Michiardi, A., Castaiio, O., & Planell, J. A. (2008). Biomaterials in orthopaedics. *Journal of the Royal Society Interface, 5*(27), 1137-1158. doi: 10.1098/rsif.2008.0151

Ng, B. D., Annergren, I., Soutar, A. M., Khor, K. A., & Jarfors, A. E. W. (2005). Characterisation of a duplex TiO2/CaP coating on Ti6Al4V for hard tissue replacement. *Biomaterials, 26*(10), 1087-1095. doi: 10.1016/j.biomaterials.2004.04.022

Niinomi, M. (2002). Recent metallic materials for biomedical applications. *Metallurgical and Materials Transactions a-Physical Metallurgy and Materials Science, 33*(3), 477-486. doi: 10.1007/s11661-002-0109-2

Niinomi, M. (2007). Fatigue characteristics of metallic biomaterials. *International Journal of Fatigue, 29*(6), 992-1000. doi: 10.1016/j.ijfatigue.2006.09.021

Ogawa, M., Tohma, Y., Ohgushi, H., Takakura, Y., & Tanaka, Y. (2012). Early Fixation of Cobalt-Chromium Based Alloy Surgical Implants to Bone Using a Tissue-engineering Approach. *Int J Mol Sci, 13*(5), 5528-5541. doi: 10.3390/ijms13055528

Ogawa, T. (2006). Medical Implants: Google Patents.

Ohring, M. (2002). *Materials science of thin films : deposition and structure* (2nd ed.). San Diego, CA: Academic Press.

Okuma, T. (2001). Magnesium and bone strength. *Nutrition, 17*(7-8), 679-680. doi: 10.1016/s0899-9007(01)00551-2

Oliver, W. C., & Pharr, G. M. (1992). Improved technique for determining hardness and elastic modulus using load and displacement sensing indentation experiments. *Journal of Materials Research, 7*(6), 1564-1583.

Onoki, T., Yamamoto, S. y., Onodera, H., & Nakahira, A. (2011). New technique for bonding hydroxyapatite ceramics and magnesium alloy by hydrothermal hot-pressing method. *Materials Science & Engineering C-Materials for Biological Applications, 31*(2), 499-502. doi: 10.1016/j.msec.2010.09.002

Oonishi, H., Yamamoto, M., Ishimaru, H., Tsuji, E., Kushitani, S., Aono, M., & Ukon, Y. (1989). The effect of hydroxyapatite coating on bone growth into porous titanium alloy implants. *Journal of Bone & Joint Surgery, British Volume, 71*(2), 213-216.

OpenCourseWare, P. A. M. a. M. Materials for Biomedical Applications.

Ortega, Y., Monge, M. A., & Pareja, R. (2008). The precipitation process in Mg–Ca–(Zn) alloys investigated by positron annihilation spectroscopy. *Journal of Alloys and Compounds, 463*(1–2), 62-66. doi: http://dx.doi.org/10.1016/j.jallcom.2007.09.044

Park, J. (2000). Metallic Biometerials in The Biomedical Engineering Handbook. *2nd ed. Edited by Brozino JD, CRC Press and IeEEE Press, 37*(20), 1-37.

Percival, M. (1999). Bone health and osteoporosis. *Appl. Nutr. Sci. Rep., 5*, 1-5.

Perera, F. H., Martínez-Vázquez, F. J., Miranda, P., Ortiz, A. L., & Pajares, A. (2010). Clarifying the effect of sintering conditions on the microstructure and mechanical properties of β-tricalcium phosphate. *Ceramics International, 36*(6), 1929-1935.

Pilliar, R. M., Lee, J. M., & Maniatopoulos, C. (1986). OBSERVATIONS ON THE EFFECT OF MOVEMENT ON BONE INGROWTH INTO POROUS-SURFACED IMPLANTS. *Clinical Orthopaedics and Related Research*(208), 108-113.

Piveteau, L. D., Girona, M. I., Schlapbach, L., Barboux, P., Boilot, J., & Gasser, B. (1999). Thin films of calcium phosphate and titanium dioxide by a sol-gel route: a new method for coating medical implants. *Journal of Materials Science-Materials in Medicine, 10*(3), 161-167. doi: 10.1023/a:1008985423644

Puleo, D. A., & Huh, W. W. (1995). Acute toxicity of metal-ions in cultures of osteogenic cells derived from bone-marrow stromal cells. *Journal of Applied Biomaterials, 6*(2), 109-116. doi: 10.1002/jab.770060205

Quadir, T. (1994). Use of ethylene/vinyl acetate polymer binders as drying pressing aids for ceramic powders: Google Patents.

Rabadjieva, D., Tepavitcharova, S., Gergulova, R., Sezanova, K., Titorenkova, R., Petrov, O., & Dyulgerova, E. (2011). Mg- and Zn-modified calcium phosphates prepared by biomimetic precipitation and subsequent treatment at high temperature. *J Mater Sci Mater Med, 22*(10), 2187-2196. doi: 10.1007/s10856-011-4415-3

Ramaswamy, Y., Wu, C., Zhou, H., & Zreiqat, H. (2008). Biological response of human bone cells to zinc-modified Ca-Si-based ceramics. *Acta Biomaterialia, 4*(5), 1487-1497. doi: 10.1016/j.actbio.2008.04.014

Ramila, A., & Vallet-Regi, M. (2001). Static and dynamic in vitro study of a sol-gel glass bioactivity. *Biomaterials, 22*(16), 2301-2306.

Ramires, P. A., Romito, A., Cosentino, F., & Milella, E. (2001). The influence of titania/hydroxyapatite composite coatings on in vitro osteoblasts behaviour. *Biomaterials, 22*(12), 1467-1474. doi: 10.1016/s0142-9612(00)00269-6

Ramirez, C., & Lei, K. S. (1996). Evaluation of the reliability and corrosivity of VOC-free, no-clean fluxes using standard, modified and electrochemical methods. *Soldering & Surface Mount Technology, 8*(1), 6-9.

Rayburn, G. L., Riffle, R. G., Walburn, F. J., & Williams, B. G. (1998). Endoscopic device and method for reinforcing surgical staples: Google Patents.

Raynaud, S., Champion, E., Lafon, J., & Bernache-Assollant, D. (2002). Calcium phosphate apatites with variable Ca/P atomic ratio III. Mechanical properties and degradation in solution of hot pressed ceramics. *Biomaterials, 23*(4), 1081-1089.

Revell, P. A., Damien, E., Zhang, X. S., Evans, P., & Howlett, C. R. (Dec). The effect of magnesium ions on bone bonding to hydroxyapatite coating on titanium alloy implants. *Key Engineering Materials, Bioceramics 16*, 447-450. doi: 10.4028/www.scientific.net/KEM.254-256.447

Roberto, V. S. (1995). The carbonate content in high-temperature apatite: An analytical method applied to apatite from the Jacupiranga alkaline complex. *American Mineralogist, 80*, 336-344.

Robins, S. P., Woitge, H., Hesley, R., Ju, J., Seyedin, S., & Seibel, M. J. (2009). Direct, enzyme-linked immunoassay for urinary deoxypyridinoline as a specific marker for measuring bone resorption. *Journal of Bone and Mineral Research, 9*(10), 1643-1649.

Rogel, M. R., Qiu, H., & Ameer, G. A. (2008). The role of nanocomposites in bone regeneration. *Journal of Materials Chemistry, 18*(36), 4233-4241.

Rude, R. K. (1998). Magnesium deficiency: A cause of heterogenous disease in humans. *Journal of Bone and Mineral Research, 13*(4), 749-758. doi: 10.1359/jbmr.1998.13.4.749

Ruksudjarit, A., Pengpat, K., Rujijanagul, G., & Tunkasiri, T. (2008). The fabrication of nanoporous hydroxyapatite ceramics. *Advanced Materials Research, 47*, 797-800.

Ryu, H. S., Youn, H. J., Hong, K. S., Chang, B. S., Lee, C. K., & Chung, S. S. (2002). An improvement in sintering property of beta-tricalcium phosphate by addition of calcium pyrophosphate. *Biomaterials, 23*(3), 909-914.

Safronova, T., Shekhirev, M., & Putlyaev, V. (2007). Ceramics based on calcium hydroxyapatite synthesized in the presence of PVA. *Glass and Ceramics, 64*(11), 408-412.

Sainz, M. A., Pena, P., Serena, S., & Caballero, A. (2010). Influence of design on bioactivity of novel CaSiO3-CaMg(SiO3)(2) bioceramics: In vitro simulated body fluid test and thermodynamic simulation. *Acta Biomaterialia, 6*(7), 2797-2807. doi: 10.1016/j.actbio.2010.01.003

Santos, J., Jha, L., & Monteiro, F. (1996). Surface modifications of glass-reinforced hydroxyapatite composites. *J. Mater. Sci., 7*, 181-185.

Saris, N.-E. L., Mervaala, E., Karppanen, H., Khawaja, J. A., & Lewenstam, A. (2000). Magnesium: An update on physiological, clinical and analytical aspects. *Clinica Chimica Acta, 294*(1–2), 1-26. doi: 10.1016/S0009-8981(99)00258-2

Saris, N. E. L., Mervaala, E., Karppanen, H., Khawaja, J. A., & Lewenstam, A. (2000). Magnesium - An update on physiological, clinical and analytical aspects. *Clinica Chimica Acta, 294*(1-2), 1-26. doi: 10.1016/s0009-8981(99)00258-2

Satomi, K., Akagawa, Y., Nikai, H., & Tsuru, H. (1988). Bone-implant interface structures after nontapping and tapping insertion of screw-type titanium-alloy endosseous implants. *Journal of Prosthetic Dentistry, 59*(3), 339-342. doi: 10.1016/0022-3913(88)90187-4

Saw, B. A. (2003). *Corrosion Resistance of Magnesium Alloys* (Vol. 13).

Scully, J. R. (2000). Polarization resistance method for determination of instantaneous corrosion rates. *Corrosion (Houston), 56*, 199-218.

Seeley, Z., Bandyopadhyay, A., & Bose, S. (2007). Influence of TiO2 and Ag2O addition on tricalcium phosphate ceramics. *Journal of Biomedical Materials Research Part A, 82A*(1), 113-121. doi: 10.1002/jbm.a.31077

Seeley, Z., Bandyopadhyay, A., & Bose, S. (2008). Tricalcium phosphate based resorbable ceramics: Influence of NaF and CaO addition. *Materials Science and Engineering: C, 28*(1), 11-17. doi: http://dx.doi.org/10.1016/j.msec.2006.12.010

Shadanbaz, S., & Dias, G. J. (2012). Calcium phosphate coatings on magnesium alloys for biomedical applications: A review. *Acta Biomaterialia, 8*(1), 20-30. doi: http://dx.doi.org/10.1016/j.actbio.2011.10.016

Sharma, A., Kalyanaraman, R., Narayan, R., Oktyabrsky, S., & Narayan, J. (2001). Carbon nanotube composites synthesized by ion-assisted pulsed laser deposition. *Materials Science and Engineering: B, 79*(2), 123-127.

Shea, J. E., & Miller, S. C. (2005). Skeletal function and structure: Implications for tissue-targeted therapeutics. *Advanced Drug Delivery Reviews, 57*(7), 945-957.

Sherman, W. (1912). Vanadium steel bone plates and screws. *Surg Gynecol Obstet, 14*, 629-634.

Shi, D. (2004). Biomaterials and Tissue Engineering. *Springer Berlin Heidelberg New York*, 2-200.

Shi, P., Ng, W. F., Wong, M. H., & Cheng, F. T. (2009). Improvement of corrosion resistance of pure magnesium in Hanks' solution by microarc oxidation with sol–gel TiO2 sealing. *Journal of Alloys and Compounds, 469*(1–2), 286-292. doi: http://dx.doi.org/10.1016/j.jallcom.2008.01.102

Singh, R. K., & Carignan, J. (1991). Theoretical aspects on spatial thickness variations in laser-deposited thin films. *MRS Online Proceedings Library, 236*, null-null.

Singh, R. K., Holland, O. W., & Narayan, J. (1990). Theoretical model for deposition of thin films using pulsed laser evaporation technique. *Journal of Applied Physics, 68*, 233-247.

Singh, R. K., & Narayan, J. (1990). Pulsed-laser evaporation technique for deposition of thin-films-physics and theoretical-model. *Physical Review B, 41*(13), 8843-8859. doi: 10.1103/PhysRevB.41.8843

Slinde, F., Grönberg, A., Engström, C., Rossander-Hulthén, L., & S., L. (2002). Individual dietary intervention in patients with COPD during multidisciplinary rehabilitation. *Respir Med., 96*(5), 330-336.

Sneddon, I. N. (1965). The relation between load and penetration in the axisymmetric Boussinesq problem for a punch of arbitrary profile. *International Journal of Engineering Science, 3*(1), 47-57.

Song, G. (2007). Control of biodegradation of biocompatable magnesium alloys. *Corrosion Science, 49*(4), 1696-1701. doi: 10.1016/j.corsci.2007.01.001

Song, G. L., & Atrens, A. (1999). Corrosion Mechanisms of Magnesium Alloys. *Advanced Engineering Materials, 1*(1), 11-33. doi: 10.1002/(SICI)1527-2648(199909)1:1<11::AID-ADEM11>3.0.CO;2-N

Song, Y. W., Shan, D. Y., & Han, E. H. (2008). Electrodeposition of hydroxyapatite coating on AZ91D magnesium alloy for biomaterial application. *Materials Letters, 62*(17–18), 3276-3279. doi: http://dx.doi.org/10.1016/j.matlet.2008.02.048

Staiger, M. P., Pietak, A. M., Huadmai, J., & Dias, G. (2006). Magnesium and its alloys as orthopedic biomaterials: A review. *Biomaterials, 27*(9), 1728-1734. doi: 10.1016/j.biomaterials.2005.10.003

Stern, M., & Geary, A. L. (1957). Electrochemical polarization .1. A theoretical analysis of the shape of polarization curves. *Journal of the Electrochemical Society, 104*(1), 56-63. doi: 10.1149/1.2428496

Suchanek, W., & Yoshimura, M. (1998). Processing and properties of hydroxyapatite-based biomaterials for use as hard tissue replacement implants. *Journal of Materials Research, 13*(1), 94-117.

Sudarshan, T. S., Srivatsan, T. S., & Harvey, D. P. (1990). Fatigue processes in metals - Role of aqueous enviroments. *Engineering Fracture Mechanics, 36*(6), 827-852. doi: 10.1016/0013-7944(90)90262-f

Sun, Y., Zhang, B., Wang, Y., Geng, L., & Jiao, X. (2012). Preparation and characterization of a new biomedical Mg-Zn-Ca alloy. *Materials & Design, 34*, 58-64. doi: 10.1016/j.matdes.2011.07.058

Suresh, S. (2004). Fatigue of materials. *2nd ed. Cambridge: Cambridge University Press*.

Tabor, D. (1951). *The Hardness of Metals*: Clarendon Press.

Tampieri, A., Fiorani, D., & Barone, A. (1995). *Euro-ceramics*.

Tanaka, H., Yamamoto, A., Shimoyama, J.-i., Ogino, H., & Kishio, K. (2012). Strongly connected ex situ MgB2 polycrystalline bulks fabricated by solid-state self-sintering. *Superconductor Science & Technology, 25*(11). doi: 10.1088/0953-2048/25/11/115022

Tang, Y., Chappell, H. F., Dove, M. T., Reeder, R. J., & Lee, Y. J. (2009). Zinc incorporation into hydroxyapatite. *Biomaterials, 30*(15), 2864-2872. doi: 10.1016/j.biomaterials.2009.01.043

Tapiero, H., & Tew, K. D. (2003). Trace elements in human physiology and pathology: zinc and metallothioneins. *Biomed Pharmacother, 57*(9), 399-411.

Technology, A. Schematic diagram of multi-target PLD method.

Thamaraiselvi, T., & Rajeswari, S. (2004). Biological evaluation of bioceramic materials - A review. *Carbon, 24*(31), 172.

Troitskii, V. V., & Tsitrin, D. N. (1944). The resorbing metallic alloy 'Osteosinthe- zit' as material for fastening broken bone. *Khirurgiia*(8), 41-44.

Uchida, A., Araki, N., Shinto, Y., Yoshikawa, H., Kurisaki, E., & Ono, K. (1990). The use of calcium hydroxyapatite ceramic in bone tumour surgery. *Journal of Bone & Joint Surgery, British Volume, 72*(2), 298-302.

Vadiraj, A., & Kamaraj, M. (2007). Effect of surface treatments on fretting fatigue damage of biomedical titanium alloys. *Tribology International, 40*(1), 82-88. doi: 10.1016/j.triboint.2006.02.064

van Blitterswijk, C., De Boer, J., Thomsen, P., Hubbell, J., Cancedda, R., de Bruijn, J. D., . . . Williams, D. F. (2008). *Tissue Engineering*: Elsevier Science.

van Dijk, K., Schaeken, H. G., Marée, C. H. M., Verhoeven, J., Wolke, J. C. G., Habraken, F. H. P. M., & Jansen, J. A. (1995). Influence of Ar pressure on r.f. magnetron-sputtered

Ca5(PO4)3OH layers. *Surface and Coatings Technology, 76–77, Part 1*(0), 206-210. doi: http://dx.doi.org/10.1016/0257-8972(95)02590-1

van Dijk, K., Verhoeven, J., Marée, C. H. M., Habraken, F. H. P. M., & Jansen, J. A. (1997). Study of the influence of oxygen on the composition of thin films obtained by r.f. sputtering from a Ca5(PO4)3 OH target. *Thin Solid Films, 304*(1–2), 191-195. doi: http://dx.doi.org/10.1016/S0040-6090(97)00104-1

Vormann, J. (2003). Magnesium: nutrition and metabolism. *Molecular Aspects of Medicine, 24*(1–3), 27-37. doi: 10.1016/S0098-2997(02)00089-4

Vu, T., & Heimann, R. B. (1997). Influence of the CaO/TiO2 ratio on thermal stability of hydroxyapatite in the system Ca5(PO4)3OH-CaO-TiO2. *Journal of Materials Science Letters, 16*(20), 1680-1682. doi: 10.1023/A:1018534300072

Walker, C. F., & Black, R. E. (2004). Zinc and the risk for infectious disease. *Annu. Rev. Nutr., 24*, 255-275.

Wallace, D. G., Smestad, T. L., McPherson, J. M., Piez, K. A., Seyedin, S., & Armstrong, R. (1988). Methods of bone repair using collagen: Google Patents.

Walz, L., Salzmann, G. M., Fabbro, T., Eichhorn, S., & Imhoff, A. B. (2008). The anatomic reconstruction of acromioclavicular joint dislocations using 2 TightRope devices a biomechanical study. *The American Journal of Sports Medicine, 36*(12), 2398-2406.

Wan, Y., Xiong, G., Luo, H., He, F., Huang, Y., & Zhou, X. (2008). Preparation and characterization of a new biomedical magnesium-calcium alloy. *Materials & Design, 29*(10), 2034-2037. doi: 10.1016/j.matdes.2008.04.017

Wan, Y. Z., Xiong, G. Y., Luo, H. L., He, F., Huang, Y., & Wang, Y. L. (2008). Influence of zinc ion implantation on surface nanomechanical performance and corrosion resistance of

biomedical magnesium-calcium alloys. *Applied Surface Science, 254*(17), 5514-5516. doi: 10.1016/j.apsusc.2008.02.117

Wang, H. X., Guan, S. K., Wang, X., Ren, C. X., & Wang, L. G. (2010). In vitro degradation and mechanical integrity of Mg–Zn–Ca alloy coated with Ca-deficient hydroxyapatite by the pulse electrodeposition process. *Acta Biomaterialia, 6*(5), 1743-1748. doi: http://dx.doi.org/10.1016/j.actbio.2009.12.009

Wang, M. (2003). Developing bioactive composite materials for tissue replacement. *Biomaterials, 24*(13), 2133-2151. doi: 10.1016/s0142-9612(03)00037-1

Wang, X. L., Fan, H. S., & Zhang, X. D. (2005). *An improvement in sintering property of β-tricalcium phosphate by addition of calcium pyrophosphate and calcium carbonate.* Paper presented at the Materials Science Forum.

Wang, Y. B., Xie, X. H., Li, H. F., Wang, X. L., Zhao, M. Z., Zhang, E. W., . . . Qin, L. (2011). Biodegradable CaMgZn bulk metallic glass for potential skeletal application. *Acta Biomaterialia, 7*(8), 3196-3208. doi: http://dx.doi.org/10.1016/j.actbio.2011.04.027

Waris, E., Konttinen, Y. T., Ashammakhi, N., Suuronen, R., & Santavirta, S. (2004). Bioabsorbable fixation devices in trauma and bone surgery: current clinical standing. *Expert review of medical devices, 1*(2), 229-240.

Watzinger, F., Luksch, J., Millesi, W., Schopper, C., Neugebauer, J., Moser, D., & Ewers, R. (2000). Guided bone regeneration with titanium membranes: a clinical study. *Br J Oral Maxillofac Surg, 38*(4), 312-315. doi: 10.1054/bjom.1999.0228

Webnode. The human skeletal system.

Weckbach, S., Losacco, J. T., Hahnhaussen, J., Gebhard, F., & Stahel, P. F. (2012). [Challenging the dogma on inferiority of stainless steel implants for fracture fixation. An end of the controversy?]. *Unfallchirurg, 115*(1), 75-79. doi: 10.1007/s00113-011-2145-0

Welch, J., & Gutt, W. (1961). High-temperature studies of the system calcium oxide–phosphorus pentoxide. *Journal of the Chemical Society (Resumed)*, 4442-4444.

Wen, C., Guan, S., Peng, L., Ren, C., Wang, X., & Hu, Z. (2009). Characterization and degradation behavior of AZ31 alloy surface modified by bone-like hydroxyapatite for implant applications. *Applied Surface Science, 255*(13-14), 6433-6438. doi: 10.1016/j.apsusc.2008.09.078

Wen, C. E., Mabuchi, M., Yamada, Y., Shimojima, K., Chino, Y., & Asahina, T. (2001). Processing of biocompatible porous Ti and Mg. *Scripta Materialia, 45*(10), 1147-1153. doi: 10.1016/S1359-6462(01)01132-0

Wen, Z., Wu, C., Dai, C., & Yang, F. (2009). Corrosion behaviors of Mg and its alloys with different Al contents in a modified simulated body fluid. *Journal of Alloys and Compounds, 488*(1), 392-399. doi: 10.1016/j.jallcom.2009.08.147

Weng, J., Liu, X. G., Zhang, X. D., & Ji, X. Y. (1994). Thermal-decomposition of hydroxyapatite structure induced by titanium and its dioxide. *Journal of Materials Science Letters, 13*(3), 159-161. doi: 10.1007/bf00278148

Wiese, A., & Pape, H. C. (2010). Bone defects caused by high-energy injuries, bone loss, infected nonunions, and nonunions. *Orthop Clin North Am, 41*(1), 1-4, table of contents. doi: 10.1016/j.ocl.2009.07.003

Willmott, P. R. (2004). Deposition of complex multielemental thin films. *Progress in Surface Science, 76*(6–8), 163-217. doi: http://dx.doi.org/10.1016/j.progsurf.2004.06.001

Willmott, P. R., Timm, R., & Huber, J. R. (1997). Reactive crossed beam scattering of a Ti plasma and a <equation>N₂</equation> pulse in a novel laser ablation method. *Journal of Applied Physics, 82*(5), 2082-2092. doi: 10.1063/1.366018

Winter, M. (1993-2012). from http://www.webelements.com/compounds/

Wise, D., Trantolo, D., Lewandrowski, K., Gresser, J., Cattaneo, M., & Yaszemski, M. (2000). Biomaterials engineering and devices human applications. *Volume Two, Humana Press, Inc. New Jersey*, 7-101.

Witte, F., Crostack, H. A., Nellesen, J., & Beckmann, F. (2011). Characterization of degradable magnesium alloys as orthopaedic implant material by synchrotron-radiation-based microtomography. *HASYLAB at DESY*.

Witte, F., Fischer, J., Nellesen, J., Crostack, H. A. H. A., Kaese, V., Pisch, A., . . . Windhagen, H. (2006). In vitro and in vivo corrosion measurements of magnesium alloys. *Biomaterials, 27*(7), 1013-1018. doi: 10.1016/j.biomaterials.2005.07.037

Witte, F., Fischer, J., Nellesen, J., Vogt, C., Vogt, J., Donath, T., & Beckmann, F. (2010). In vivo corrosion and corrosion protection of magnesium alloy LAE442. *Acta Biomaterialia, 6*(5), 1792-1799. doi: http://dx.doi.org/10.1016/j.actbio.2009.10.012

Witte, F., Hort, N., Vogt, C., Cohen, S., Kainer, K. U., Willumeit, R., & Feyerabend, F. (2008). Degradable biomaterials based on magnesium corrosion. *Current Opinion in Solid State & Materials Science, 12*(5-6), 63-72. doi: 10.1016/j.cossms.2009.04.001

Witte, F., Hort, N., Vogt, C., Cohen, S., Kainer, K. U., Willumeit, R., & Feyerabend, F. (2009). *Degradable biomaterials based on magnesium corrosion*: Elsevier.

Witte, F., Kaese, V., Haferkamp, H., Switzer, E., Meyer-Lindenberg, A., Wirth, C. J., & Windhagen, H. (2005). In vivo corrosion of four magnesium alloys and the associated bone response. *Biomaterials, 26*(17), 3557-3563. doi: 10.1016/j.biomaterials.2004.09.049

Wolf, F. I., & Cittadini, A. (2003). Chemistry and biochemistry of magnesium. *Molecular Aspects of Medicine, 24*(1-3), 3-9. doi: 10.1016/s0098-2997(02)00087-0

Wolff, D. M. B., Ramalho, E. G., & Acchar, W. (2006). *Phase transition behaviour of tricalcium phosphate (TCP) doped with MgO and TiO2 as additives.* Paper presented at the Materials science forum.

Wong, H. M., Yeung, K. W. K., Lam, K. O., Tam, V., Chu, P. K., Luk, K. D. K., & Cheung, K. M. C. (2010). A biodegradable polymer-based coating to control the performance of magnesium alloy orthopaedic implants. *Biomaterials, 31*(8), 2084-2096. doi: 10.1016/j.biomaterials.2009.11.111

Wood, D. S., Zollman, J., Reuben, J. P., & Brandt, P. W. (1975). Human skeletal muscle: properties of the" chemically skinned%" fiber. *Science (New York, NY), 187*(4181), 1075.

Wu, C., Ramaswamy, Y., Chang, J., Woods, J., Chen, Y., & Zreiqat, H. (2008). The effect of Zn contents on phase composition, chemical stability and cellular bioactivity in Zn-Ca-Si system ceramics. *Journal of Biomedical Materials Research Part B-Applied Biomaterials, 87B*(2), 346-353. doi: 10.1002/jbm.b.31109

Xin, R., Leng, Y., Chen, J., & Zhang, Q. (2005). A comparative study of calcium phosphate formation on bioceramics in vitro and in vivo. *Biomaterials, 26*(33), 6477-6486. doi: http://dx.doi.org/10.1016/j.biomaterials.2005.04.028

Xu, L., Pan, F., Yu, G., Yang, L., Zhang, E., & Yang, K. (2009). In vitro and in vivo evaluation of the surface bioactivity of a calcium phosphate coated magnesium alloy. *Biomaterials, 30*(8), 1512-1523. doi: http://dx.doi.org/10.1016/j.biomaterials.2008.12.001

Xu, L., Yu, G., Zhang, E., Pan, F., & Yang, K. (2007). In vivo corrosion behavior of Mg-Mn-Zn alloy for bone implant application. *Journal of Biomedical Materials Research Part A, 83A*(3), 703-711. doi: 10.1002/jbm.a.31273

Xu, L., Zhang, E., Yin, D., Zeng, S., & Yang, K. (2008). In vitro corrosion behaviour of Mg alloys in a phosphate buffered solution for bone implant application. *Journal of Materials Science-Materials in Medicine, 19*(3), 1017-1025. doi: 10.1007/s10856-007-3219-y

Xue, W., Dahlquist, K., Banerjee, A., Bandyopadhyay, A., & Bose, S. (2008). Synthesis and characterization of tricalcium phosphate with Zn and Mg based dopants. *J Mater Sci Mater Med, 19*(7), 2669-2677. doi: 10.1007/s10856-008-3395-4

Yamamoto, A., & Tsubakino, H. (2003). Surface treatment of magnesium alloys by artificial corrosion-oxidization method. *MATERIALS TRANSACTIONS, 44*(4), 511-517.

Yamamoto, A., Watanabe, A., Sugahara, K., Tsubakino, H., & Fukumoto, S. (2001). Improvement of corrosion resistance of magnesium alloys by vapor deposition. *Scripta Materialia, 44*(7), 1039-1042.

Yamasaki, Y., Yoshida, Y., Okazaki, M., Shimazu, A., Kubo, T., Akagawa, Y., & Uchida, T. (2003). Action of FGMgCO3Ap-collagen composite in promoting bone formation. *Biomaterials, 24*(27), 4913-4920. doi: 10.1016/S0142-9612(03)00414-9

Yamasaki Y, Y. Y., Okazaki M, Shimazu A, Uchida T, Kubo T, Akagawa Y, Hamada Y, Takahashi J, Matsuura N. (2002 Oct). Synthesis of functionally graded MgCO3 apatite accelerating osteoblast adhesion. *J Biomed Mater Res., 62*(1), 99-105.

Yamashita, K., Arashi, T., Kitagaki, K., Yamada, S., Umegaki, T., & Ogawa, K. (2005). Preparation of Apatite Thin Films through rf-Sputtering from Calcium Phosphate Glasses. *Journal of the American Ceramic Society, 77*(9), 2401-2407.

Yang, J., Cui, F.-z., Lee, I. S., & Wang, X. (2010). Plasma surface modification of magnesium alloy for biomedical application. *Surface & Coatings Technology, 205*, S182-S187. doi: 10.1016/j.surfcoat.2010.07.045

Yang, W., Zhang, P., Liu, J., & Xue, Y. (2006). Effect of long-term intake of Y3+ in drinking water on gene expression in brains of rats. *Journal of Rare Earths, 24*(3), 369-373. doi: 10.1016/s1002-0721(06)60126-9

Yue, S., Pilliar, R. M., & Weatherly, G. C. (1984). The fatigue strength of porous-coated Ti–6% Al–4% V implant alloy. *Journal of Biomedical Materials Research, 18*(9), 1043-1058. doi: 10.1002/jbm.820180908

Zeng, R., Dietzel, W., Witte, F., Hort, N., & Blawert, C. (2008). Progress and challenge for magnesium alloys as biomaterials. *Advanced Engineering Materials, 10*(8), B3-B14. doi: 10.1002/adem.200800035

Zhang, E., Xu, L., & Yang, K. (2005). Formation by ion plating of Ti-coating on pure Mg for biomedical applications. *Scripta Materialia, 53*(5), 523-527. doi: http://dx.doi.org/10.1016/j.scriptamat.2005.05.009

Zhang, E., Yang, L., Xu, J., & Chen, H. (2010). Microstructure, mechanical properties and bio-corrosion properties of Mg-Si(-Ca, Zn) alloy for biomedical application. *Acta Biomaterialia, 6*(5), 1756-1762. doi: 10.1016/j.actbio.2009.11.024

Zhang, E., Yin, D., Xu, L., Yang, L., & Yang, K. (2009). Microstructure, mechanical and corrosion properties and biocompatibility of Mg-Zn-Mn alloys for biomedical

application. *Materials Science and Engineering C, 29*(3), 987-993. doi: 10.1016/j.msec.2008.08.024

Zhang, F., Chang, J., Lu, J., Lin, K., & Ning, C. (2007). Bioinspired structure of bioceramics for bone regeneration in load-bearing sites. *Acta Biomaterialia, 3*(6), 896-904.

Zhang, S., Zhang, X., Zhao, C., Li, J., Song, Y., Xie, C., . . . Bian, Y. (2010). Research on an Mg-Zn alloy as a degradable biomaterial. *Acta Biomaterialia, 6*(2), 626-640. doi: 10.1016/j.actbio.2009.06.028

Zhang, Y., Yang, J. X., Cui, F. Z., Lee, I. S., & Lee, G. H. (2010). Characterization and degradation comparison of DLC film on different magnesium alloys. *Surface & Coatings Technology, 205*, S15-S20. doi: 10.1016/j.surfcoat.2010.02.069

Zhou, W., Zhong, X., Wu, X., Yuan, L., Shu, Q., Xia, Y., & Ostrikov, K. K. (2007). Plasma-controlled nanocrystallinity and phase composition of TiO2: a smart way to enhance biomimetic response. *J Biomed Mater Res A, 81*(2), 453-464. doi: 10.1002/jbm.a.30987

Znamenskii, M. (1945). Metallic osteosynthesis by means of an apparatus made of absorbing metal. *Khirurgiia*(12), 60-63.

Zreiqat, H., Howlett, C. R., Zannettino, A., Evans, P., Schulze-Tanzil, G., Knabe, C., & Shakibaei, M. (2002). Mechanisms of magnesium-stimulated adhesion of osteoblastic cells to commonly used orthopaedic implants. *J Biomed Mater Res., 62*(2), 175-184.

Zreiqat, H., Ramaswamy, Y., Wu, C., Paschalidis, A., Lu, Z., James, B., . . . Dunstan, C. R. (2010). The incorporation of strontium and zinc into a calcium-silicon ceramic for bone tissue engineering. *Biomaterials, 31*(12), 3175-3184. doi: 10.1016/j.biomaterials.2010.01.024